OPTICAL INTERCONNECTS ON PRINTED CIRCUIT BOARDS

A Thesis
Presented to
The Academic Faculty

by

Fengtao Wang

In Partial Fulfillment
of the Requirements for the Degree
Doctor of Philosophy in Electrical and Computer Engineering

Georgia Institute of Technology
December 2010

COPYRIGHT 2010 BY FENGTAO WANG

OPTICAL INTERCONNECTS ON PRINTED CIRCUIT BOARDS

Approved by:

Dr. Ali Adibi, Advisor
School of Electrical and Computer Engineering
Georgia Institute of Technology

Dr. Azad J Naeemi
School of Electrical and Computer Engineering
Georgia Institute of Technology

Dr. Gee-Kung Chang
School of Electrical and Computer Engineering
Georgia Institute of Technology

Dr. Stephen H. Sprigle
School of Applied Physiology
Georgia Institute of Technology

Dr. Stephen E Ralph
School of Electrical and Computer Engineering
Georgia Institute of Technology

Date Approved: 07/ 23 /2010

To my wife, parents, and family.

ACKNOWLEDGEMENTS

I would like to first thank my advisor, Prof. Ali Adibi, for his guidance, support, and encouragement, and also for giving me the freedom to pursue my academic research. I am deeply grateful to Dr. Fuhan Liu, a great tutor and a good friend, for all the help throughout my PhD program. I have been working with Prof. Gee-Kung Chang and Prof Thomas K. Gaylord at the Packaging Research Center, and would like to thank them for sharing their precious knowledge and aggressive attitude in research. I would like to sincerely thank Prof. Gee–Kung Chang, Prof. Stephen E Ralph, Prof. Azad J Naeemi, Prof. Stephen H. Sprigle for reviewing my thesis and being the members of my PhD defense committee. I also appreciate Prof. Stephen H. Sprigle and Dr. Linghua Kong who give me the opportunity to work on the multispectral imaging project during my PhD program.

I am also sincerely grateful to the holographic team, including Jerry, Arash and Omid, for the collaborations and invaluable discussions in my project. I am proud of being the member in one of the best research groups in the world, Photonics Research Group, and grateful to work with the brilliant colleagues, including JD, Siva, Henry, Babak, Samon, Charles, Mohammad, Majid, Ehsan, Saeed, Reza, Murtaza, Amir, Hossein, Pouyan, Charlie, Maysam, Ye, Ali, Qing, Majid, Reza, and Zhixuan. I also would like to express my gratitude to my friends, in particular, Dr. Lynn Yang and Prof. Haizheng Li, for their friendship and enjoyable life in Atlanta.

And finally, from bottom of my heart, I would like to thank my parents, my brother, my sisters, and my dear wife, Yuan (Leda), for all their endless love, support, and patience throughout my life.

TABLE OF CONTENTS

LIST OF TABLES

LIST OF FIGURES

LIST OF ABBREVIATIONS

1D	One Dimensional
2D	Two Dimensional
3D	Three Dimensional
AFM	Atomic fForce Microscopy
BGA	Ball Grid Array
CCD	Charge Coupled Device
CSP	Chip Scale Package
DIP	Dual Inline Package
D.I.	De-ionized
FSOI	Free-Space Optical Interconnects
MEMS	Micro-Electro-Mechanical Systems
NA	Numerical Aperture
PCB	Printed Circuit Board
PLC	Planar Lightwave Circuits
PRC	Packaging Research Center
QFP	Quad Flat Package
RIE	Reactive Ion Etch
RMS	Root-Mean-Square
SAP	Semi-Additive Processes
SBVH	Spherical Beam Volume Hologram
SEM	Scanning Electron Microscopy
SIP	System-in-Package
SMT	Surface Mount Technology

SOP	System on Package
TIR	Total Internal Reflection
UV	Ultra Violet
VCSEL	Vertical Cavity Surface Emitting Laser

SUMMARY

The ever-increasing need for higher bandwidth and density is one of the motivations for extensive research on planar optoelectronic structures on printed circuit board (PCB) substrates. Among these applications, optical interconnects have received considerable attention in the last decade. Several optical interconnect techniques, such as free space, guided wave, board level and fiber array interconnects, have been introduced for system level applications. In all planar optoelectronic systems, optical waveguides are crucial elements that facilitate signal routing. Low propagation loss, high reliability and manufacturability are among the requirements of polymer optical waveguides and polymer passive devices on PCB substrates for practical applications. Besides fabrication requirements, reliable characterization tools are needed to accurately and nondestructively measure important guiding properties, such as waveguide propagation loss. In three-dimensional (3D) fully embedded board-level optical interconnects, another key challenge is to realize efficient optical coupling between in-plane waveguides and out-of-plane laser/detector devices.

Driven by these motivations, the research presented in this thesis focuses on some fundamental studies of optical interconnects for PCB substrates, e.g., developing low-loss optical polymer waveguides with integrated efficient out-of-plane couplers for optical interconnects on printed circuit board substrates, as well as the demonstration of a novel free-space optical interconnect system by using a volume holographic thin film. Firstly, the theoretical and experimental investigations on the limitations of using mercury i-line ultraviolet (UV) proximity photolithography have been carried out, and the metallization

techniques for fine copper line formation are explored. Then, a new type of low-loss polymer waveguides (i.e., capped waveguide) is demonstrated by using contact photolithography with considerable performance improvement over the conventional waveguides. To characterize the propagation properties of planar optical waveguides, a reliable, nondestructive, and real-time technique is presented based on accurately imaging the scattered light from the waveguide using a sensitive charge coupled device (CCD) camera that has a built-in integration functionality. To provide surface normal light coupling between waveguides and optoelectronic devices for optical interconnects, a simple method is presented here to integrate 45° total internal reflection micro-mirrors with polymer optical waveguides by an improved tilted beam photolithography (with the aid of de-ionized water) on PCBs. A new technique is developed for a thin layer of metal coating on the micro-mirrors to achieve higher reflection and coupling efficiency (i.e., above 90%). The combination of the capped waveguide technique and the improved tilted UV exposure technique along with a hard reusable metal mask for metal deposition eliminates the usage of the traditional lift-off process, greatly simplifies the process, and reduces fabrication cost without sacrificing the coating quality. For the study of free-space optical interconnects, a simple system is presented by employing a single thin-film polymeric volume holographic element. One 2-spherical-beam hologram is used to link each point light source with the corresponding photodetector. An 8-channel free-space optical interconnect system with high link efficiency is demonstrated by using a single volume holographic element where 8 holograms are recorded.

CHAPTER 1

INTRODUCTION

The speed and complexity of integrated circuits are increasing rapidly as integrated circuit technology advances to ultra large scale integrated circuits. As the number of devices per chip, the number of chips per board and the modulation speed continue to increase, electrical interconnects are facing their fundamental bottlenecks, such as bandwidth, packaging density and power dissipation. This ever-increasing need for higher bandwidth and density is one of the motivations for extensive research on planar optoelectronic structures on PCB substrate [1]. Among many applications, optical interconnects [2-33] have received considerable attention in the last decade. Several optical interconnect techniques such as free space [4], guided wave [5], board level and fiber array interconnects have been introduced for system level applications.

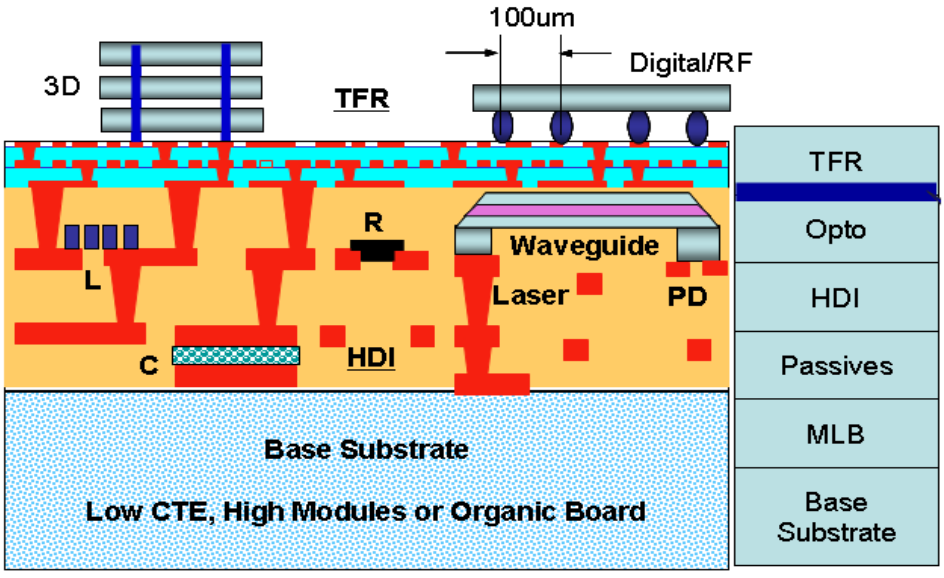

Figure 1.1. The concept of high density and high speed system-on-package

Because optical interconnects are still bulky and less reliable, and have packaging difficulties, many ideas are introduced to address these problems. These ideas mainly focus on reducing packaging volume and vulnerability to the external environment. Scientists use matured semiconductor technology to build optical components. Their initial effort is fabricating planar lightwave circuits (PLC) integrated on a solid or flexible substrate. Figure 1.1 shows the concept of high density and high speed system on package (SOP), where optical waveguide circuit is embedded in a multi-layer high speed substrate, along with digital/RF modules, passive devices (resistors, capacitors, and inductors) and active devices (lasers and photodiodes). For optical interconnects on PCB substrates, low propagation loss, high optical quality and manufacturability are among the requirements of polymer optical waveguide circuit for practical applications. During the late 1980's, early attempts were focused on the integration of polymer waveguides on PCBs for optical interconnects [6]. Several technologies have been developed, such as photolithography, reactive ion etch (RIE), laser ablation molding/embossing, lamination and monomers diffusion, etc., to define optical waveguides [7-10]. Among these technologies, photolithography has excellent ability to define smooth and high definition waveguides. However, there are process-related challenges that limit the manufacturability of such waveguides. For example, dust particles, contaminations, scratches, mechanical damages, chemical swells, corrosions and over-etching degrade the performance of high quality waveguides and other polymer-based devices. Further efforts on fabrication process optimization are needed to minimize the process-induced defects in integrated optoelectronics.

Photolithography is a dominant process used in microfabrication on both semiconductor and packaging board substrates. It uses UV light to transfer and define a latent pattern from a photomask to a light-sensitive photoresist. Then, chemical treatments will engrave the relief pattern into the material underneath the photoresist. There are three basic UV photolithography methods: contact printing [58], proximity printing [59] and projection imaging [59]. Proximity and contact printing technologies play a dominant role in the PCB and packaging industry, while projection imaging is generally used in semiconductor integrated circuit manufacturing. To be compatible with the PCB industry, the integrated optical waveguide circuit on PCB substrate in this thesis is fabricated by the photolithography using the PCB facilities.

Besides fabrication requirements, reliable characterization tools are needed for an accurate and nondestructive measurement of important waveguide properties such as the propagation loss. Several techniques, such as the cutback method [11], sliding prism technique [12, 13], multiple reflections method [14] and photographic approach [15-17], have been developed to measure the propagation loss of planar waveguides. The widely used cutback method requires a relatively long waveguide sample, especially for low propagation loss (i.e., less than 0.1dB/cm) waveguides. Furthermore, the cutback method is destructive, time consuming and hard to implement for waveguides integrated on PCB substrates that are difficult to cleave. The sliding prism method, in which a prism is moving along the light propagation direction, is also widely employed, but it is hard to maintain the coupling efficiency constant, especially for polymer waveguides on PCB substrates. The multiple reflection method provides a nondestructive solution for loss

measurement; however, it involves the complicated reflectometer alignment and is not suitable for studying the local propagation properties in detail.

The photographic method is a simple and accurate way to characterize the properties of planar waveguides, such as waveguide propagation loss, bending behavior and cross talk among adjacent waveguide channels. This technique uses a video camera to record the entire streak of light scattered from the waveguide, and then analyzes the power of the scattered light on the computer. However, this method is hard to use for the loss measurement in a waveguide with small scattering, due to low sensitivity of the video camera [15]. The method is improved later by coating the waveguide with a fluorescent layer to enhance the detection of the scattered light [16]. Strasser and Gupta [17] used photographic films with high sensitivity to record the image of the low-intensity scattered light. Although this method has high sensitivity, it is not a real-time measurement. Further research efforts are required to develop a simple, real-time, accurate and nondestructive technique for the characterization of optical waveguides with low scattering loss on PCB substrates.

In three-dimensional fully embedded board-level optical interconnects, another key challenge is to realize highly efficient optical coupling between in-plane waveguides and laser/detector devices. 45° total internal reflection (TIR) micro-mirrors and grating devices [3] integrated on waveguides have been studied as surface normal couplers. 45° TIR mirror couplers are more widely employed as waveguide couplers compared with the grating couplers, because they are coupling-efficient, easy to fabricate and relatively insensitive to wavelength variation.

Various techniques can be used to construct 45° TIR micro-mirrors, such as laser ablation [18–20], grayscale lithography [21], hard molding [22], soft molding [23], reactive ion etching (RIE) [24], micro-dicing [25], the X-ray lithography [26] and deep proton writing [27]. Among these technologies, photolithography is commonly used in printed circuit and semiconductor fabrication, micro-electro-mechanical systems (MEMs), bio samples and optical polymer devices, because of its excellent ability to define smooth and high definition micro-structures. Devices with precise structure profile and optical smooth surface required for optical application can be achieved by photolithography technology. Photolithography is the least disruptive technology to implement optical interconnects on PCBs, because it is easy, cost effective and compatible with the present-day PCB processing. Other techniques might yield better quality micro-mirrors, but may be more "exotic", therefore less compatible with high-volume and large-scale PCB production.

In most cases, the device structures are defined by utilizing UV beam normally incident into the polymer so that the structures have vertical side walls. The tilted beam lithography can make tapered structure, as the UV beam is traveling inside the polymer material at an inclined angle. It can be used to make polymer waveguides with tapered micro-mirrors integrated at the end. Taken the refractive index of most photo polymers as 1.5, according to Snell's Law, the maximum slope angle that can be formed in photo polymers by using the tilted beam lithography in the air is 41.8° (i.e., smaller than 45°). Additionally, to achieve this maximum angle, the UV exposure beam has to be tilted at an angle close to 90° in the air, which leads to the huge reflection loss on the air-polymer

interface. Therefore, it is impossible to fabricate micro-mirrors with 45° by simply tilting the UV exposure beam in the air.

In order to have the UV exposure beam traveling inside the polymer waveguide core layer at an angle greater than 41° (e.g., at 45°), a prism can be used on top of the polymer core layer [28]. However, there are some practical issues in using prism for the micro-mirror integration on polymer waveguides on PCB substrates. First, the desired waveguide circuits usually reach longer than 10 cm. Thus multiple prisms have to be placed at the different locations of the waveguides where micro-mirrors are needed. Furthermore, the edge of the prism will cause UV beam distortion during exposure. Lastly, because the substrate or the optical board is not ideally smooth and flat, there will be air gaps at the interface between the prism and the photo mask, as well as the interface between the polymer core layer and the photo mask. Usually these air gaps are filled with index matching glue during the UV exposure process, which is cleaned out thereafter. Another solution of reducing the mismatch of refractive index between air and photo resist is reported in 3-dimentional inclined polymer microstructures fabrications, where Glycerol is employed as an index matching material between the photo mask and photo resist Su-8 during tilted beam exposure to compensate the refractive index difference, thus extending the possible inclined angle of UV beam in the photo resist [29].

Compared with optical fiber or waveguide interconnects, free-space optical interconnects [4] (FSOIs) offer more flexible routing of signal beam as a result of using the third spatial dimension for beam propagation. The space between two circuit boards that need to communicate with each other is purely empty; therefore, it is called free space. Light signals coming out from the sources substrate propagate to designated

locations on the object substrate. Usually the architecture is simple; however, realization is very difficult. The relative positions among the optical components and two substrates should be precisely controlled. Another disadvantage of the free space interconnects is that the system is vulnerable to the external environment such as vibration and thermal fluctuation, thus maintenance of the system is extremely difficult.

There are several physical implementations of FSOI systems, based on monolithic micro-lenses [30], a modified folded 4-f imaging system [31] and optical substrate-mode holograms [32], etc. Compared to the FSOIs that use planar integrated free-space components and lenses (micro-lenses or macro-lens) to collimate and collect the light [30, 31], lensless FSOIs are simpler and require less packaging efforts. A hologram is generally recorded by the interference pattern of two coherent beams. One of the recording beams can be reconstructed by reading the hologram with the other recording beam under the Bragg matching condition. The holography was first demonstrated by Lippman in 1891 by interfering a beam of light with its own reflection [33]. With the invention of the laser in the early 1960's, the holography technology became practical for storing and retrieving images. In 1966, E. N. Leith and his colleagues demonstrated the multiple-image storage in three-dimensional media by rotation of the photographic plate [34], which started the journey of numerous applications of "volume hologram". Volume holograms have more restrict Bragg matching condition, compared to thin holograms, due to the thickness of the holographic medium. Thus, based on the unique property of high selectivity of the reading angle and reading wavelength in thick holographic media, thousands of data pages can be recorded in a small common volume through the multiplexing techniques, such as angular multiplexing [35], wavelength multiplexing [37,

38], phase-coded multiplexing [39], shift multiplexing [40], spatial multiplexing [41] and combinations of multiplexing methods [42, 43]. During the past 50 years, volume holographic technology has been widely used in many applications, including data storage [35-43], pattern recognition [44, 45], telecommunication [46-48] and optical neural networks [49]. Volume holograms multiplexed in thick polymer film have also been proposed for optical interconnects [50]. The high Bragg selectivity of thick holograms can provide low cross talk noise in FSOIs. The thin film polymer holographic media usually offers larger dynamic range than the doped $L_iN_bO_3$ crystal media, and as a result, multiple strong holograms can be recorded within the same volume of the thin film holographic polymer and provide high link efficiency for FSOIs.

In summary, optical interconnects have many advantages over the copper interconnects, which include immunity to the electromagnetic interference, independency from impedance mismatch, less power consumption, and higher bandwidth. This technology will provide a new path for the system performance improvement, other than relying on incremental reduction of the size of transistors; however, they are still faced difficulties in packaging, fabrication feasibility, signal tapping, and reliability. At present, metal-based electrical interconnects still dominate inter- and intra-chip interconnects for the obvious reason: there is no viable cost effective alternative. If optical interconnects can provide reliable and cost effective solutions, in areas where conventional electrical interconnects fail to function, i.e., ultra high density and high speed interconnects, optical interconnects will be the most promising technology.

1.1 Thesis Organization

This thesis focuses on some fundamental studies of optical interconnects for PCB substrates.

In Chapter 2, the theoretical and experimental investigations on the limitations of using mercury i-line UV proximity photolithography have been carried out, and the metallization techniques for fine copper line formation are explored. The theoretical analysis based on the Fresnel diffraction indicates that the key factor that hinders the finer feature size formation through proximity photolithography is the air gap between the photoresist and the mask. An expression for the minimum transferable feature size is obtained from the experiments. The experimental data confirm the validity of the theoretical analysis.

In Chapter 3, a new type of low-loss polymer waveguides (i.e., capped waveguide) is demonstrated by using contact photolithography with a considerable performance improvement over the conventional optical polymer waveguides. By simultaneously patterning the core and the top cladding layers in capped waveguides, the effect of fabrication defects can be considerably reduced, and the propagation lose is reduced by at least 20% compared to the conventional waveguides.

In Chapter 4, to characterize the propagation properties of planar optical waveguides, a reliable, nondestructive and real-time technique is presented based on accurately imaging the scattered light from optical waveguides using a sensitive CCD camera that has a built-in integration functionality. This technique can be used for real-time investigation of the propagation properties (loss, mode profile, bending properties, etc.) and the fabrication quality of planar waveguides, with high sensitivity. Using the

characterization tool developed in Chapter 3, we measured capped waveguides with loss coefficients of $\alpha_1 = 0.065$ dB/cm at $\lambda = 850$ nm, and $\alpha_2 = 0.046$ dB/cm at $\lambda = 980$ nm with the accuracy of 0.008 dB/cm.

To provide surface normal light coupling between waveguides and optoelectronic devices for optical interconnects, a simple method is presented in Chapter 5 to integrate 45° total internal reflection micro-mirrors with polymer optical waveguides by an improved tilted beam photolithography (with the aid of de-ionized water) on PCBs. A new technique is developed for a thin layer of metal coating on the micro-mirrors to achieve higher reflection and coupling efficiency (i.e., above 90%). The combination of the capped waveguide technique and the improved tilted UV exposure technique along with a hard reusable metal mask for metal deposition eliminates the usage of the traditional lift-off process, greatly simplifies the process, and reduces the fabrication cost without sacrificing the coating quality.

In Chapter 6, for the study of free-space optical interconnects, a novel and simple system is developed by employing a single thin-film polymeric volume holographic element. One 2-spherical-beam hologram is used to link each point light source with the corresponding photodetector. An 8-channel FSOI system with high link efficiency is demonstrated by using a single volume holographic element where 8 holograms are recorded.

Chapter 7 addresses the future extension of this research, and the conclusion of the thesis is discussed in Chapter 8.

CHAPTER 2

PROXIMITY LITHOGRAPHY IN SUB-10 MICRON PACKAGING CIRCUITRY

Rapid changes in the semiconductor industry will continue toward higher functionality that leads to higher I/O counts, pushing packaging towards higher density architectures. In the next 2 to 3 years, the I/O pitch will fall within 100 μm for area array die and 30μm for periphery die. That raises an important question to the packaging industry: How will the rapid shrinkage of the I/O pitch affect the package substrate for chip attaching? The answer is sub-10 micron copper line technology. In this chapter, the theoretical and experimental studies on the limitations of using mercury i-line UV photolithography have been carried at the Packaging Research Center at Georgia Tech. Furthermore, ultra fine copper line routing substrates are demonstrated for flip chip attaching by using semi-additive metallization process [68].

2.1. Introduction to Photolithography

The International Technology Roadmap for Semiconductors [51] predicts that the pad pitch of microprocessor packages will be 120 μm in 2011 and down to 95 μm in 2016 for area array flip chips [52] while the periphery pad pitch would be down to 25 μm in 2016. A build-up substrate consisting of multiple wiring layers with routing line width and space below 10 μm will be needed. Figure 1 illustrates the needs of routing line width and space for an area array flip chip with I/O pitch of 100 μm and pad diameter of 40 μm. For 60 μm spacing between two adjacent pads, the line width must be 20 μm or less so

that two rows of copper lines can be routed between the pitches. When three signal rows need to be accessed, 12 μm line width and space are required. If four signal rows need to be accessed, 8.5 μm line and space becomes necessary. The maximum number of I/O escaped per layer is calculated and listed in Fig. 2.1. The more the number of I/Os that are achieved (or fanned out per layer), the greater is the reduction in layer count. The main advantage with lower layer count is the reduction in material consumption and the time saving in fabrication, which result in lower cost. Using fewer layers, the number of processing steps is also reduced, and the yield will be increased. In addition, the package will be more reliable. The realization of such fine feature size, while maintaining low cost, is a key challenge for the packaging industry.

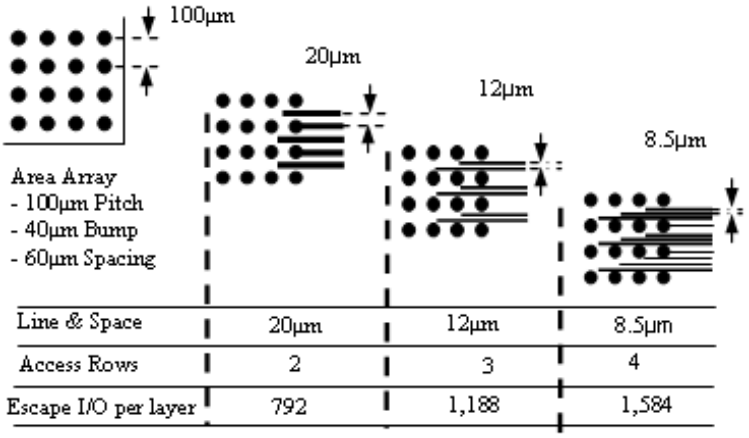

Figure 2.1. Routing Requirements for an area array flip chip with 100 μm pitch

Figure 2.2 illustrates the advances of packaging technologies from earlier Dual Inline Package (DIP) technology [53] in the 1970's, to surface mount technology (SMT) in the 1980's, such as Quad Flat Package (QFP) [54], etc. to current advanced IC packages, such as Ball Grid Array (BGA), Chip Scale Package (CSP) [55] etc, in the 1990's, and system-in-package (SIP) [56] in the 2000's, and to highly integrated system-

on-package (SOP) system technology [57]. The SOP offers advantages over the three-dimensional packaging and the SIP. The 3-D packaging is a general concept of stacking of similar or dissimilar chips such as DRAMs with processor and flash memory. The SIP goes beyond to embed actives and passives that are discrete, thick, and bulky components. The SOP goes further in the ultimate 3-D integration of components in thin-film form at microscale in the short term, and nanoscale in the long term.

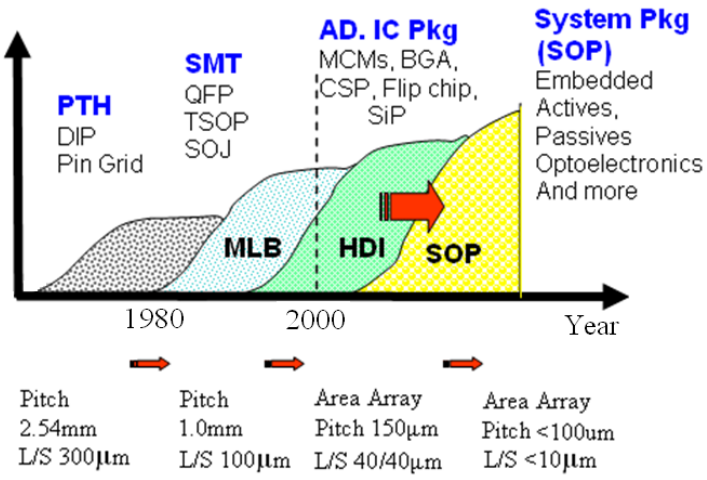

Figure 2.2. Packaging advances and Trends: DIP type package (1970's), SMT (1980's), advanced IC packages (BGA, CSP etc. 1990's, and SiP, 2000's), and next generation SOP.

Photolithography is a dominant process used in microfabrication on both semiconductor and packaging board substrates. It uses UV light to transfer and define a latent pattern from a photomask to a light-sensitive photoresist. Then, chemical treatment will engrave the relief pattern into the material underneath the photoresist. There are three basic UV photolithography methods: contact printing [58], proximity printing [59], and projection imaging [59]. Proximity and contact printing technologies play a dominant role in the printed circuit board (PCB) and packaging industry, while projection imaging is used in semiconductor IC manufacturing.

The semiconductor industry has developed features of 30 nm for high performance microprocessors. While the feature size that the packaging industry can produce is about 15~20 μm, a huge technical gap exists between semiconductor industry and packaging industry. In order to keep the pace with semiconductor process development, a process for finer pitch wiring substrate is necessary. In this chapter, we investigate the key factors that hinder the finer feature size formation on packaging substrates and explore the minimum size of lines and spaces that can be obtained based on the high pressure mercury i-line photolithography.

2.2. Theoretical Analysis of Proximity Photolithography

The pattern definition in the resist in proximity photolithography is a two-step process consisting of a latent image formation via the exposure, followed by development process to generate a relief structure. Therefore, limitation factors in both exposure and development processes will be considered. The exposure process, as well as the post processes (e.g., baking and developing), have to be optimized to realize fine lines and spaces.

The primary resolution limitation of proximity photolithography is diffraction of light at the edge of an opaque feature on the photomask as the collimated UV beam passes through an adjacent clear area. To simplify the analysis, the discussions of diffraction effect are based on the assumption of fully spatially coherent UV exposure light. Due to diffraction, the propagating light is then “bent” and diverted through an equal line and space grating (i.e., a grating with equal width of the wire and the space between the adjacent wires) on the mask. The intensity distribution of UV light inside the photoresist can be estimated by computer simulation based on the Fresnel diffraction

theory [60]. The theory of Fresnel diffraction is based on the assumption that the incident wave is multiplied by the aperture function $p(x,y)$ and propagates in free space (or uniform media) in accordance with the Fresnel approximation. If the incident wave is a plane wave, at the wavelength of λ, traveling in the z-direction with intensity I_i, the complex amplitude immediately after the aperture is $f(x,y) = I_i^{1/2} p(x,y)$. Then the diffraction pattern $I(x,y)$ at a distance d is:

$$I(x,y) = \frac{I_i}{(\lambda d)^2} \left| \int_{-\infty}^{\infty} \int p(x',y') \exp\left[-j\pi \frac{(x-x')^2 + (y-y')^2}{\lambda d} \right] dx'dy' \right|^2 \tag{2.1}$$

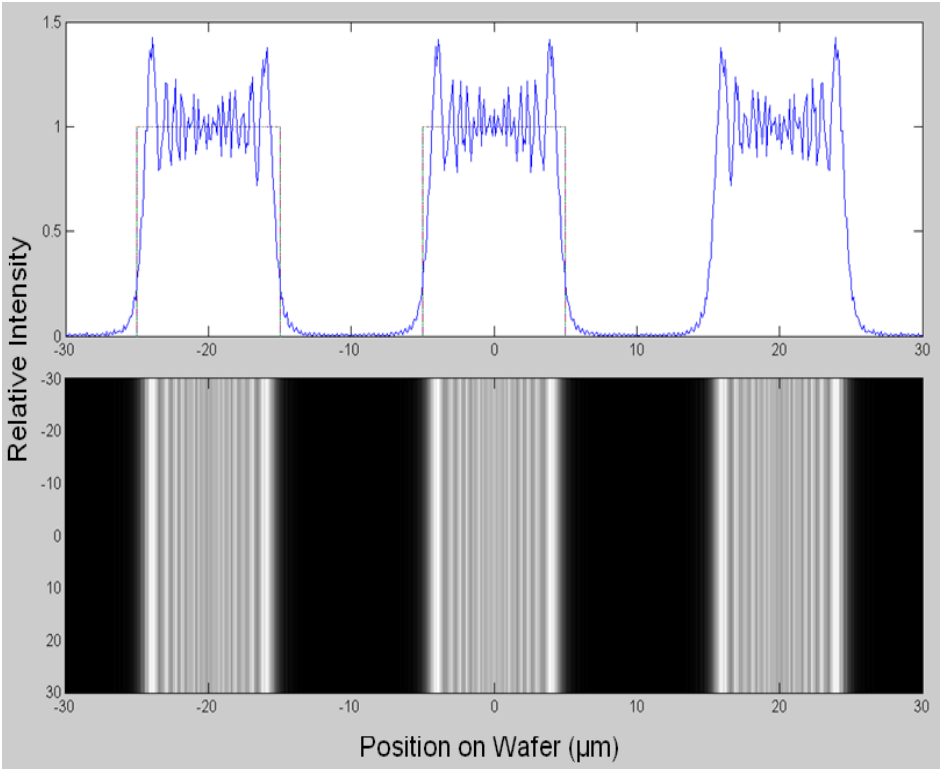

Figure 2.3. The simulation of light intensity distribution at the distance $d = 4\mu m$ through the photomask of 10 µm line and 10 µm space. The wavelength of the plane wave is 365 nm.

The light intensity distribution of the UV beam after propagating a distance of 4 μm through a photomask (with 10 μm line and space grating) is shown in Fig. 2.3, by using Eq. (2.1). Since the propagation distance is short enough, the diffraction does not spread the light widely, and the light intensity is still well confined inside the desired areas. However, as the light propagates further from the photomask, the diffraction of light becomes apparent. Figure 2.4(a) illustrates how light is "bent" and diverted by an equal line and space grating on the mask due to diffraction. As another example, the light intensity distribution of the UV beam passing through a photomask (with 10 μm line and space grating) on the photoresist is shown in Fig. 2.4(b), by using Eq. (2.1), given an 80 μm air gap between the photomask and the resist. The light intensity of the UV beam on the resist outside the desired exposure area (as shown in Fig. 2.4(b), especially where the intensity is above the red line) is comparable to the threshold sensitivity of the resist, which will result in the resist residue between the desired patterns on the substrate and make it difficult to form structures with 10 μm resolvable feature size under such exposure conditions. While the air gap is reduced, the maximum light intensity diffracted outside the open area of the mask decreases and will eventually become negligible compared to the sensitivity threshold of the resist. An example of this case for the fabrication with a 30 μm air gap is shown in Fig. 2.4(c). It is clear from Fig. 2.4(c) that 10 μm feature size structures can be achieved under this exposing condition with 30 μm air gap using the optimized developing process.

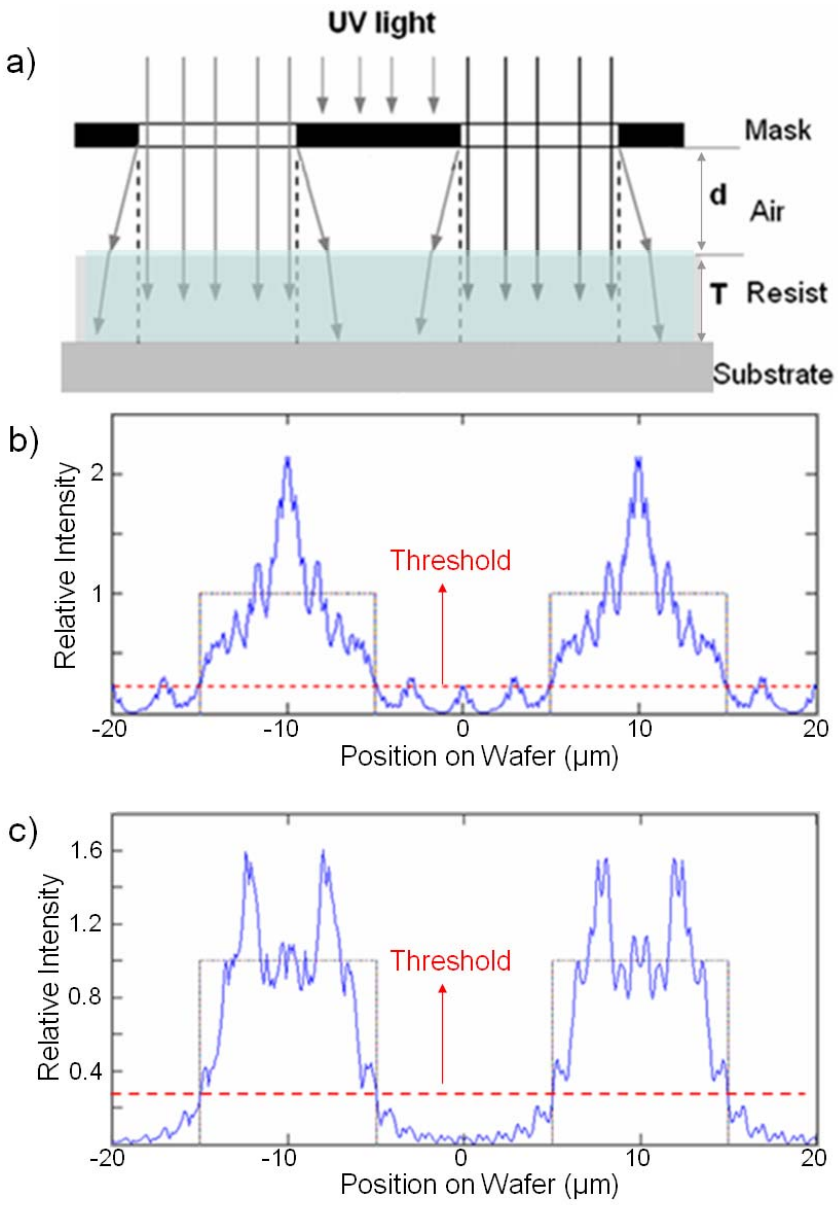

Figure 2.4. a) Schematic of UV light propagation through a photomask containing a grating with equal lines (white rectangles) and spaces (black rectangles); And simulation of light intensity distribution inside the photoresist at the wavelength of 365 nm under the photomask of 10 μm line and 10 μm space, with b) the air gap of 80 μm, and c) the air gap of 30 μm. The dotted lines in b) and c) show the sensitivity threshold of the photoresist. For light intensity above the threshold, the change in the material properties occurs.

2.3. Experimental Study and Discussion on Gap Effect

To optimize the exposing and development processes, it is necessary to study the sensitivity of the photoresist experimentally. A layer of 7.5 μm thick photoresist NT-90

was spin-coated on a bare silicon substrate. The sample was covered by a moving opaque mask at a constant speed under UV exposure, so that the exposure dose varies linearly along the sample. Then, the whole sample experiences the same post-process (baking and developing). The residual photoresist thickness was measured by a contact surface profiler (DekTek 303). Figure 2.5 shows the relationship between the residual photoresist NT-90 thickness and the exposure dose. From Fig. 2.5, we can define two important parameters representing the threshold properties of this negative photoresist: D_{min} =62 mJ/cm^2 (the minimum exposure dose required to produce insolubilized residue) and D_{ful} =200 mJ/cm^2 (the minimum exposure dose for the full sensitization of the resist). In the following experiments, a 10% over-exposing dose over D_{ful} (i.e., 0.1*D_{ful} =20 mJ/cm^2) is applied to ensure the full sensitization of the whole layer of the photoresist.

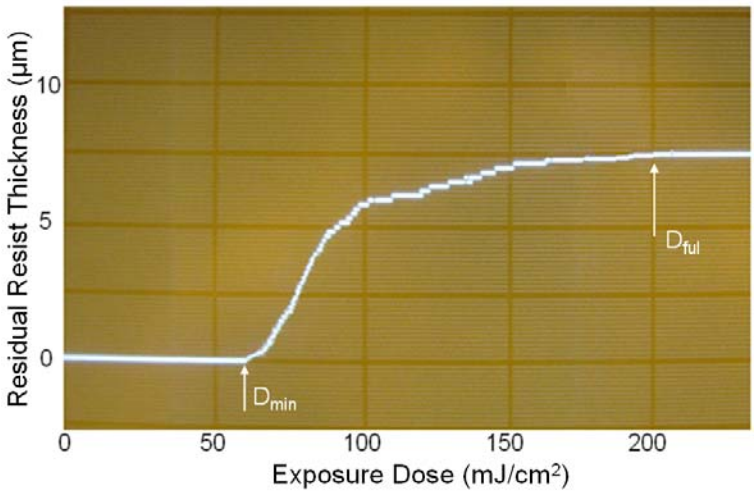

Figure 2.5. Experiment results for the residual photoresist thickness dependence on the light exposure dose. The initial photoresist NT-90 thickness is 7.5 μm, and the light intensity is 24 mW/cm^2 at the wavelength of 365 nm.

Well-controlled process conditions are necessary since the minimum achievable feature size is very sensitive to the process conditions, such as exposure dose, baking (temperature and time), development (solution concentrations, temperature and time), etc.

Our experimental steps are as follows: 1) design a photomask with three groups of testing comb structures. Each pattern group contains comb structures with different lines and spaces from 2 μm to 84 μm, and these three groups are placed in parallel at equal distance on the chromium mask, 2) spin-coat a layer of 8 μm thick resist NT-90 on a silicon substrate, 3) place the photomask on the photoresist with a small tilting angle of 0.3 degree, so that these test structures at different locations on the photomask will have different air gaps to the photoresist, as shown in Fig. 2.6, 4) full-field UV exposure at the dose of 220 mJ/cm^2, 5) bake and develop, and 6) measure the resolvable minimum feature sizes by studying the defined features with optical microscopy and scanning electron microscopy (SEM). All the patterns go through the same exposure and development simultaneously. Figure 2.6 shows the schematic of the mask design and exposure experimental setup. The gap distances between the mask and the photoresist are 30 μm (d1), 60 μm (d2), and 90 μm (d3) for the three different groups, respectively. A high pressure mercury UV light source with collimated i-line output is employed in the experiment. The minimum lines and spaces achieved in our experiments are 7, 10 and 12 μm for gaps at 30, 60, and 90 μm respectively. Figure 2.7 shows the microscope image of a comb structure with lines and spaces of 7 μm fabricated on an 8 μm thick photoresist at the air gap of 30 μm. It is also found that the contrast of line edge deteriorates as the gap distance increases. When the photomask is laid down onto the photoresist in the contact mode, i.e., the air gap is almost zero, 5 μm line and space is achieved. Feature sizes less than 6 μm are difficult to recognize under an optical microscope, thus, SEM pictures are used for evaluation of such structures.

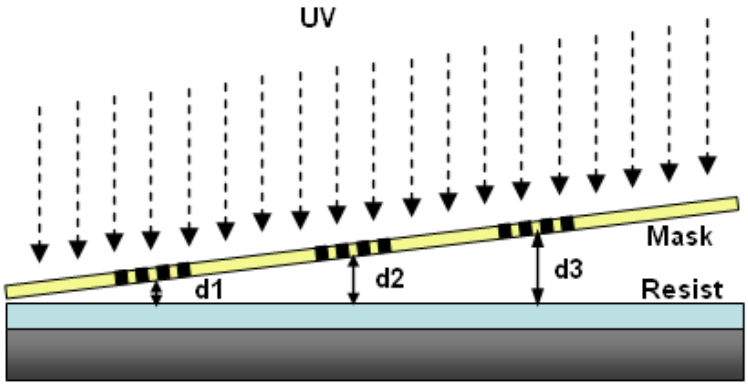

Figure 2.6. Schematic of mask design and experimental setup for UV exposure at different air gaps.

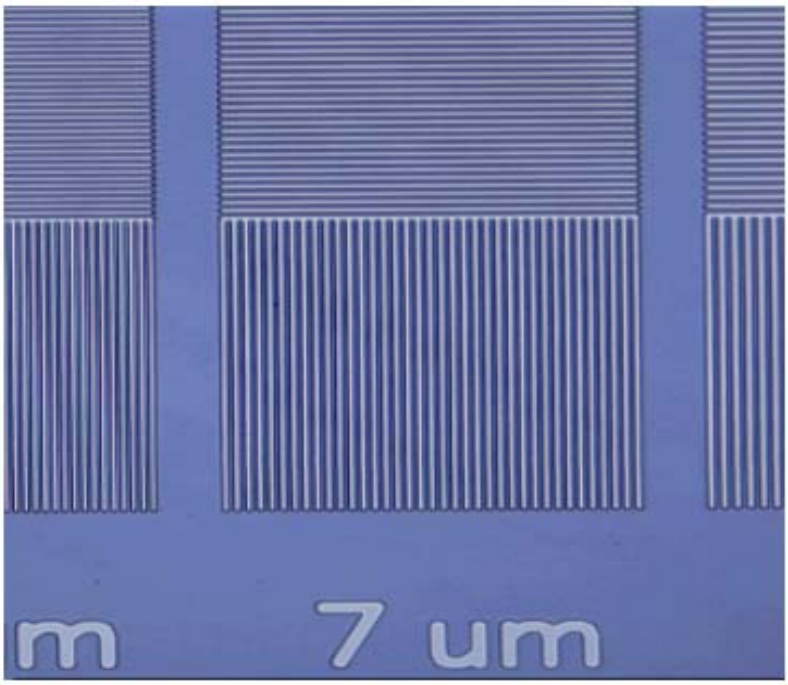

Figure 2.7. Microscopic picture of fabricated comb structures with equal line width and space. 7 μm lines and spaces are resolved on an 8 μm thick photoresist at a gap of 30 μm by using i-line UV lithography.

The Fresnel's diffraction theory predicts a square root relationship between the minimum definable feature size L_{min} of a periodic structure and the product of the

wavelength λ and the air gap d between mask and wafer [60]. Considering the thickness of the photoresist, the minimum achievable L_{min} can be expressed as [61],

$$2L_{\min} = k\sqrt{\lambda(d + T/2)} \tag{2.2}$$

where T is the thickness of the photoresist. The proportionality factor k is usually determined experimentally. If small tolerances of exposure and development in the photoresist are allowed, k is given a value of 3 [62]. Based on this assumption, the following expression of L_{min} is now widely used.

$$2L_{\min} = 3\sqrt{\lambda(d + T/2)} \tag{2.3}$$

Given the optimized fabrication recipe for NT-90 photoresist and the facilities and environment in our substrate clean room, the factor k determined from our experimental data is 4. Thus, in our experiment, L_{min} is expressed as,

$$2L_{\min} = 4\sqrt{\lambda(d + T/2)} \tag{2.4}$$

The difference of proportionality factor k in Eq. (2.3) and Eq. (2.4) is the overall consequence of the entire fabrication factors, such as, the difference in sensitivity of the chosen photoresist, properties of the collimated UV light, and the mechanical stability of the exposure system. Figure 2.8 shows the curves of experimental minimum transferrable feature sizes and corresponding calculated value, according to Eq. (2.3) and Eq. (2.4) at different air gaps. The experimental data agree well with Eq. (2.4), except at the zero air gap. The big size difference at the contact mode can be explained by the process effect. In general, the aspect ratio of features that can be developed for most resists is 1:1. In this experiment, the thickness of the photoresist is 8 μm. If 2 μm line and space needs to be resolved, the aspect ratio will be 4:1. It becomes harder to remove the thick un-exposed

polymer with high aspect ratio in the development process. The finest line and space that we obtained is 5 μm (with the aspect ratio of 1.6:1).

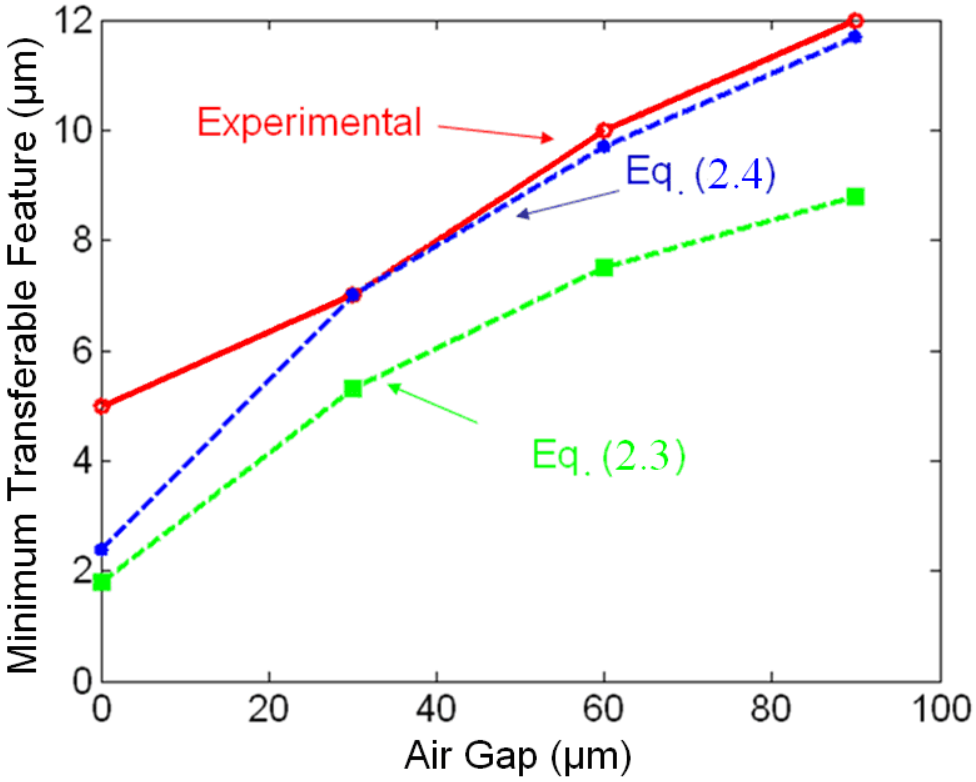

Figure 2.8. Calculated (dash lines) and fabricated minimum (solid) line and space L_{min} at various air gaps between the photomask and the photoresist on an 8 μm thick NT-90 photoresist under UV exposure.

2.4. Metallization Techniques for Fine Copper Line Formation

Photoresists, dry film or liquid, are used for image transfer from photomasks to substrates [63]. A dry film is supplied as a three-layer sandwich with a polyester cover layer and a polyethylene separator sheet. This stack provides a reliable imaging system with a suitable resolution and a simple process for high volume production. The dry film has been the dominant process for the image formation in the packaging and PCB industry. In general, the minimum line and space that can be formed is about 1.2~1.5

times the thickness of the resist in a manufacturing environment and down to 0.7~1.0 in a laboratory. The thinnest dry film photoresist currently provided at production volume is 15 μm (i.e., 0.6 mil). Therefore, the finest circuit traces that can be fabricated by using dry film photoresist is about 18~22 μm in production and 10~15 μm in the laboratory. Liquid photo-resist has higher imaging resolution ability and can be formed in any thickness. As the advanced package moves towards higher pin counters, finer pitch, and thinner profile, liquid photoresist technology should be used. As the stripes of photoresist get finer, the adhesion becomes weaker, and photoresist adhesion promoter is needed.

In the metallization process, a layer of metal is deposited on the substrate surface to provide electrical contact to the devices. Two types of processes typically used by the industry for metallization are subtractive process and additive process [64]. The subtractive metallization process involves the build-up of a blanket layer of metal on the substrate, and then uses a photoresist and chemical solution to etch copper away through open areas of photoresist to form the circuitry. Figure 2.9 shows copper traces of 20 μm feature size by etching 12 μm clad copper foil with subtractive process on a Bismaleimide-Triazine (BT) laminate board. Note that the etched copper traces have sharp vertical walls and equal line and space widths. Further reduction of the copper line width is limited by the roughness of the bottom surface of the copper foil. Additive process utilizes electrolytic plating to fill copper in the patterned photoresist (pattern plating). Electrolytic plating requires a thin conductive layer as electrode, called the seed layer. There are two ways to provide the electrode: (I) a very thin copper foil, e.g., 3 μm, using resin coated copper (RCC) technology [65], or (II) electroless copper plating [66] (0.5 μm thick) on resin. The additive processes I and II actually are semi-additive

processes (SAP) [67]. The SAP consists of dielectric film surface treatment [66], a thin layer of conductive layer (seed layer) formation, photoresist application, UV exposure, development, and electrolytic plating. The surface treatment usually uses permanganate etching to create topography of the resin, especially for epoxy. For some advanced dielectrics, plasma is used to micro-roughening of the resin or a combination of the two methods. The created topography and micro-roughening of resin greatly increases the surface area that results in the enhancement of adhesion of plated copper on the resin. The thin layer of conductive layer is typically formed by electroless copper plating in the PCB and packaging substrate fabrication. After copper is plated to a designed thickness, the photoresist is stripped away and the seed layer is etched off. This technology is currently well used in high density packaging substrates and the PCB industry. The method of SAP-II has the advantages of achieving fine feature copper lines and high traces definition since only a half micron copper seed layer needs to be removed. The minimum line width achieved depends on the minimum size of the photoresist structures and the quality of process controls.

We have produced 10 μm copper lines and spaces by using dry film photoresist in the Next Generation Substrate Laboratory of the Packaging Research Center (PRC) at Georgia Tech. Figure 2.10 shows 4 pairs of copper traces with lines and spaces of 10, 15, 20, and 25 μm on an ajinomoto build-up film-based (ABF-based) BT substrate by using a dry film DuPont photoresist (MAX5015) with the thickness. The developer of the DuPont photoresist is 0.8%-1.0% disodium carbonate. The copper traces with the thickness of 18 μm are plated using SAP II.

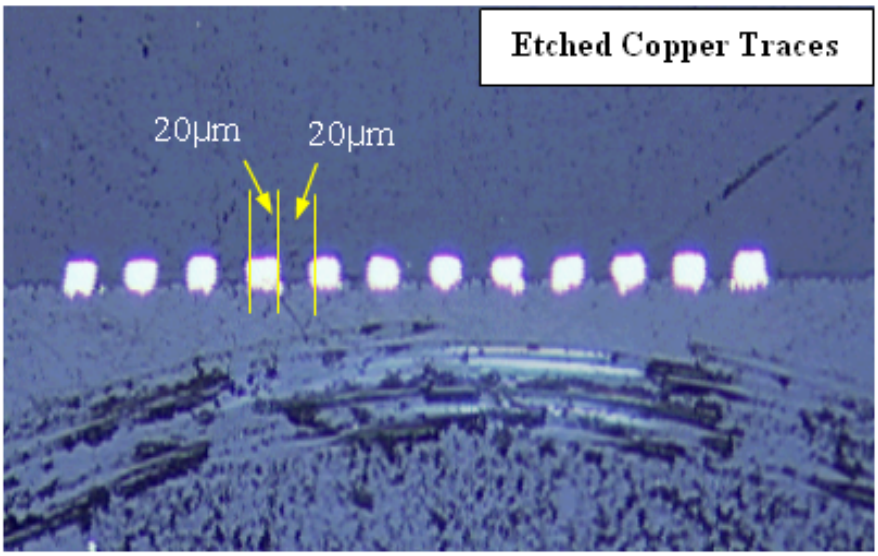

Figure 2.9. Microscopic picture of wet-etched copper traces of 20 μm line and space on a 12 μm thick copper foil on BT laminate. Note that the etched copper traces have vertical walls, and rough surface of the copper foil limits the fine line formation by etching.

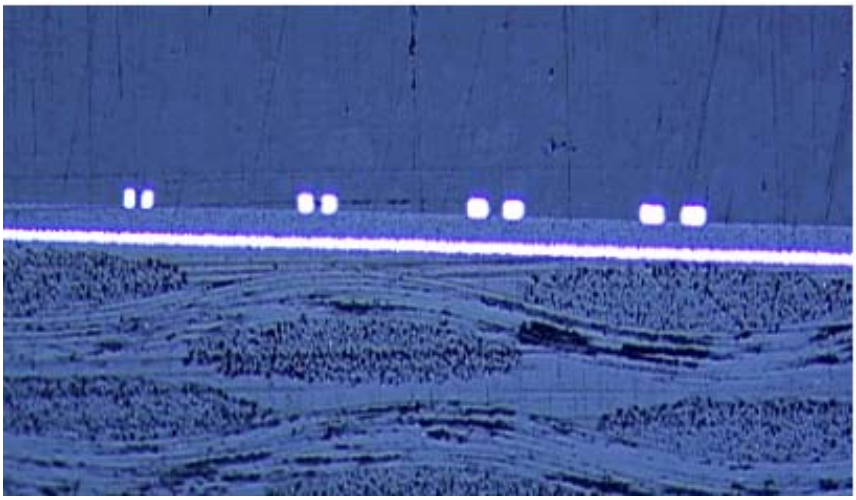

Figure 2.10. Microscopic picture of plated copper traces with line width and space width of 10/15/20/25 μm on an ABF/BT substrate by using a dry film photoresist provided by DuPont. The copper thickness is 18 μm.

Figure 2.11 shows the top view and the cross section of flip chip mounting pad structures and routing lines on an ABF/BT substrate by using the SAP II process. The pad diameter is 40 μm and the pitch is 100 μm. Also, there are three metal lines routed in the

pitch. The space between the adjacent pads is 60 μm, so the minimum routing line width is less than 8.6 μm. The routing capability of 4 rows per pitch and 10,000 pads/cm^2 can be achieved. Copper thickness measured is 8.5 μm. The aspect ratio is 1:1. With process optimization, it is possible to form line and space widths down to 5-6 μm with the SAP II process. Figure 2.12 shows a SEM picture of copper lines with 7 μm line widths and 6 μm wide spaces. Again, the dielectric film is ABF, and the substrate is glass fiber reinforcement BT laminate.

In order to improve SAP plated copper adhesion to the dielectric surface and enhance catalyst adsorption, micro-roughening the dielectric is required. The complex dielectric surface structure under the copper lines is shown in the magnified picture in Figure 2.12. It consists of particles embedded in the resin. The particles are fillers added to the resin for reducing the coefficient of thermal expansion (CTE). The micro-roughness is formed due to the permanganate etching during the chemical besmear process. The micro-roughness interlocks the plated copper to make the bond strength as high as more than 1kg/cm. However, the surface topography and roughness creates a big challenge to fine line and space formation. During development, the photoresist may lift off the particles and leave residues in the recessed areas. It becomes difficult to form the circuitry traces when the filler size becomes comparable to the line and space size. Another factor that will affect the fine line lithography is an undulating surface. The undulating surface is often caused by the buried copper traces. The unexposed photoresist is easily washed off on the convex areas and is difficult to wash off from the concave areas on the undulating surface during development. A smooth and flat surface is necessary for ultra fine line lithography.

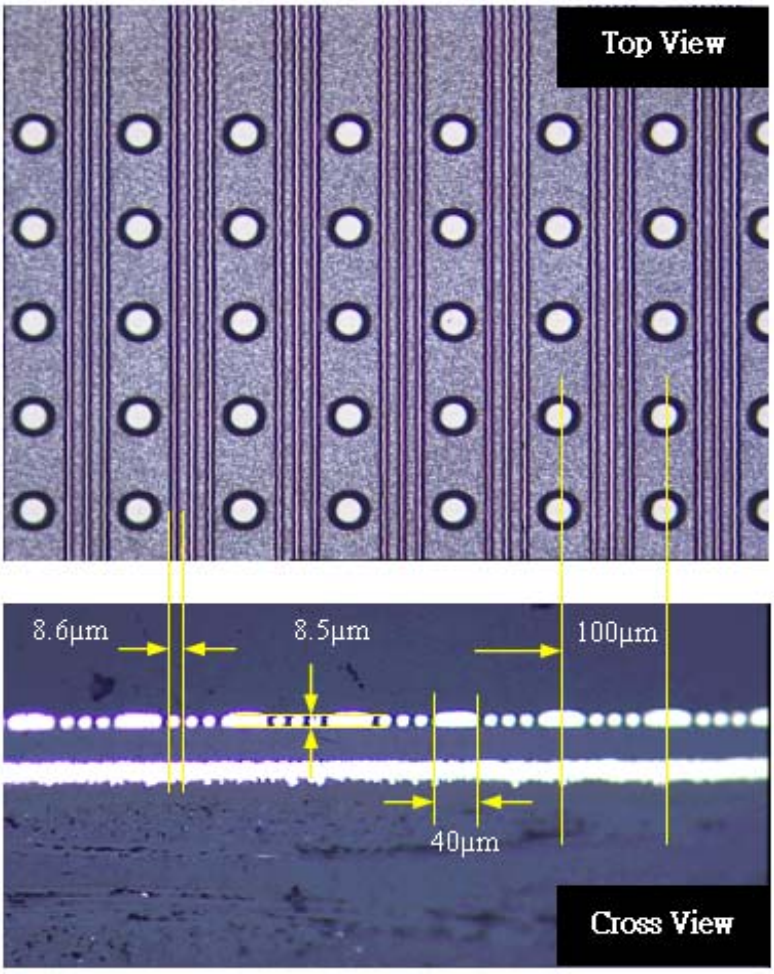

Figure 2.11. Microscopic picture of the ultra-fine line routing on ABF build-up for flip chip with 100 µm pitch. Bonding pad size is 40 µm in diameter. Line and space is 8.6 µm; 3 lines are routed within a pitch; and copper thickness is 8.5 µm. Routing capability is 4 rows per pitch and 10,000 Pads/cm^2.

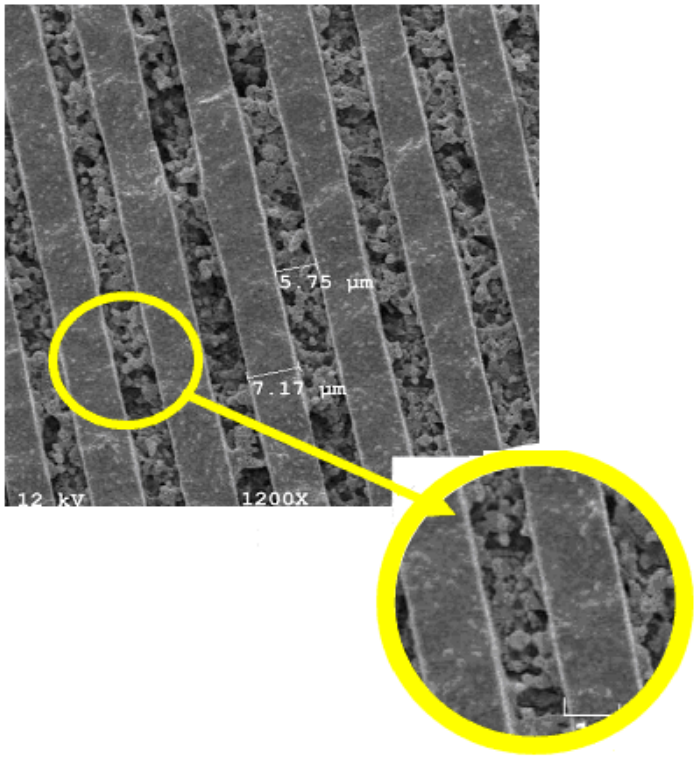

Figure 2.12. SEM micrograph of copper traces with 7 µm lines and 6 µm spaces on an ABF/BT substrate. The lower right shows a close look of the copper traces and the dielectric surface.

2.5. Chapter Summary

Photolithography is a dominant process used in microfabrication on packaging board substrates. The theoretic analysis based on Fresnel diffraction indicates that the key factors that hinder the finer feature size formation through proximity photolithography is the air gap between the photoresist and the mask. To experimentally study the dependence of the minimum transferable feature size on the air gap, we designed a simple and unique experiment that guarantees the same resist thickness and the same optimized fabrication process for the group samples under different air gaps. The experimental data confirm the validity of the theoretic analysis. We also showed that an expression for the minimum transferable feature size is obtained from the experiments. Furthermore, in this chapter, we explored the metallization techniques for fine copper line

formation, and demonstrated 8.5 μm copper line routing substrates by using semi-additive metallization process in the PRC at Georgia Tech. We believe that this investigation on the Sub-10 μm copper routing circuitry technique is important and fundamental for the future flip chip substrate packaging [68].

CHAPTER 3

CAPPED OPTICAL POLYMERIC WAVEGUIDES

In this chapter, we present here a new type of polymer waveguides (i.e., capped waveguide) fabricated using contact photolithography with considerable performance improvement over the conventional waveguides. We also show that by simultaneous patterning of the core and the top cladding in capped waveguides, we can considerably reduce the effect of fabrication defects and reduce the propagation lose by at least 20% compared to conventional waveguides [69].

3.1. Introductions to Waveguide Fabrication Techniques

The widespread use of the advanced package technologies, such as Ball Grad Array (BGA), Chip Scale Packaging (CSP), flip chip, and wafer-level-packaging, has promoted the development of high density substrates and printed circuit boards [1]. To realize high speed in these substrates, it is essential to develop processes for the integration of high speed optics. One of the most important components for this integration is the optical polymer waveguide, and there have been extensive efforts on the development of fabrication techniques for waveguides and waveguide-based devices. As an example, integration of optical waveguides and polymer passive devices on high density substrate/PCB is a major area of research in optoelectronics. During the later 1980's, early attempts were focused on the integration of polymer waveguides on printed circuit boards for interconnection use [6]. Several technologies have been developed such as photolithography, reactive ion etch (RIE), laser ablation, molding/embossing, lamination, and monomers diffusion, etc., to define optical waveguides [7-10]. Among

these technologies, photolithography has excellent ability to define smooth and high definition waveguides. However, there are process-related challenges that limit the manufacturability of such waveguide. For example, dust particles, contaminations, scratches, mechanical damages, chemical swells, corrosions, and over-etching degrade the performance of a high quality waveguide and other polymer-based devices. In this chapter, we introduce a novel cap-clad approach for creating high quality waveguides by minimizing the process-induced defects and improving waveguide definition that result in the improvement of the manufacturability of such waveguides for the integrated optoelectronics.

3.2. Optical Waveguide Materials

In this study, a pair of optical polymers, LighLink^{TM}, provided by Rohm & Haas Electronic Materials was used. The LightLink^{TM} is a negative acting photoimaging polymeric system which is based on an inorganic-organic hybrid platform [70]. It consists of two parts with refractive indices of 1.5196 and 1.4908. The higher index material is used for the waveguide core and the lower one is used for the cladding. Since the materials are in monomer liquid form, they are applied either by spin coating, slot coating, or meniscus coating on a substrate which can be silicon, glass, ceramic, organic package substrate, or printed circuit board. Both the core and the cladding are photoimaging with high resolution. The photolithography process allows us to define a few micron to a few hundred micron structures with high degree of accuracy so that high performance single mode and multimode waveguides and polymer related passive devices can be made for the integrated optoelectronics. Figure 3.1 shows an atomic force microscopy (AFM) picture of a 4 micron wide waveguide on an 8 micron pitch multi-

channel waveguide with a few nanometer smooth surfaces. This high density polymeric channel waveguides were formed by using the low cost printed circuit board (PCB) facility and process in a class-1000 substrate laboratory at the Packaging Research Center (PRC) at Georgia Institute of Technology.

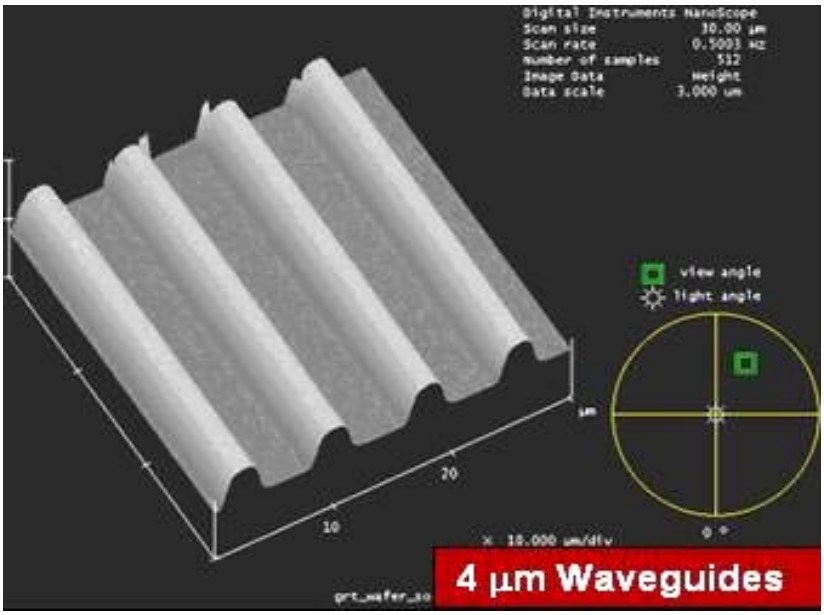

Figure 3.1. An AFM picture showing 4 µm multi-channel waveguides made by PCB facilities with nano-smooth surfaces for single-mode applications.

Propagation loss is one of the most important properties of optical waveguides. Unlike the optical glass fibers, optical polymer waveguides have much higher propagation losses. For example, the loss of a typical optical fiber at 1550 nm is about 0.1dB/km, while that of a typical un-fluorinated polymer waveguide is 0.2~0.3 dB/cm at 1310 nm and 0.5~1.5 dB/cm at 1550 nm. This loss can be as low as 0.02~0.1 dB/cm at 850 nm, but it is quite sensitive to the process [70]. Thus, the fabrication of low-loss waveguides is crucial for using polymer waveguides in the practical applications. The propagation loss of a typical waveguide can be divided into intrinsic loss and extrinsic loss. The intrinsic loss is caused by material absorption and compositional

inhomogeneity, while the extrinsic loss is mostly caused by the fabrication process. Practically, scattering from defects such as contaminations, bubbles, dimples, bumps, cracks, surface roughness, and also poor definition are responsible for most of the waveguide loss. Optical waveguides with good performance must have clear, defect-free and smooth surfaces. An ultra clean environment is required for the large area board level optoelectronics integration, which results in high fabrication cost. In this section, we show a reliable procedure for almost complete elimination of the fabrication-related defects by using capped waveguides without requiring ultra clean fabrication environment to reduce the fabrication cost considerably.

3.3. Manufacture Challenges and Environment Requirements

A typical optical polymer waveguide is a triple-layer structure: bottom cladding, core, and top cladding. The waveguide is formed layer by layer from the bottom cladding to the top cladding in a sequential process. The process includes coating, soft-baking, and curing. In addition, the core is patterned after soft-baking. For board-level integration, soft-baking usually takes around 10 minutes at low temperatures (for example, 90 ^{o}C) while curing takes about 1 hour to a few hours at a higher temperature (for example, 150 ^{o}C). In the formation of the core, a contact mode UV exposure is used followed by post-baking and development in a chemical solution, and then curing is performed in a convectional oven. In the long-period processes, the top surface of the core layer goes through mechanic contact, chemical solution, and convectional oven resulting in defects and damages (including contamination, dust, scratch, dimple, and bubble) and thus a rough waveguide surface. In addition, very low electrical conductivity of the polymers results in the build up of static charges on the core surface, which can attract dust

particles even in very clean environments. The light scattering from such dust particles can be considerable if the particle size is comparable to the optical wavelength (typically in the range of 850 – 1550 nm for most practical applications).

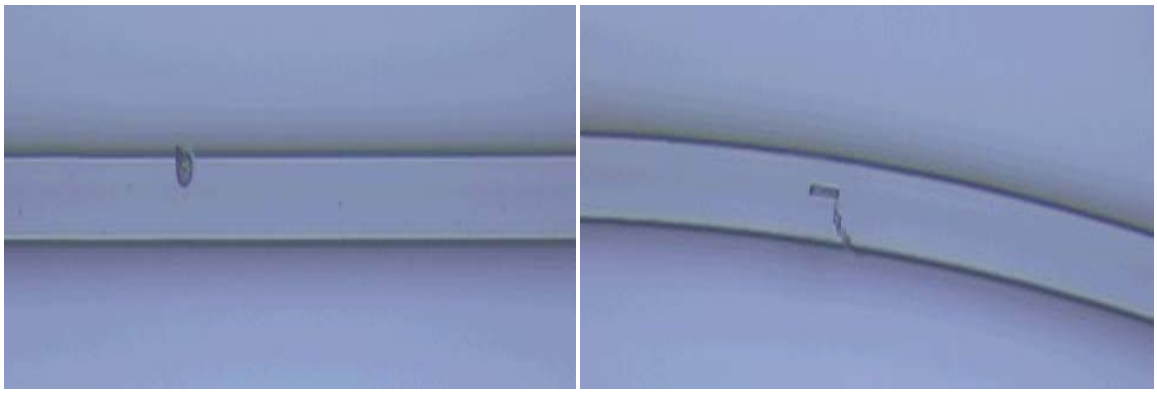

(a) (b)

Figure 3.2. Typical contaminations on top of a 50×50 μm^2 waveguide core: a) a particle on top of a waveguide formed in a convectional oven, and b) debris re-deposited on top of a waveguide produced from the development.

Figure 3.2(a) shows a particle with 10 μm diameter attached to the top of a well defined waveguide during the curing process in a convectional oven. Figure 3.2(b) shows debris of the polymer residue with size of 5×30 μm^2 attached to the waveguide core during the process of chemical development. Once these particles attach to the waveguide, they can not be removed. Thus, usually for low-loss waveguide processing, ultra-clean fabrication environment, special storage, special handling techniques, and careful precautions, are required.

Another important requirement for fabricating practical optical devices like waveguides is the accuracy of the fabricated structures. This requires very good resolution in forming feature sizes using photolithography. The resolution (or the

minimum achievable feature size, L_{min}) in photolithography with a UV lamp at wavelength λ is represented by Eq. (2.4)

$$2L_{\min} = 4\sqrt{\lambda(d + T/2)}$$

with d being the separation or gap between the lithography mask and the polymer film and h being the thickness of the polymer film. Eq. (2.4) clearly shows that in order to achieve very fine resolutions, the mask needs to be in contact with the polymer.

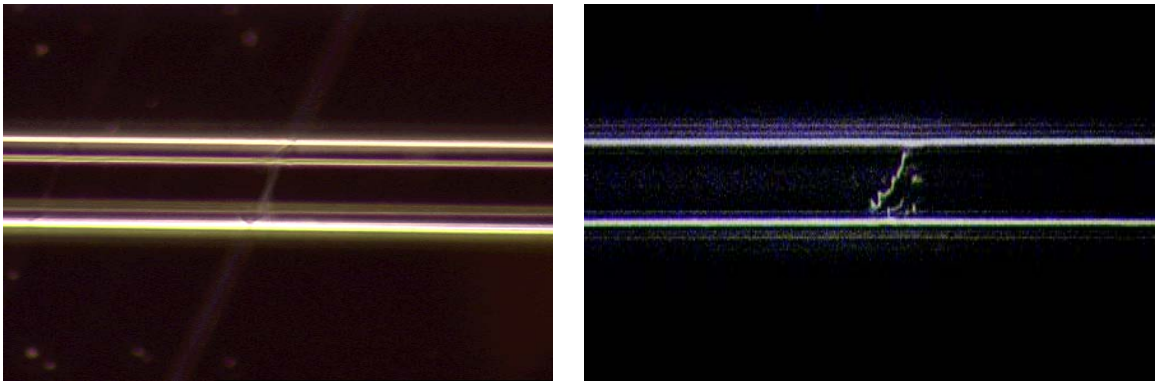

(a) (b)

Figure 3.3. Microscope pictures (dark field) of Surface damages on a 50×50 μm^2 waveguide core: a) a scratch caused by handling, and b) damage caused by contacting with the photomask.

The gap or the separation of the mask and the polymer layer (i.e., d in Eq. (2.4)) results in poor resolution and poor definition due to the wave diffraction effect. Thus, contact mode is commonly used for high-definition waveguide formation. However, the physical contact between the mask and the polymer can potentially cause mechanical damages to the core of the waveguide. For example, Figure 3.3(a) shows a scratch on the waveguide happened because of the handling during lithography, and Figure 3.3(b) shows a typical surface damage caused by mask contact during waveguide formation.

Dark field photography was used in Figures 3.3(a) and 3.3(b) to clearly show the defects. All these defects cause the increasing of scattering loss. So, defect-free or defect-

less smooth surface and high definition are required for fabricating low-loss waveguides and other passive devices. In the next section, we describe a new approach to form such low-loss waveguides, without requiring ultra-clean fabrication environment.

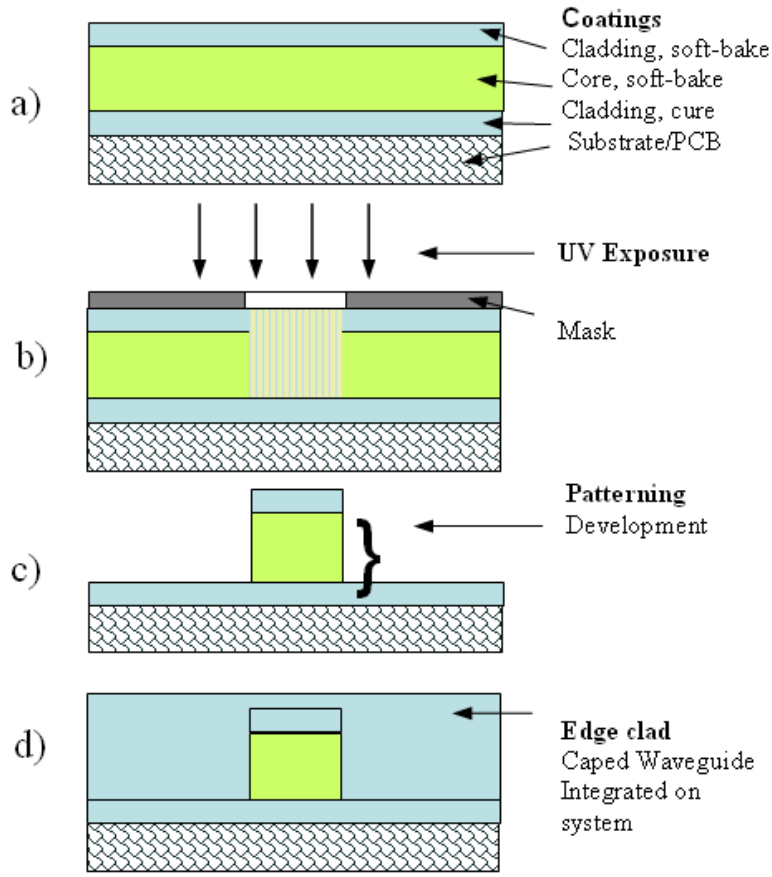

Figure 3.4. Capped waveguide fabrication process flow: a) coat and cure the bottom cladding layer, coat and soft-bake the core layer, and then coat and soft-bake the top cladding layer, b) expose two top layers to an appropriate dose of UV radiation through a mask, c) develop the pattern using a wet process, and d) finally, apply a layer of polymer to clad the sides of the core as well as the top of the core.

3.4. Fabrication of Capped Waveguides

The key step in the fabrication of capped waveguides developed in this research is the simultaneous photolithographic formation of the core and the top cladding layer of the waveguide. This avoids the formation of defects or attachment of dust particles to the

core surface, which is the most sensitive place in the waveguide to defects. The sequential steps in the fabrication of a capped waveguide (also demonstrated graphically in Figure 3.4) are as follows: 1) Coat the bottom cladding layer on the substrate or the printed circuit board (PCB) and cure it, 2) coat the core layer and soft-bake it, 3) coat the cladding layer on top of the core layer and soft-bake it, 4) expose two layers to an appropriate dose of UV radiation through a mask, 5) develop the pattern using a wet process. The developer used for patterning of LightLink^{TM} is an aqueous solution (2% Alkaline). Developments are carried out in room temperature for about 3 minutes. Unexposed areas are dissolved and washed away and the exposed areas remain. The cladding layer on top of the core acts as both cap and cladding. We call it cap-clad, and we call the waveguide the capped waveguide. In this structure the surface of the core is protected by the cap-clad during the later processes. 6) Finally, the capped waveguide is completed by applying a layer of polymer to clad the sides of the core as well as the top of the core.

Since the core and the cap-clad are patterned simultaneously, the problem of the formation of defects on top of the core layer in conventional waveguides does not exist in the capped waveguides. Instead, almost all existing defects occur on the top of the cap-clad layer and have much less effect on light propagation in the waveguide due to lower field intensity in the cladding (the thickness of the cap-clad is much larger than the wavelength of the light guided in the core layer). Furthermore, the side walls of the capped waveguide have similar quality to those of the conventional waveguide due to the similarity of the development process. In both waveguides, the probability of defect formation on the side walls is much less than that on the top surface. There is also no

contact damage on side walls, as the mask will only contact the top surface. Similarity, the probability of the attachment of dust particle to the side walls is far less than that for the top surfaces. As a result, capped waveguides can have considerably lower propagation loss than the conventional waveguides fabricated in the same environment.

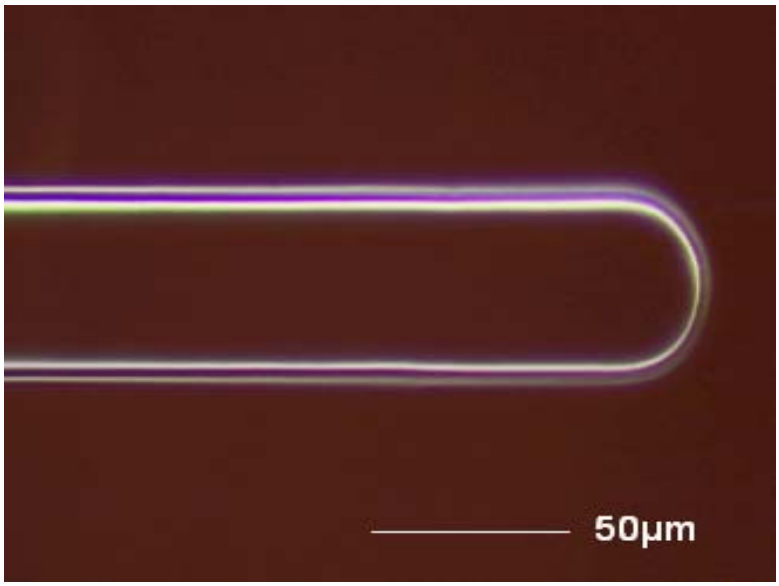

(a)

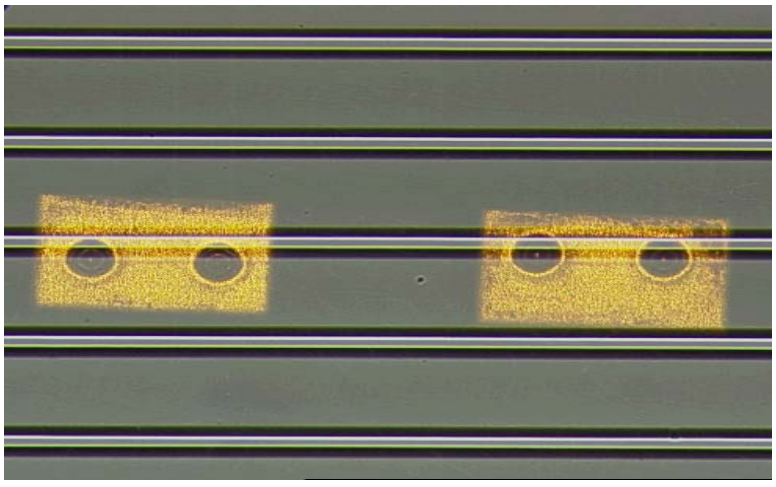

(b)

Figure 3.5. Microscope images of a) a polymeric waveguide with a 50×50 μm^2 core, b) waveguide channels on high definition circuit board (above micro-vias), c) light guided inside multi-channel waveguide integrated on a HDI board (end surface), d) the enlarged end face view of the light inside a multimode polymer waveguide on PCB substrate, and e) waveguide channels above high definition copper lines.

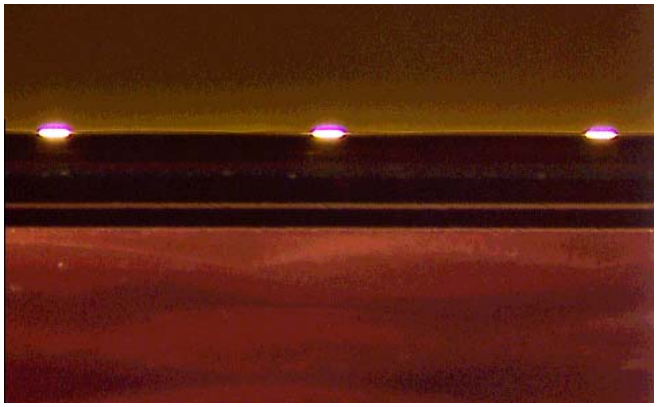

(c)

(d)

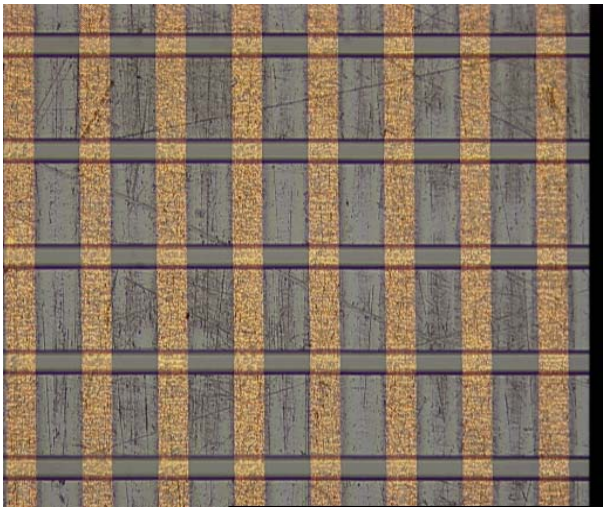

(e)

Figure 3.5. continued

Figure 3.5 shows the microscopic images of defect-free optical polymer waveguides on PCB substrates, by using the capped waveguide technology. Another advantage of the capped waveguide technology is the possibility of forming high definition passive devices such as Y-splitter, H-tree, and multimode interference (MMI) that require good definition and accurate structures or require square (or rectangular) shapes with sharp edges. Using conventional waveguides, it is difficult to form such devices accurately, as the top surface of the core tend to have a round shape instead of a square or a rectangle due to overetching of the sharp edges in wet etching processes. However, this problem can occur only for the cladding surface in a capped waveguide, as the core is buried under the cladding during the etching process. Figure 3.6 shows the microscope image of a fabricated capped waveguide with a 50×50 μm^2 core and a cap-clad with thickness of 10 μm. A microscopic light source is used to illuminate the waveguide, so the white light is guided inside the waveguide core. As seen in Fig. 3.6, the core has a well-defined square shape while minor rounding at the cladding surface is visible. Since most of the guided light energy is concentrated in the core of the waveguide, moving non-ideal features like round surface, from the core to the cladding results in improved performance of the optical devices fabricated using capped waveguide technology.

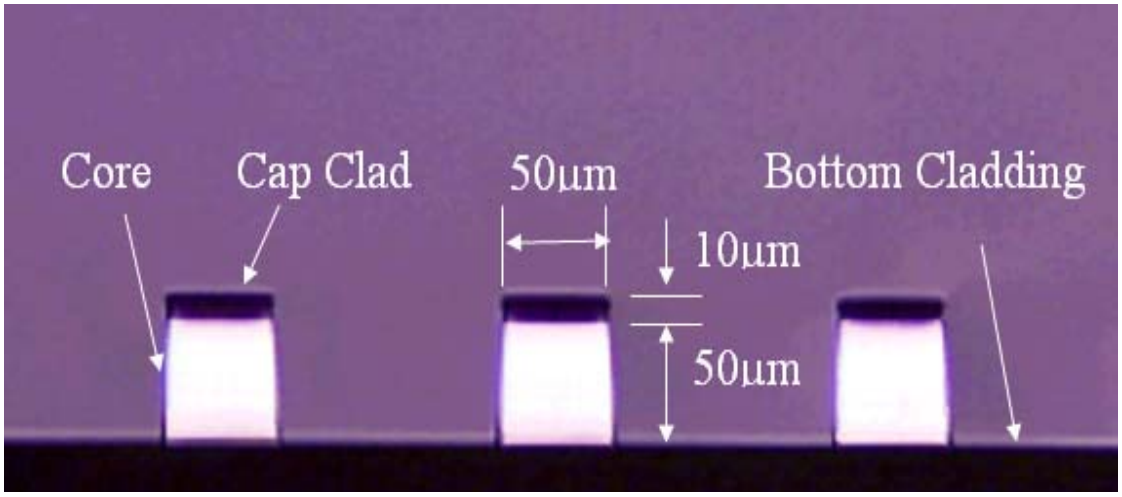

Figure 3.6. Microscope image of a capped polymeric waveguide with a 50×50 μm^2 core and a 10 μm cap-clad.

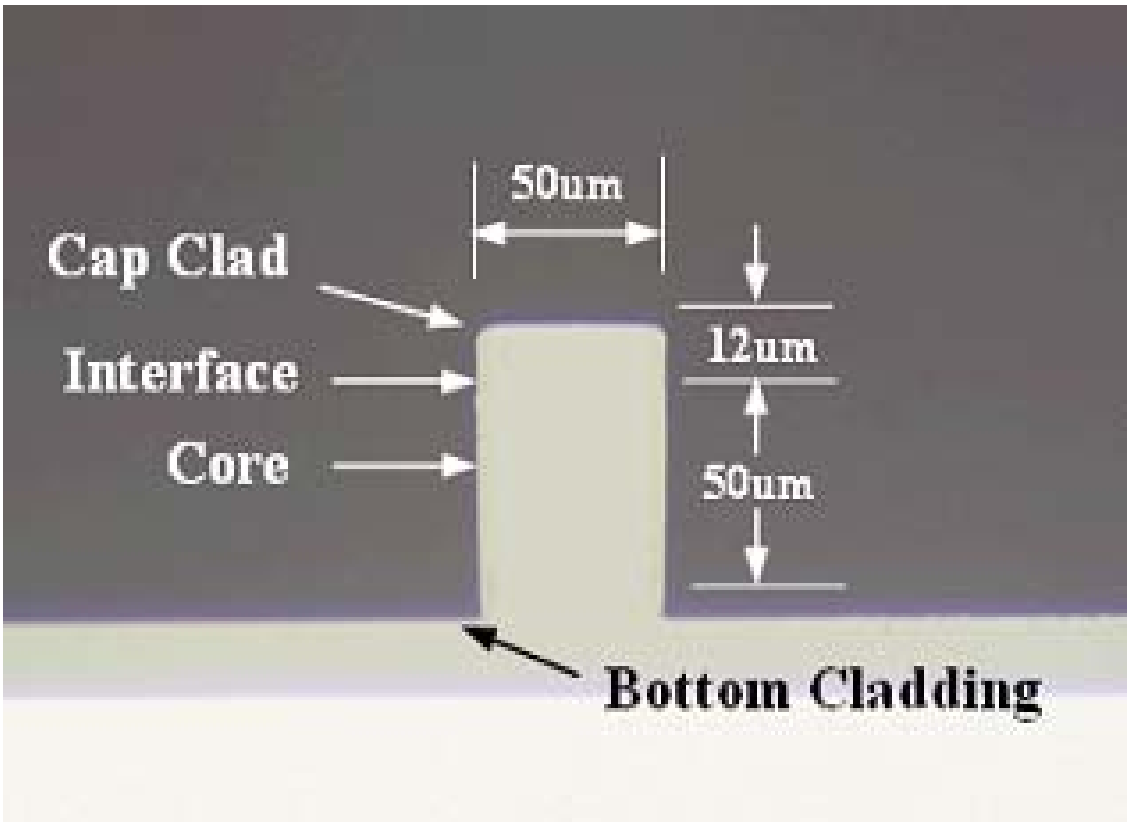

Figure 3.7. Microscope image of a capped polymeric waveguide with a 50×50 μm^2 core and a 12 μm top cap-clad and a 10 μm bottom cap-clad.

With the similar fabrication process, the waveguides with both top and bottom caps can also be integrated on PCB substrate, as shown in Fig. 3.7. The sandwiched waveguide core layer will thus be protected by the top and bottom caps from the defects.

3.5. Characterization of Propagation Loss in Capped Waveguides

Several techniques such as cutback method [11], sliding prism technique [12, 13], multiple reflections method [14], and photographic approach [15-17], etc., have been used for loss measurement in optical waveguides. In this section, we use a non-destructive technique based on the scattering loss measurement along the propagation direction of the waveguide under investigation [71, 72]. Light is coupled to the waveguide using free-space optics and the scattering pattern on top of the waveguide is monitored by a fast, high precision, and sensitive integrated CCD camera through a two-lens imaging system. Since the scattered intensity from the waveguide is a function of light intensity inside the waveguide, the variation of the scattered intensity with propagation length can be used for the measurement of the propagation loss coefficient. The details of this technique will be described in the next chapter.

Using this technique, we measure the loss coefficients of $\alpha_1 = 0.064\,dB/cm$ at $\lambda = 850nm$ and $\alpha_2 = 0.045\,dB/cm$ at $\lambda = 980nm$ for the capped waveguide. To compare the propagation loss of the capped waveguide with that of a conventional one, we fabricated the latter using a layer-by-layer process with a 50×50 μm^2 core and a 10 μm thick top cladding. And the measured propagation loss coefficient is $\alpha_3 = 0.085\,dB/cm$ for the conventional waveguides.

We repeated the experiments for several waveguides and found similar loss coefficients. Our results suggest that under the same fabrication environment, the capped

waveguide has at least 20% less propagation loss compared to the conventional waveguide. Furthermore, the effect of local defects in the capped waveguide is highly suppressed as they moved from the core (as in the conventional waveguide case) to the cladding. Thus, our results suggest that the capped waveguide technology proposed in this chapter is a much better candidate for the formation of passive optical devices using simple photolithography.

3.6. Chapter Summary

In this chapter, we presented a new type of waveguide (i.e., capped waveguide) with improved manufacturability for integrated optoelectronics. The key feature in these waveguides is the simultaneous fabrication of the core and the cap-clad layers. This results in almost no defect on the core surface. Instead, the defects appear only on the cap-clad surface, which has much less effect on the light propagation. Furthermore, the capped waveguide technology is suitable for the formation of high definition optical devices due to the possibility of defining sharp feature on the waveguide core. Finally, we showed that the capped waveguide has at least 20% less propagation loss compared to the conventional waveguide fabricated in the same environment. We conclude that the proposed capped waveguide will have a big impact on the improvement of manufacturability of optical waveguide and related passive devices for the optoelectronics integration on the system packages. This new capped waveguide technology can be extended to almost all other fabrication methods, such as RIE, molding/embossing, direct writing etc., for waveguides and waveguide-based devices which need low loss and high definition.

CHAPTER 4

PRECISION MEASUREMENTS OF WAVEGUIDE PROPAGATION PROPERTIES BY IMAGING OF SCATTERED LIGHT

In this Chapter, we presented here a reliable, non-destructive, and real time technique for characterization of propagation properties of planar optical waveguides based on accurate imaging the scattered light from the optical waveguide using a sensitive CCD camera with built-in integration functionality. This technique can be used for real-time investigation of the propagation properties (loss, mode profile, bending properties, etc.) as well as the fabrication quality of planar optical waveguides. With this technique, we have evaluated high definition polymer optical waveguides on PCB substrates with very low loss of 0.065 dB/cm at the wavelength of 850 nm, and the measurement accuracy is less than 0.01 dB/cm. We expect this technique with the given CCD camera to be suitable for measuring loss coefficients well below 0.1 dB/cm reliably [71, 72].

4.1. Introduction to the Waveguide Loss Measurement Techniques

In all planar optoelectronic systems, optical waveguides are crucial elements that facilitate signal rooting. The development of optical structures like waveguides on high density organic printed circuit boards has been a major focus of research on board-level interconnection. Low propagation loss, high optical quality, possibility of bending

without excessive loss, and manufacturability are among the requirements of polymer optical waveguides on PCB substrates for practical applications.

Besides fabrication requirements, reliable characterization tools are needed for the accurate and nondestructive measurement of important guiding properties like propagation loss in such waveguides. Several techniques, such as such as the cutback method [11], sliding prism technique [12, 13], multiple reflections method [14], and photographic approach [15-17], have been studied and used to measure the propagation loss of planar waveguides. The widely used cutback method requires the long waveguide sample, especially for low-loss (i.e., less than 0.1dB/cm) waveguides. Furthermore, the technique is destructive, time consuming, and hard to implement for waveguides integrated on PCB substrates, which are difficult to cleave. The sliding prism method, in which a prism is moving along the light propagation direction, is also widely employed, but it is hard to maintain the coupling efficiency constant, especially for the polymer waveguides on PCB substrates. The multiple reflection method provides a non-destructive means for loss measurement, however, it involves the complicated reflectometer alignment and it is not suitable for studying the local propagation properties in details. Figure 4.1 shows the schematics of the common waveguide measurement techniques.

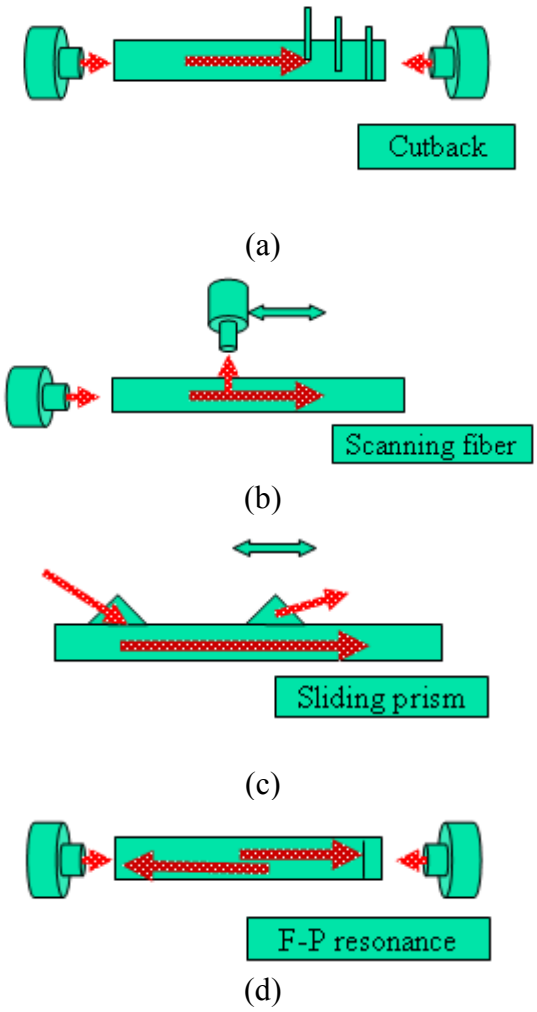

Figure 4.1 shows the schematics of the common waveguide measurement techniques: a) cutback method, b) scanning fiber method, c) sliding prism method, and d) F-P resonance.

Photographic method is a simple and accurate way to characterize the properties of planar waveguides, such as waveguide propagation loss, bending behavior, and crosstalk among adjacent waveguide channels. In this technique, a video camera is used to record the entire streak of light scattered from the waveguide, and then a computer was employed to analyze the power of the scattered light. However, this method is hard to use for the loss measurement in a waveguide with small scattering, due to low sensitivity of the video camera [15]. The method is improved later by coating the waveguide with a

fluorescent layer to enhance the detection of the scattered light [16]. Strasser and Gupta [17] used photographic films with high sensitivity to record the image of the low-intensity scattered light. Although this method has high sensitivity, it is not a real-time measurement. Further research efforts are required to develop a simple, real-time, accurate, and nondestructive technique for the characterization of optical waveguides with low scattering loss on PCB substrates.

4.2. Waveguide Measurement by Imaging the Scattered Light

In this section, we present a simple, real-time, accurate, and non-destructive technique for the characterization of loss in such optical waveguides that have low scattering losses such that the application of other loss measurement techniques for the study of these waveguides is not possible.

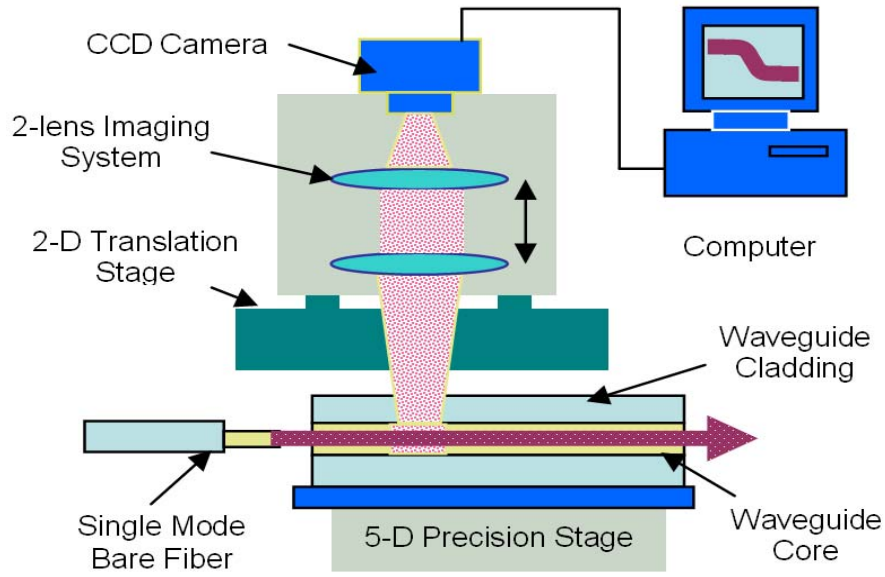

Figure 4.2. The schematic of the experimental setup used to characterize the propagation of the polymer waveguides. A single-mode bare fiber is used as the facet coupler to excite the waveguide modes. The polymer waveguide is mounted on a five-axis precision stage. The adjustable two-lens imaging system with numerical aperture of 0.15 along with the CCD camera is mounted on a two-dimensional (2D) large-range translation stage.

The propagation loss in optical waveguides is primarily due to material absorption, scattering, and radiation. The scattered and radiated light can be observed from the top as a streak of light in the waveguide. The intensity of the observed light above the waveguide is directly proportional to the intensity of the guided light inside the waveguide. Therefore, the propagation loss of the optical waveguide can be non-destructively measured by monitoring the intensity of the scattered light I along the propagation direction and fitting this variation with a mono-exponential formula:

$$I = I_o \exp(-\alpha x), \tag{4.1}$$

with I_o being the incident intensity at the waveguide input at $x = 0$, x being the coordinate along the propagation direction, and α being the loss coefficient.

Equation 4.1 can be rewritten (by taking the logarithm of both sides) as:

$$\ln I = \ln I_o - \alpha x. \tag{4.2}$$

The loss coefficient α of the waveguide is then calculated as the slope of the linear function of $\ln I$, which can be obtained by simply fitting the data with a linear function.

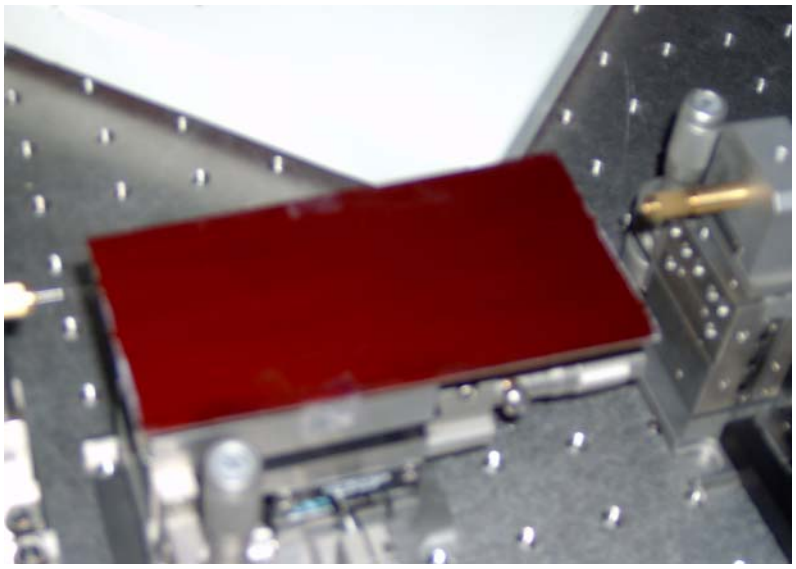

Figure 4.3. Multi-channel optical polymer waveguides integrated on PCB board are under test by imaging the scattered light through a CCD camera.

Figure 4.2 shows the schematic of the experimental setup used to characterize the propagation properties of our polymer waveguides. A single-mode bare fiber is used as the facet coupler to excite the waveguide modes (a prism-film coupler can also be used to couple light into the waveguide; however, an extra stop must be used to block the scattered light from the edge of the input prism). The polymer waveguide is mounted on a five-axis precision stage, as shown in Fig. 4.3. A high sensitive commercial CCD camera (Model: SBIG ST-7XME) with a built-in integration function is utilized to observe the light streak in two dimensions through a two lens imaging system with numerical aperture (NA) of 0.15. By changing the magnification ratio of the imaging system, we can study the scattered light to obtain detailed information about waveguide propagation properties such as guided mode profiles, defect distributions, bending behavior, etc. The imaging system along with the CCD camera is mounted on a two-dimensional (2D) large-range translation stage, which enables the investigation of different locations of the

waveguide structure. The output data of the CCD camera are sent to a computer through an analog to digital converter to characterize the propagation properties of the waveguide structure. The high sensitivity and built-in integration function of the CCD camera with the dark current of 1 e/pixel/sec, 765×560 pixel array (with 9μm × 9μm pixel size) and a 6×104 dynamic range enables the system to detect low intensity scattering light and thus to measure the low loss coefficients. This technique has the advantage of being nondestructive, low guided power, readily automated, independent of the coupling efficiency and facet reflectivity, and applicable to complex waveguide circuits.

4.3. Low-loss Waveguide Measurement Results

By adjusting the imaging system, a clear image, as shown in Figure 4.4(a), of the scattered light on top of a capped waveguide with a $50\mu m \times 50\mu m$ core area and a $10\mu m$ thick cap-clad waveguide, is captured by the CCD camera with 10 seconds integration time. The length of the measured waveguide is 1.7 cm. The variations of the scattered light with propagation length detected by the camera at two different wavelengths (850 nm and 980 nm) are illustrated in Figure 4.4(b).

The loss analysis is performed by sampling the light intensity in 2D (both longitudinal and transverse) along the propagation direction. The relative intensity at each position along the propagation direction is then obtained by the integration of the light intensity perpendicular to the propagation direction within the width of waveguide. The logarithm of the relative scattered power versus the propagation position is then plotted. A linear least-square fit of this plot gives the propagation loss coefficient for the waveguide under test. Note that this technique is quite general and can be used for any waveguide geometry (straight, bent, etc.).

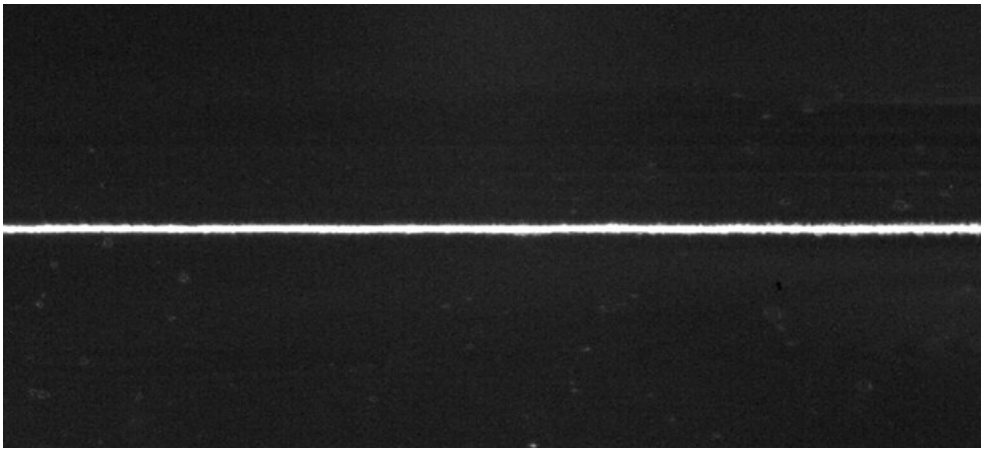

(a)

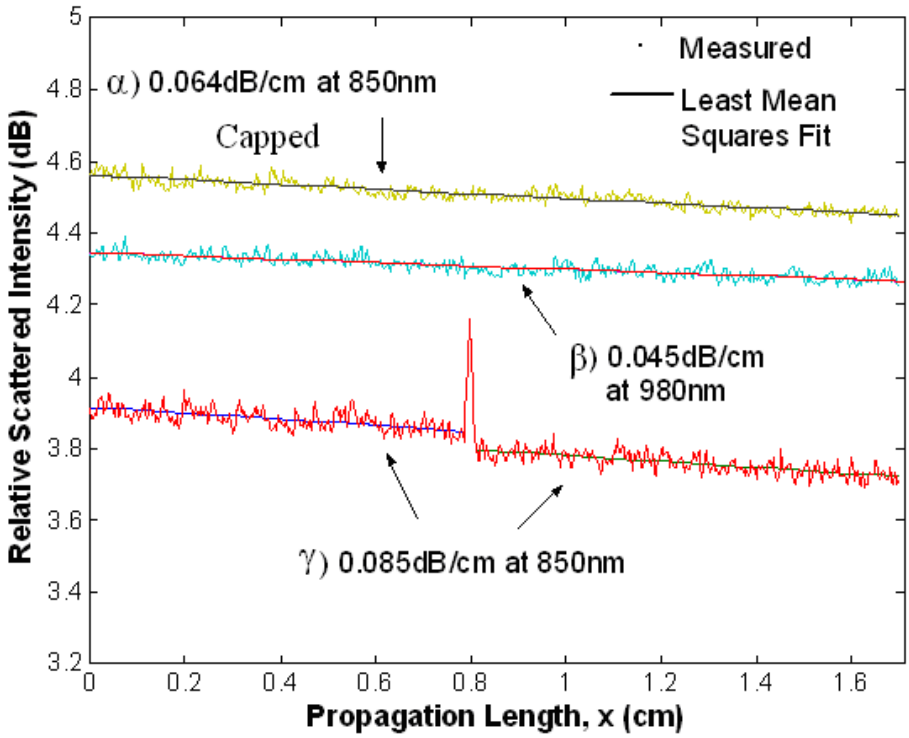

(b)

Figure 4.4. (a) The image captured by the CCD camera of the scattered intensity of the multimode waveguide shown in Figure 1. The propagation length of the waveguide is L=1.7 cm, and the integration time of the CCD camera is 10 seconds. The wavelength of the coupled light is 850 nm. (b) Relative scattered intensity versus the propagation length (α) at 850 nm and (β) at 980 nm for the capped waveguide, and (γ) at 850 nm for a conventional waveguide with the same feature size with the capped waveguide. The lines are the least-squares fits of the measured relative scattered intensity with a mono-exponential function.

From Figure 4.4, we measured loss coefficients of $\alpha_1 = 0.065 dB/cm$ at $\lambda = 850nm$ and $\alpha_2 = 0.046 dB/cm$ at $\lambda = 980nm$ for the capped waveguides. To examine the repeatability of these results, we repeated the experiment with 5 different groups of channel waveguides with 8 waveguides in each group (with the same feature size) under different input coupling conditions and we obtained less than 10% variation of loss coefficients in all 40 measurements. The accuracy of the loss coefficient measurement can be obtained by analyzing the deviation of the linear fitting. The standard deviation of the linear fitting shown in Figure 4.4(b) is less than ±0.004dB/cm. We believe this technique with the given CCD camera has accuracy better than 0.01dB/cm, and therefore is suitable for measuring loss coefficients well below 0.1dB/cm reliably.

To compare the propagation loss of the capped waveguide with that of a conventional one, we fabricated the latter using a layer-by-layer process with a $50\mu m \times 50\mu m$ core and a $10\mu m$ thick top cladding. The variation of the relative scattered intensity with propagation length at 850 nm for the conventional waveguide is also shown as in Figure 4.4(b). The local scattering peak for this case corresponds to a local defect formed during fabrication. We use linear curve fitting on both sides of this defect and then average the slope of the fitting lines in these two curves to find a propagation loss coefficient of $\alpha_3 = 0.085 dB/cm$. We repeated the 40 experiments for a total of 5 groups of channel waveguides and found loss coefficients with less than 10% variation. Our results suggest that under the same fabrication environment, the capped waveguide has at least 20% less propagation loss compared to the conventional waveguide.

Table 4.1. The comparison of the optical propagation loss of polymer waveguides integrated on PCB substrates.

	R. Chen [23]	IBM [19]	D.W. Kim KR [73]	Bamiedakis UK [74]	Dangel Swiss [75]	Capped Waveguide
Core size (μm^2)	50 × 50	35 × 35	50 × 50	50 × 50	50 × 50	50 × 50
Loss (dB/cm)	0.1 at 850 nm	0.16 at 985 nm	0.16 at 850 nm	0.05 at 850 nm	0.05 at 850 nm	0.065 at 850 nm 0.045 at 980 nm
Polymer Material	Perfluorinated acrylate	acrylate	UV-curable epoxy resins	Polydimethyl-siloxane PDMS	Silsesquioxanes Siloxane-based	Shipley LightLink™ polysiloxane-based

Compared with the reported results for similar polymer waveguides on PCB substrate [19, 23 73, 74, 75], as shown in Table 4.1, we believe that the losses reported here are among the smallest values reported for polymer waveguides fabricated using the basic contact photolithography on a PCB substrate. We think that the lower loss obtained at 980nm is primarily due to the lower material absorption at 980nm. Assuming allowable total loss is 20dB of which 10dB budgets are used for coupling losses and 10 dB for waveguide propagation. The waveguide working distance could reach up to 150cm at the wavelength of 850nm. This small loss makes the presented waveguides excellent candidates for the implementation of optical interconnects on PCB boards.

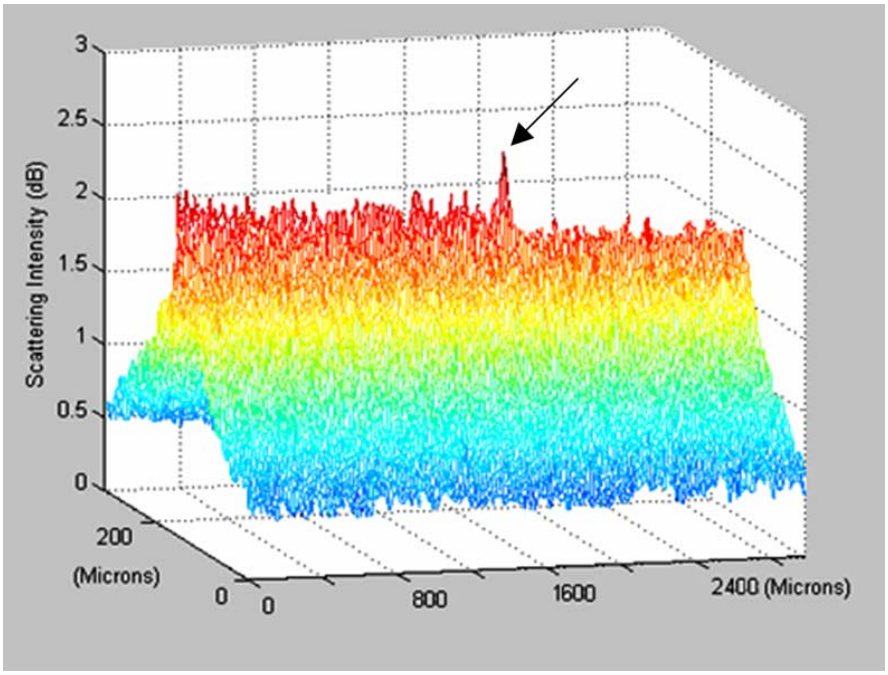

Figure 4.5. The 2D scattered light intensity from a traditional multimode polymer waveguide when an air bubble exists in the waveguide core. This waveguide was fabricated layer by layer (not with the capped waveguide technique) and has the same core and cladding dimensions as the capped waveguide in Figure 1. The air bubble causes a local peak in the scattered intensity.

While the main focus of this technique is the loss measurement, the characterization setup described in Figure 4.2 can be used to investigate several other properties of the planar waveguides. As an example, Figure 4.5 shows the 2D scattered light intensity from a traditional multimode polymer waveguide when an air bubble exists in the waveguide core. This waveguide is fabricated layer by layer, not with the capped waveguide technique, and it has the same core and cladding dimensions as the capped waveguide. As shown in Figure 4.5, the air bubble causes a local peak in the scattered intensity. The spatial extent of the peak is directly related to the size of the air bubble. Thus, the experimental set up presented in this chapter can be used to investigate the fabrication quality of the waveguides as well. As another example, Figure 4.6(a) shows a strong local scattered center from a conventional optical polymer bending waveguide, as

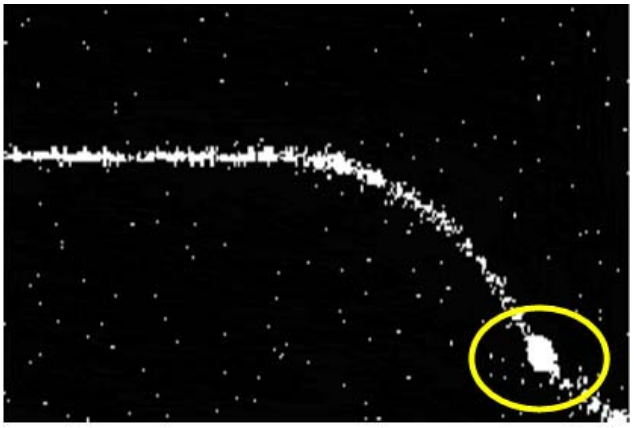

(a)

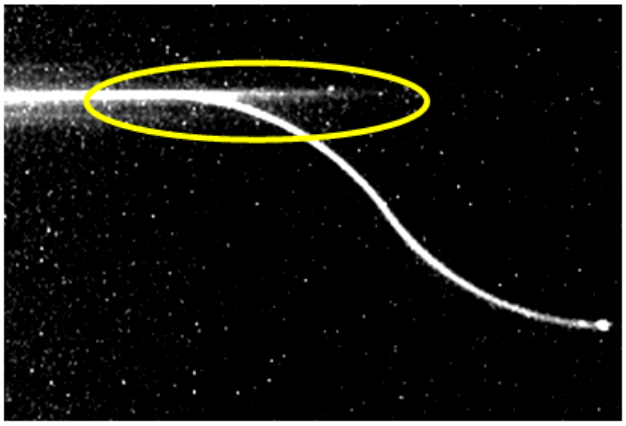

(b)

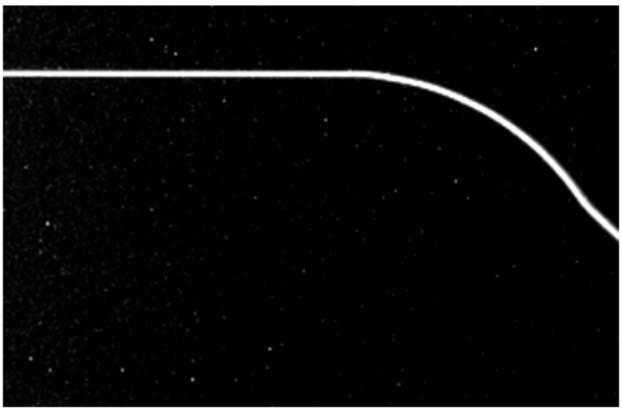

(c)

Figure 4.6. The images captured by the CCD: a) an image showing a defect detected, as a scattering center, b) an image showing an extra loss due to the misalignment of the input fiber to waveguides, and c) an image of light propagation through the bending area without extra loss.

circled on the bottom right of the image. This was induced by a defect on the waveguide. In general, a defect is a scattering center. Usually a strong scattering happens, when a beam travels through the defect. The defect can be a particle, a bubble, mechanical scratch or some other kinds of damages. The spatial extent of the peak is directly related to the size of the defect. Thus, the experimental set up presented here can be used to investigate the fabrication quality of the waveguides as well. Figure 4.6(b) shows another unexpected loss caused by bending structure and mis-alignment. The light escaped is noticeable from the transaction area from straight line to curvature. Once the input light is perfectly aligned, the extra loss disappears and the collected scattering light becomes a smooth curve, as shown in Figure 4.6(c). Thus this technology can be used to monitor and adjust the alignment between devices and components in light wave circuits that are critical to optical interconnect.

4.4. Chapter Summary

In summary, we presented here a reliable, non-destructive, and real time technique for characterization of propagation properties of planar optical waveguides based on accurate imaging the scattered light from the waveguide using a sensitive CCD camera with built-in integration functionality. This technique can be used for real-time investigation of the propagation properties (loss, mode profile, bending properties, etc.) as well as the fabrication quality of planar waveguides with better sensitivity compared to other techniques. Using this characterization tool, we measured capped waveguides with loss coefficients of $\alpha_1 = 0.065\,dB/cm$ at $\lambda = 850nm$ and $\alpha_2 = 0.046\,dB/cm$ at $\lambda = 980nm$ with accuracy of 0.008dB/cm. To the best of our knowledge, these data are among the lowest loss coefficients reported for polymer waveguides on PCB substrates to

date. This makes our capped waveguides an excellent candidate for board-level optical interconnects.

CHAPTER 5

45º METAL COATED POLYMER MICROMIRROR INTEGRATION

In this chapter, we introduce a simple method of integrating 45º total internal reflection micro-mirrors with polymer optical waveguides by an improved tilted beam photolithography on printed circuit boards to provide surface normal light coupling between waveguides and optoelectronic devices for optical interconnects. De-ionized water is used to couple UV beam through the waveguide core polymer layer at 45º angle during the photo exposure process. This technique is compatible with PCB manufacturing facility and suitable to large panel board-level manufacturing. The mirror slope is controlled accurately (within ±1º) with high repeatability. The insertion loss is 1.6 dB for an uncoated micro-mirror, and 0.46 dB for a silver coated micro-mirror [76, 77].

5.1. Introduction to 45º Micro-Mirror Fabrication Techniques

In three-dimensional fully embedded board-level optical interconnects, one key challenge is to realize efficient optical coupling between in-plane waveguides and laser/detector devices. 45º total internal reflection micro-mirrors and grating devices integrated on waveguides have been studied as surface normal couplers. 45º TIR mirror couplers are more widely employed as waveguide couplers compared with the grating couplers, because they are coupling-efficient, easy to fabricate, and relatively insensitive to wavelength variations.

Various techniques can be used to construct 45° TIR micro-mirrors, such as laser ablation [18–20], grayscale lithography [21], hard molding [22], soft molding [23],

reactive ion etching (RIE) [24], micro-dicing [25], the X-ray lithography [26], deep proton writing [27]. Among these technologies, Photolithography is commonly used in printed circuits, semiconductor fabrication, MEMs, bio samples, and optical polymer devices, because of its excellent ability to define smooth and high definition micro-structures. Devices with precise structure profile and optical smooth surface required for optical application can be achieved by photolithography technology. Photolithography is the least disruptive technology to implement optical interconnects on PCBs, because it is easy, cost effective, and compatible with present-day printed circuit board processing. Other techniques might yield better quality micro-mirrors, but may be more "exotic", therefore less compatible with high-volume and large-scale PCBs production.

5.2. Discussions on Tilted Beam Lithography

In most cases, the device structures are defined by utilizing UV beam normally incident into the polymer so that the structures have vertical side walls. The titled beam lithography can make tapered structure when UV beam is traveling inside the polymer material at an inclined angle. It can be used to make polymer waveguides with tapered micro-mirrors integrated at the ends. The principle of titled beam photolithography is shown in Fig. 5.1. Two different types of tapered micro-mirrors (with positive slope and with the negative slope) will be defined at the different ends of the optical polymer waveguide core layer in one photo exposure step.

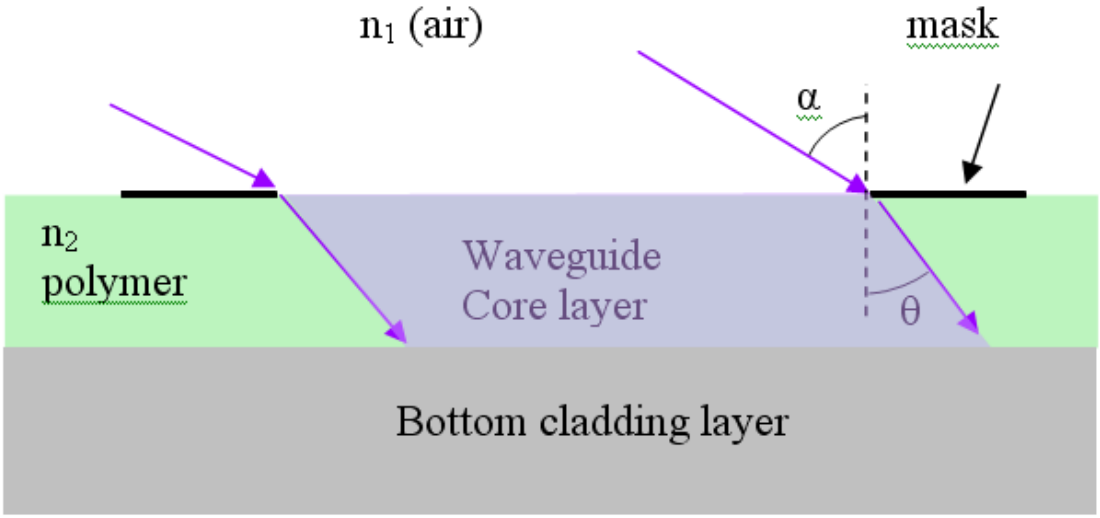

Figure 5.1. Schematic of titled beam photolithography. (α and θ being the incident angles in air and in the polymer respectively)

In most cases of the photolithography, the UV beam is incident from air to the polymer. The UV beam propagation at the interface between air and polymer obeys the Snell Law:

$$n_1 \sin\alpha = n_2 \sin\theta \tag{5.1}$$

with n_1 and n_2 being the refractive index of air (media 1) and the optical polymer (media 2) respectively, and α and θ being the incident angles in media 1 and media 2 respectively.

The refractive index n_2 of most photo polymers at the wavelength of the UV exposure beam (i.e., 365 nm, i-line of the mercury lamp), is above 1.5, depending on the type of polymer material chosen. Taken the refractive index of photo polymer as 1.5, according to the Snell's Law the maximum slope angle θ that can be formed in photo polymer by using the tilted photolithography is 41.8º, which is smaller than 45º. And to achieve this maximum angle, the UV exposure beam has to be tilted at the angle α close to 90º in the air, which suffers from the huge reflection loss on the air-polymer interface. Thus it is impossible to fabricate micro-mirrors with 45º by simply tilting the UV

exposure beam. A polymer optical waveguide channel with a 31.5º negative tapered mirror facet integrated at the end is demonstrated on a silicon substrate by simply tilting the UV exposure beam at 52.7º in the air, as shown in Fig. 5.2. A waveguide (50 μm in height and 200 μm in width) is carefully cleaved along the waveguide propagation direction to show the mirror facet in details at the waveguide end. The imperfections (as circled in Fig. 2) near the mirror facet and inside the waveguide are introduced by the cleaving damage. A pair of optical polymers with low optical loss, LighLink^{TM}, provided by Rohm & Haas Electronic Materials is used to fabricate optical waveguides and micro-mirrors. The LightLink^{TM} is a negative acting photoimaging polymeric system that is based on an inorganic-organic hybrid platform. It consists of two parts with refractive indices of 1.5196 and 1.4908 for the waveguide core layer and cladding layer.

In order to have the UV exposure beam travel inside the polymer waveguide core layer at an angle greater than 41º, i.e., with 45º, a prism can be used on top of the polymer core layer to couple light [28]. However, there are some practical issues in using prism for the micro-mirror integration on polymer waveguides on PCB substrates. Firstly, the desired waveguide circuit length can usually reach more than 10cm. Thus multiple prisms have to be placed at the different mirror locations on the waveguide core layer. Furthermore, the edge of the prism will cause the UV beam distortion during the exposure. At last, because the substrate or optical board is not ideally smooth and flat, there will be air gaps at the interface between the prism and the photo mask, as well as the interface between the polymer core layer and photo mask. Usually these air gaps have to be filled with index matching glue during the UV exposure process and then be cleaned out thereafter. Another solution of reducing the mismatch of the refractive index

between air and photo resist was reported in 3D inclined polymer microstructures fabrications, as Glycerol was employed as an index matching material between the photo mask and photo resist Su-8 during tilted beam exposure to compensate the refractive index difference, thus extended the possible inclined angles in the resist [29].

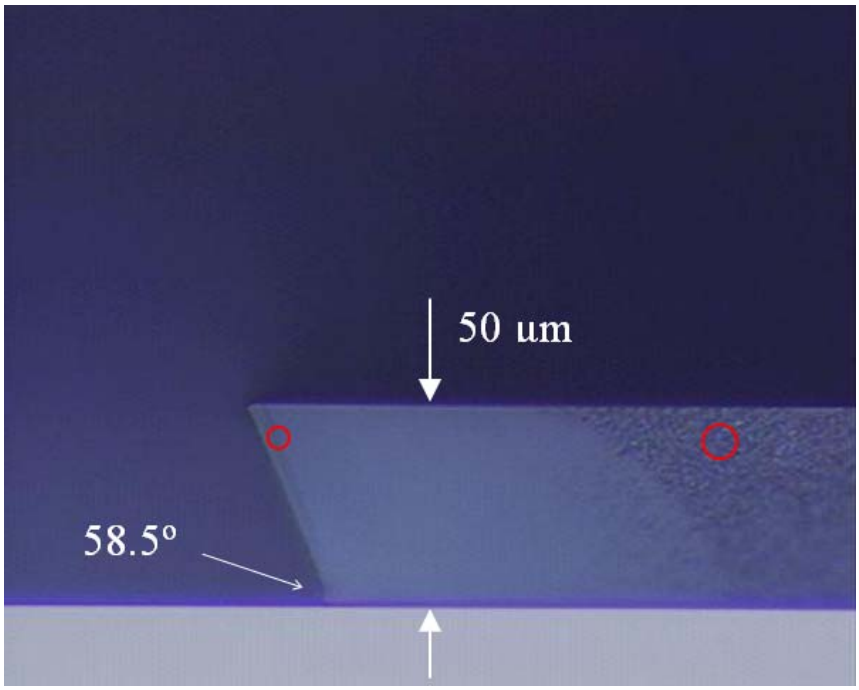

Figure 5.2. Microscope image of a cleaved 50 μm thick polymeric waveguide core layer with a 31.5º negative tapered mirror integrated at the end on silicon substrate by using the air-polymer tilted beam (52.7º) contact photolithography.

5.3. Design of Improved Tilted Beam Lithography

Here in this chapter, we introduce a simple method to fabricate the polymer optical waveguides with precisely integrated 45º TIR micro-mirrors at waveguide ends on PCB substrate with an improved titled-beam photolithography method. The key task here is to find an alternative solution of the prism coupler during the UV exposure. This solution should be cost-efficient, convenient, compatible to PCB manufacturing technology, and practical to large area processing on large size panel board-level optical polymer waveguide circuits. We notice the refractive index of D.I. water at the

wavelength of 365 nm (i-line of mercury lamp) is 1.35. With some straightforward setup, it can be used to replace the prism to match the refractive index difference between optical polymer and air during UV exposure. At the interface of polymer and water, in order to have the UV beam to propagate inside the waveguide core polymer layer at 45º angle, the beam incident angle in D.I. water should be close to 52.7º, which is practical.

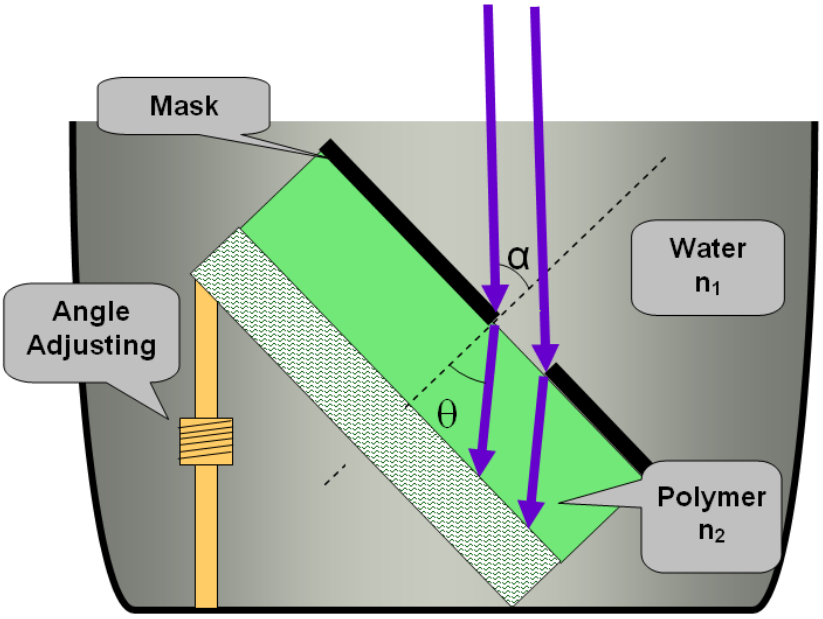

Figure 5.3. Schematic of improved UV photolithography on PCB substrate. (α and θ being the incident angles in water and polymer respectively)

Figure 5.3 shows the schematic of the improved tilted beam photolithography. In this improved system, the whole PCB substrate along with polymer waveguide core layer and photo mask aligned above is titled at 52.7º and immersed in a tank filled with D.I. water. The UV exposure beam is normal to the water surface in the water tank so that the reflection of UV exposure beam at the air-water surface is negligible. Because the PCB substrate is tilted, UV beam at different location of polymer core layer has different propagation length in water, thus the absorption loss of D.I. water is different. Fortunately, the absorption coefficient of D.I. water at 365 nm is very low and the

absorption loss of 10 cm water is less than 0.1%, as shown in Fig. 5.4 [78]. Thus the different propagation path in water will not affect the UV exposure process. This method allows fabricating the 45º micro-mirrors for large panel manufacturing for the optoelectronics industry with almost no extra cost. Thus a tank of D.I. water provides a cost-effective solution to match the refractive index difference between air and polymer material. By this method, the tapered angle can reach up to 60º for most photo resist material, and people in MEMS may find application in fabrication of large slope structures, i.e., V-groove holders.

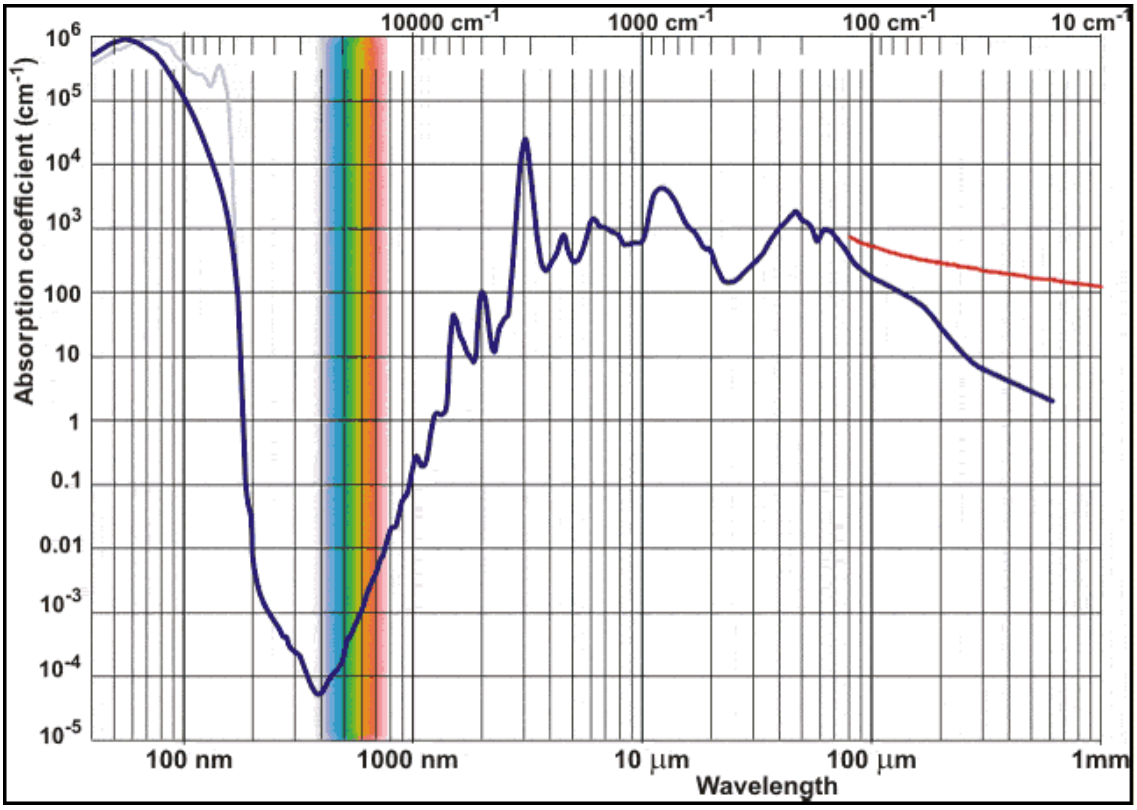

Figure 5.4. Absorption spectrum of DI water. And the absorption coefficient at 365 nm is less than 10^{-4} cm^{-1} [78].

5.4. Fabrication and Test of TIR 45º Micro-Mirrors

In this study, a 10cm × 10cm FR4 substrate is employed to build planar optical waveguide circuits. A pair of optical polymers, LighLink^{TM}, is used. The sequential fabrication steps of the integration of 45º tapered TIR micro-mirrors at the ends of waveguides are as follows: 1) spin-coat the bottom cladding layer on the FR4 board and cure it, 2) coat the core layer and soft-bake it, 3) immerse the FR4 board at a tilted angle in the D.I. water tank, and expose the core layer to an appropriate dose of UV radiation through a mask, as illustrated in Fig. 5.3, Special attention is needed to remove any air bubbles between the interface of photo mask and photo resist. Any air bubbles will block UV beam from propagation during the exposure, thus there will be no patterns defined inside the resist under the air bubbles. Additionally, the photo mask should be aligned with the photo resist inside the water tank to avoid any air bubbles between the photo mask and photo resist, and the air bubbles can be easily removed by a soft tissue inside the water tank. 4) develop the pattern using a wet process. The developer used for patterning of LightLink^{TM} is an aqueous solution (2% Alkaline). Developments are carried out at room temperature for about 3 minutes. Unexposed areas are dissolved and washed away and the exposed areas remain. In this process, the 45º TIR micro-mirrors are defined simultaneously with the waveguide core at the end of the waveguides.

Figure 5.5 shows the microscope images of a 50×50 μm^2 polymer waveguide integrated with 45º positive or negative tapered mirror facets on FR4 substrate. It is critical to maintain an accurate 45º tapered mirror angle for the optimum light coupling between waveguides and out of plane optoelectronic devices. The tapered angle of the micro-mirrors is measured by the contact surface profiler (DekTek 303). The surface

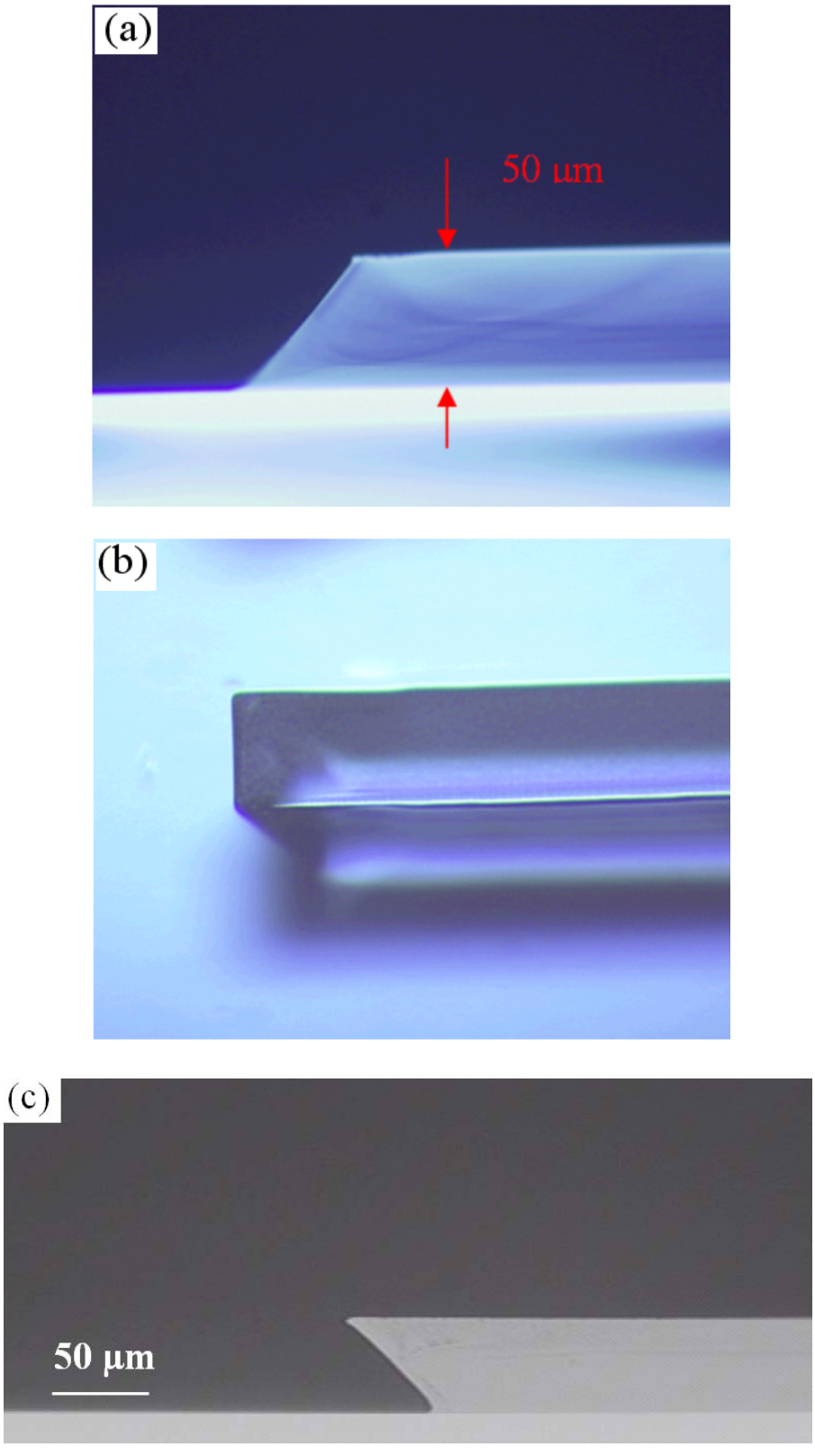

Figure 5.5. Microscope images of a 50×50 µm^2 polymer waveguide with a 45º (a) positive (b, c) negative tapered mirror facet in the ends on FR4 substrate.

profile measurement of the positive tapered mirror (as shown in Fig. 5.5(a)) confirms an exact 45º mirror angle, as shown in Fig. 5.6, compared with the fact that the mirror sample fabricated under the same condition can only achieve 31.5º (as shown in Fig. 5.2). The surface profile measurement of the micro-mirrors on different waveguide channels, as well as on different FR4 substrates, demonstrates an angle accuracy of ±1º and a high repeatability.

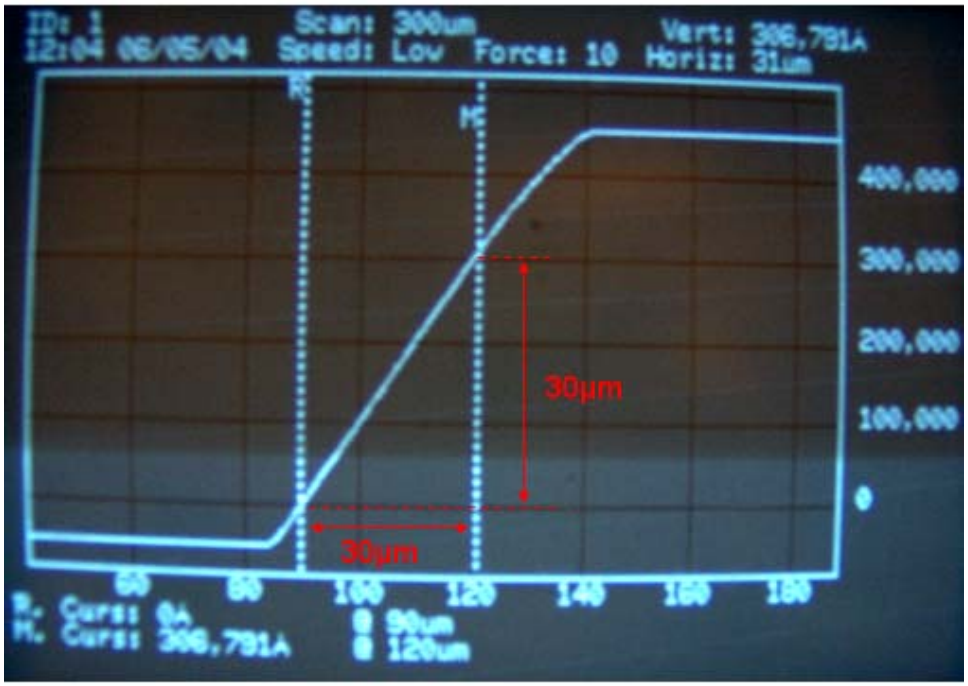

Figure 5.6. Surface profile of the positive tapered mirror (as in Fig. 5.5(a)) at the waveguide end measured by the contact surface profiler (DekTek 303).

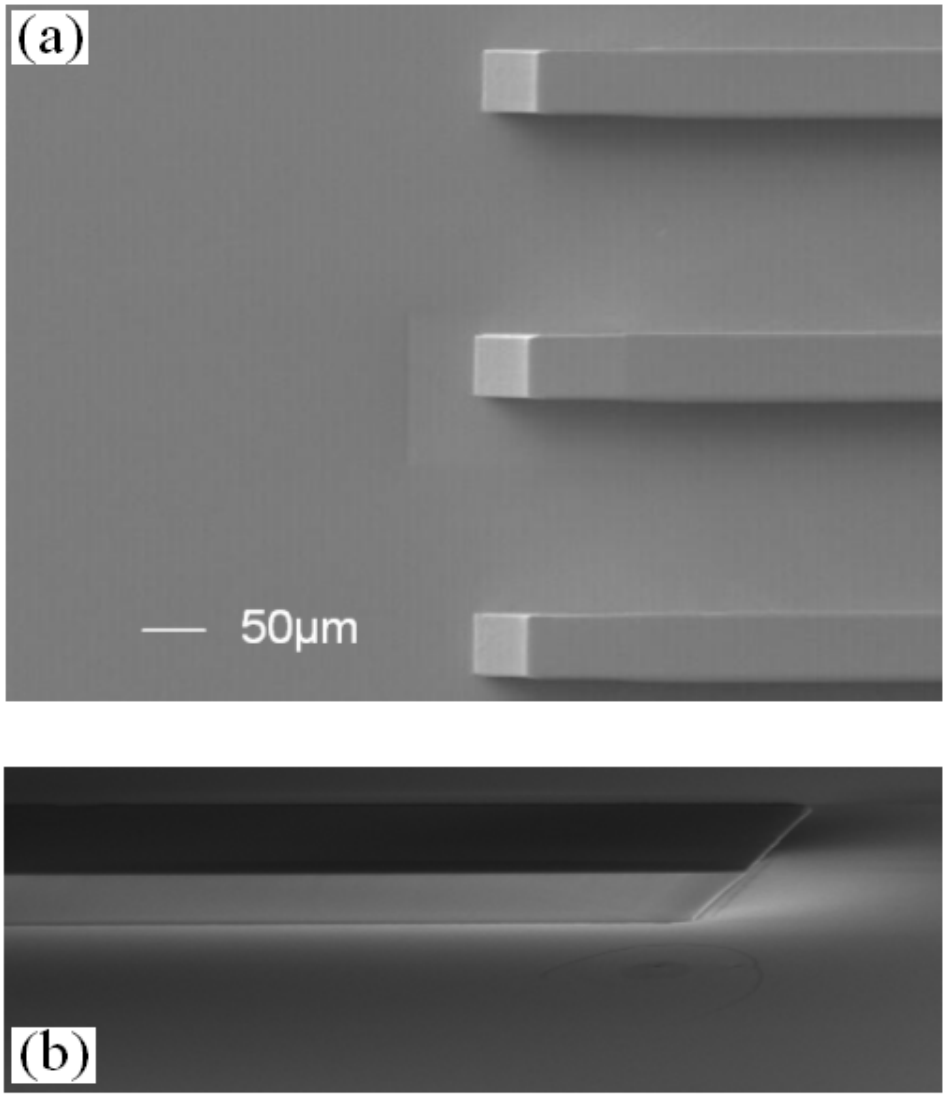

Figure 5.7. SEM images showing the top views of (a) positive tapered and (b) negative tapered 45º micro-mirrors at the ends of 50×50 μm^2 multimode waveguides on PCB substrate.

Scanning electron microscope (SEM) images confirm the smooth surface of the tapered mirror that is essential for a low scattering loss, as shown in Fig. 5.7. Clear and smooth rectilinear mirror planes are achieved for both positive and negative tapered mirrors. The surface root-mean-square (rms) roughness of the positive tapered 45º mirror facet is measured by AFM. The average surface roughness measured for different positive tapered mirror samples is 40 nm rms with small variation, as measured over an

area of 10×10 μm^2. A similar surface roughness is expected on the negative tapered mirror facets. This small surface roughness guarantees that the tapered facets can be used as high quality 45º TIR mirrors.

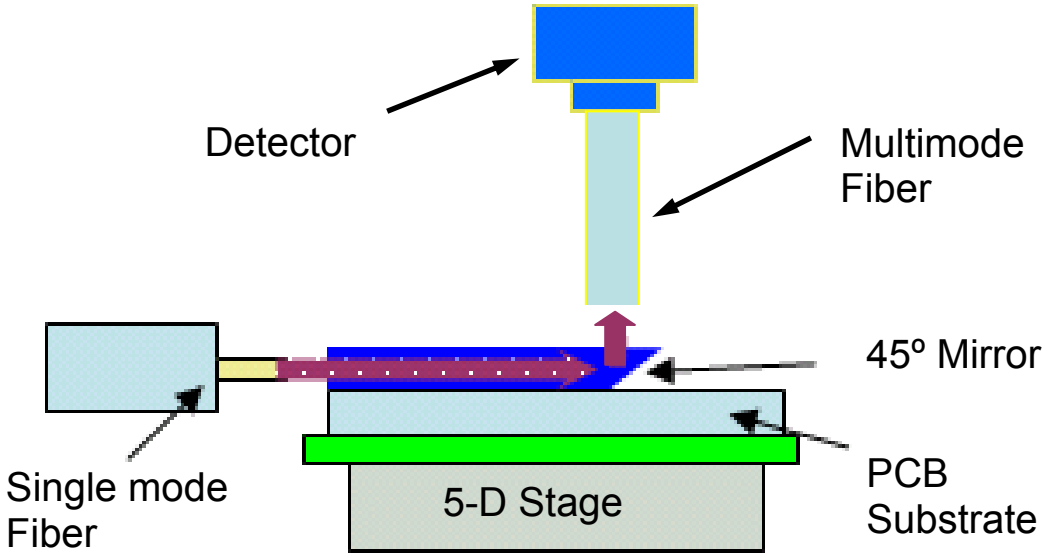

Figure 5.8. Schematic of the measurement system to test the integrated 45º micro-mirrors at the end of optical polymer waveguides on PCB substrate.

Optical waveguides fabricated on FR4 substrates in this study have very low propagation loss at the wavelength range of 850 - 1000 nm, which is rather tedious to measure by using the conventional destructive cutback method due to the difficulty to cleave the FR4 board. We have developed a reliable, non-destructive, and real time technique for characterization of propagation properties of planar optical waveguides based on accurate imaging the scattered light from the waveguide using a sensitive CCD camera with built-in integration functionality. Using this characterization tool, the optical waveguides show loss coefficients of $0.085\,dB/cm$ at $\lambda = 850nm$ with great accuracy.

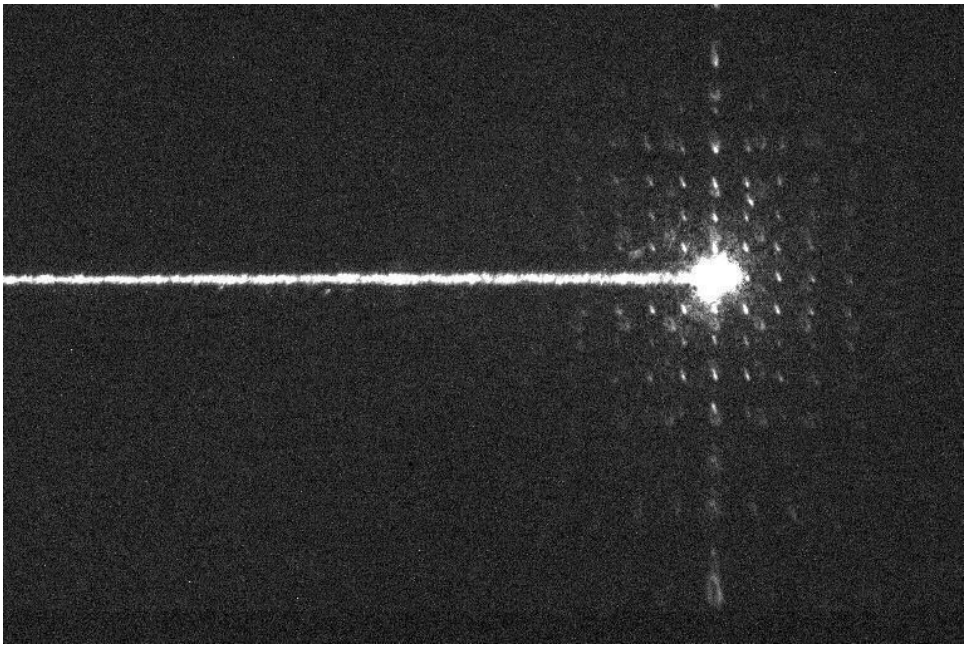

Figure 5.9. Microscope image of the light coupled out in z-direction for the optical waveguide on PCB substrate by an integrated 45º micro-mirror.

To characterize the surface normal coupling efficiency of the integrated micro-mirrors, the negative tapered facet (as shown in Fig. 5.5(b)) is tested. The schematic of the measurement setup is shown in Fig. 5.8. The probe laser beam is coupled into the waveguide through a 9 μm single mode fiber from air. The numerical aperture is 0.29 for the waveguide and 0.14 for the single mode fiber. Then the coupled beam propagating inside the waveguides is reflected out of the waveguide circuit plane by the micro-mirror at the end, as shown in Fig. 5.9. And the reflected light is collected by a 62.5 μm multimode fiber (with a NA of 0.275) above the negative tapered 45º TIR mirror. By comparing the insertion loss measurement from the waveguides of the same length with and without the micro-mirror, the excess loss of the mirror is obtained as 1.6 dB, corresponding to a coupling efficiency of 69%. We have tested 3 FR4 substrates with 5 micro-mirrors on each substrate, and less than 10% variation of the mirror insertion loss

was observed in all measurements. The performance of the air-polymer interface based TIR 45º micro-mirrors can be further improved by metal coating on the surface.

5.5. Metal Coating on 45º Micro-Mirrors

The unprotected TIR mirror facets are vulnerable to contaminations and a thin layer of metal coating on the mirror surface is necessary for a high performance and reliable system. With the knowledge and the techniques developed in the previous research, this section will be focused on the development of a new technique for a thin layer of metal coating (e.g., silver) on micro-mirrors integrated on optical waveguides to achieve higher reflection and coupling efficiency (i.e., above 90%) than the uncoated TIR mirrors.

Lift-off process in microstructuring technology is a method of creating structures of a target material on the surface of a substrate using a sacrificial material. Lift-off process is mostly used to create metallic deposition on semiconductor wafers [79]. As shown in Fig. 5.10, the lift-off process is a complicated additive technique. An inverse pattern is first created in the sacrificial photoresit photoresist, deposited on the surface of the substrate. This is done by etching openings through the layer such that the target material can reach the surface of the substrate in those open regions, where the final pattern is to be created. The target metal material (e.g., silver or gold) is deposited over the whole area of the wafer, reaching the surface of the substrate in the etched open regions and staying on the top of the sacrificial layer in the regions, where it was not previously etched. When the sacrificial layer is washed away (photoresist in a solvent), the material on the top is lifted-off and washed together with the sacrificial layer below.

After the lift-off, the target material remains only in the regions where it had a direct contact with the substrate.

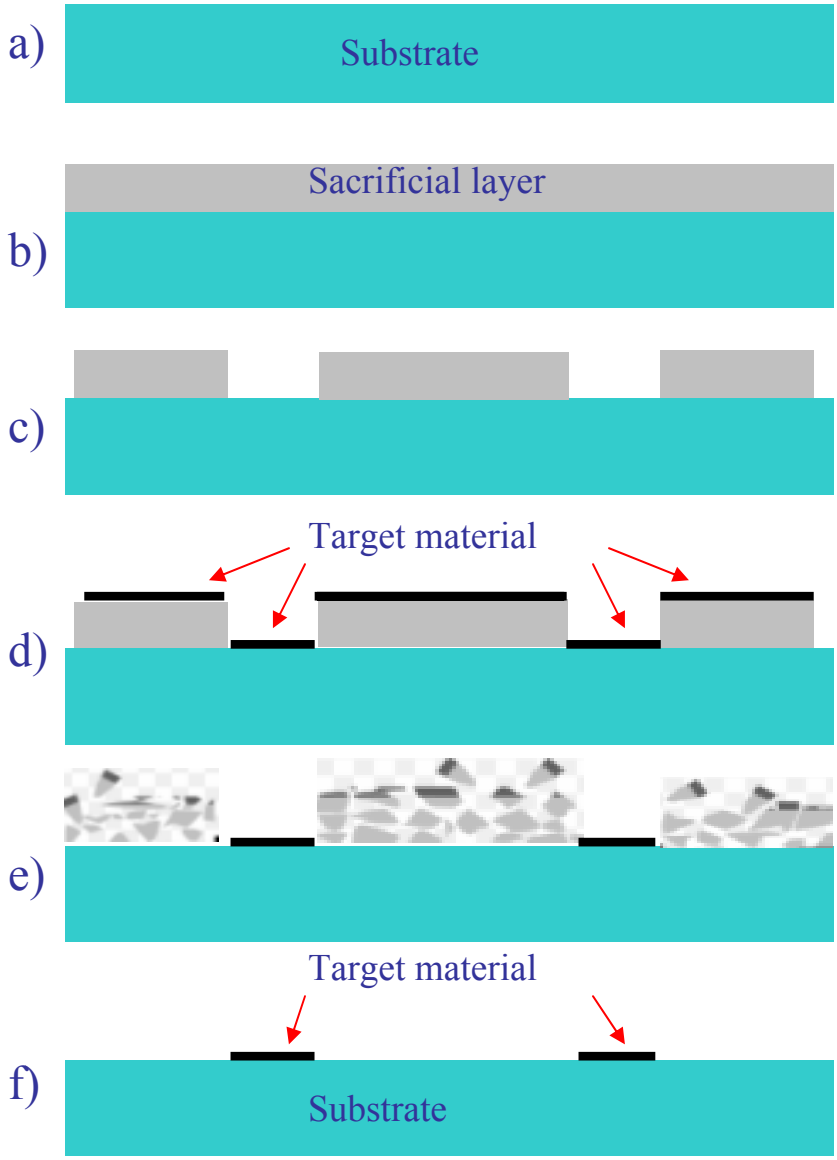

Figure 5.10. Schematic of lift-off process: a) preparation of the substrate, b) deposition of the sacrificial stencil layer, c) etching the sacrificial layer to create an inverse pattern, d) deposition of the target material, e) washing out the sacrificial layer together with the target material on the surface, and f) the final target material patterned on the substrate.

Lift-off process has major challenges, such as retention, ears, and redeposition. Retention is the worst problem for the lift-off process. The unwanted parts of the metal layer will remain on the wafer, because the metal has adhered so well to the sacrificial photoresist and prevented the resist below from being dissolved properly. When the metal is deposited, and it may cover the sidewalls of the resist, "ears" can be formed. Also, it is possible that these ears will fall over on the surface, causing an unwanted shape on the substrate. During the washing of the sacrificial photoresist in the liftoff process, it is possible that particles of metal will become re-deposited to the surface, at random locations. It is very difficult to remove these redeposition particles after the wafer has dried.

The key to successful lift-off is the ability to ensure the existence of a distinct break between the layer of target material deposited on top of the sacrificial resist and the layer of target material deposited on top of the wafer substrate. Such a separation allows the dissolving liquid to reach and attack the sacrificial resist layer. Several technical attempts haven been reported to address these challenges [79, 80, 81]. Hatzakis developed a lift-off metallization technique with UV exposure of a single layer of AZ-type photoresist [80]. The process consists of soaking the resist layer for a predetermined time either in chlorobenzene or other aromatic solvents such as toluene and benzene before or after exposure. After development, resist profiles with overhangs suitable for lift-off metallization were obtained. The lift-off process can also involve multiple layers of different types of resist [81]. This can for instance be used to create shapes that will prevent side walls of the resist being covered in the metal deposition stage. However, no solution based on metal coating on the micro-structures without the involvement of the

lift-off process has been reported. The combination of the capped waveguide technique and the tilted beam exposure technique mentioned in the preliminary research along with a reusable hard metal mask for metal deposition will provide a solution that eliminates the usage of traditional lift-off process, which will greatly simplify the process and reduce fabrication cost without sacrificing the coating quality. Furthermore, the common defects induced in the traditional lift-off process, such as retention, ears, and redeposition, will be avoided in the new metal deposition process. In this section, the fabrication process of metal coating on the 45º micro-mirrors integrated on the polymer waveguides by electron beam (E-beam) evaporation is studied, and the performance of the metal-coated micro-mirrors is evaluated.

The processes for this new technique of metal coating on micro-mirrors integrated with capped waveguides, as shown in Fig. 5.11, are as follows:

a) Coat the bottom cladding layer on the substrate and cure it. Then coat the core layer and soft-bake it followed by coating the cladding layer on top of the core layer and soft-bake it. A pair of LightLink^{TM} polymers for core and cladding is used in this research. This is the same process as the first two steps described for the fabrication of capped waveguides in Section 3.4.

b) Immerse the whole substrate at a tilted angle in the D.I. water tank, expose the top two layers to an appropriate dose of UV radiation through a photo mask, and develop the pattern using a wet etching process. The exposure setup is similar to the one described for improved tilted beam exposure in Section 5.3. Development process (i.e., wet etching) is carried out at room temperature. Unexposed areas are dissolved and washed away, and the exposed areas remain. 45^{o} micro-mirrors are now integrated at the end of capped

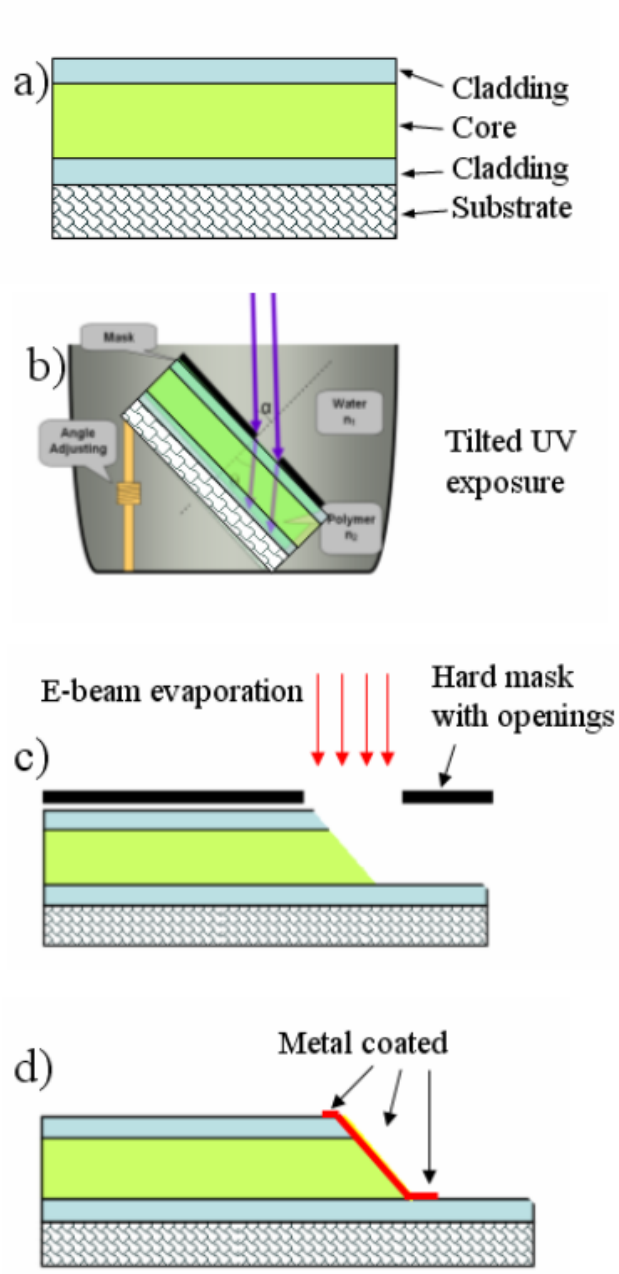

Figure 5.11. Improved process flow of metal coating on micro-mirrors integrated with capped waveguides: a) formation of core and cladding layers; b) immerse the whole substrate at a tilted angle in the D.I. water tank, expose the top two layers to an appropriate dose of UV radiation through a photo mask, and develop the pattern using a wet etching process; c) cover the capped waveguides with a hard metal mask with openings, while the openings of the hard mask is aligned on top of the micro-mirrors integrated at the end of the capped waveguides. Put the whole structures inside an E-beam evaporator for a thin layer of metal coating; d) remove the hard mask after the metal deposition, and apply a thin layer of polymer to clad the sides and the top of the core.

waveguides. In capped waveguides, the surface of the core is protected by the cap-clad during the following processes. And the 45º micro-mirrors are open from the cap-clad layer.

c) The capped waveguides are then covered with a hard metal mask with openings, with the open windows of the hard mask aligned on top of the integrated micro-mirrors. The open windows on the hard mask are fabricated by the chemical etching process used in defining the copper circuits. The size of these open windows is larger than the feature size of the micro-mirrors, such that the whole mirrors are covered inside the windows, and the alignment tolerance is loose (e.g., 25 μm). The surface of the core is protected from contact with the hard mask by the cap-clad during handling. The whole structures are then inserted in the chamber of an E-beam evaporator for the deposition of a thin metal layer (e.g., silver or gold) with the thickness of 150 nm. The E-beam evaporator is used to coat micro-mirrors with metals, because unlike sputtered films, E-beam evaporators only coat the surface facing away from the substrate and will provide very little coating to the side walls of micro-mirrors, which are perpendicular to the surface of the substrate.

d) Remove the hard mask after the metal deposition. The metal coating only occurs on the surfaces of the micro-mirrors and the small areas around them. The air gap between the capped waveguides and the above hard metal mask ensures the existence of a distinct break between the layer of metal material deposited on top of the reusable hard mask and the layer of metal material deposited on top of the mirror facets and the adjacent areas. Such a separation prevents the peel-off of the coated metal layer on the 45º mirror facets when removing the reusable hard mask after the metal deposition. There

will be side slope connecting the capped waveguides and the hard mask, due to the air gap, so no such "metal ears" will be formed during the deposition process. There will be no retention and redeposition, which are hard to prevent in the lift-off process, left on the waveguide surface and on the 45º micro-mirror facets, because the process of washing the sacrificial resist layer is avoided. There may be some damages (e.g., scratches) on the surface of the clad layer, due to the contact with the hard mask during the alignment. However, these possible damages are far away from the waveguide core layer, and have little effects on the waveguide performance. The capped waveguides are completed by further applying a layer of polymer to clad the sides and the top of the core.

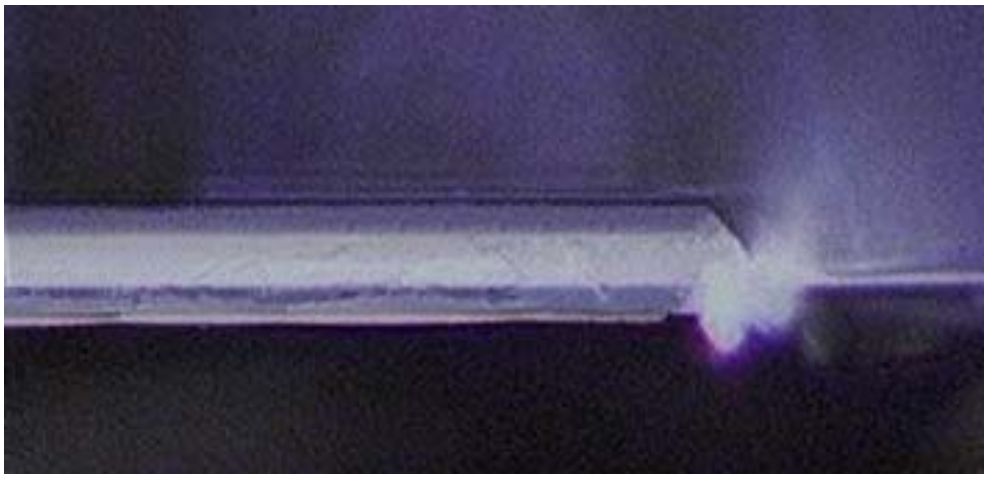

Figure 5.12. The microscopic picture of a cross section of a capped waveguide with silver coated 45º micro-mirror integrated in the end. The waveguide core size is of 50×50 μm^2, and the thickness of the top-clad layer is 20 μm. The cross section is along the waveguide propagation direction. The light guided inside the waveguide core is reflected out-of-plane by the silver coated mirror.

Figure 5.12 shows how light propagating inside a capped waveguide is coupled out-of-plane by the integrated 45º mirror with 150 nm silver coating. The capped waveguide are fabricated on a FR4 substrate. The surface roughness of metal coated mirrors measured by AFM is 40 nm, the same with the uncoated TIR mirrors. The

reflection of the metal-coated 45° micro-mirrors is evaluated by using the same measurement setup for the uncoated 45° mirrors. Micro-mirrors with 150 nm thick silver coating show more than 90% reflection at both 850 nm and 980 nm.

5.6. Chapter Summary

In summary, we introduce in this chapter a simple method to fabricate polymer optical waveguides with integrated 45º TIR micro-mirrors on printed circuit boards by improved tilted beam contact photolithography (with the aid of D.I. water) for fully embedded optical interconnects. The 45º TIR coupling mirrors are shaped at the ends of the waveguides in one exposure step to provide surface normal light coupling between waveguides and optoelectronic devices by using the low cost PCB facility in a class-1000 substrate laboratory. The optical polymer waveguides on PCB substrate show propagation loss of $0.085\,dB/cm$ at $\lambda = 850nm$. The slope of the 45º TIR mirrors can be accurately controlled within ±1º and has a high reproducibility. The average insertion loss of the 45º TIR uncoated mirrors is around 1.6 dB with less than 10% variation. Given the length of such a waveguide channel integrated with 45º mirrors to be 10cm, the total power penalty required will be less than 2.4 dB, which is practical in the real optoelectronic system.

The coupling efficiency of the 45º TIR mirrors is further improved by the metal coating by using a single process. The new metal deposition process combines the capped waveguide technique and the tilted beam exposure technique along with a reusable hard metal mask for metal deposition in E-beam evaporator. This simple process eliminates the usage of traditional lift-off process, and thus greatly simplifies the process and reduces fabrication cost without sacrificing the coating quality. Furthermore, the common

defects induced in the traditional lift-off process, such as retention, ears, and redeposition, will be avoided in the new metal deposition process. Micro-mirrors with 150 nm thick silver coating show more than 90% reflection at both 850 nm and 980 nm. This technique is compatible with PCB manufacturing technology, and offers a low-cost solution to large panel board-level manufacturing for optical interconnects.

CHAPTER 6

FREE-SPACE OPTICAL INTERCONNECT WITH A SINGLE VOLUME HOLOGRAPHIC ELEMENT

The issues of electrical interconnect between chips and boards approaching their performance limit can be alleviated by use of optical carriers to transmit parallel data. Parallel free-space beams for board-to-board interconnects, when combined with electronics, offer a potential solution. In this chapter, we present a novel free-space optical interconnect system realized by a single thin-film polymeric volume holographic element. The only element required for the interconnect system is the thin film holographic element between the light source array and detector array. One 2-spherical-beam volume hologram is used to link each light source with the corresponding photodetector. We demonstrate an 8-channel free-space optical interconnect using a single volume holographic polymer thin film with a channel pitch of 250 μm. Volume holograms are subsequentially recorded with a recording schedule in the same volume of a photopolymer thin film using shifting multiplexing technique at the wavelength of 532 nm. The interconnect length between the light source and detector arrays is 80 mm, with the average link efficiency above 60% with small variation at the wavelength of 532 nm. The effect of wavelength fluctuation on link efficiency of the volume holograms is studied theoretically. Other important system performances, such as cross-talk, mechanical misalignment tolerances, are characterized both theoretically and experimentally [82].

6.1. Introduction to Free-Space Optical Interconnects

As a result of rapid development of VLSI technology enabled by the scaling down of device feature size and the increase of integration density, current electronic interconnection technology has many limitations with respect to bandwidth and packaging density. The bandwidth capacity is limited by the inductance and capacitance of copper wires used as electrical interconnects, as well as the two-dimensional nature of electrical interconnects. Optical interconnect has low cross-talk and low sensitivity to electromagnetic interference, thus provides a promising solution to meet the bandwidth demand. Optical interconnect systems designed for different packaging levels have been studied [1-4]. Compared with optical fiber or waveguide interconnects, free-space optical interconnects [4] (FSOIs) offer more flexible routing of signal beam as a result of using the third spatial dimension for beam propagation. In free space optical interconnects, the distance between two circuit boards that need to communicate with each other is purely empty space. Light signals coming out from the sources substrate propagate in free space to designated locations on the object substrate. Despite of the simplicity of the architecture, the realization of free space system is usually difficult, because the relative positions among the optical components and two substrates should be precisely controlled. The free space interconnect system is also vulnerable to the external environment such as temperature fluctuation and vibration, making the system maintenance an extremely hard task.

There are several physical implementations of FSOI systems, based on monolithic micro-lenses [30], a modified folded 4-f imaging system [31], optical substrate-mode

holograms [32], etc. Compared to the FSOIs that use planar integrated free-space components and lenses (micro-lenses or macro-lens) to collimate and collect the light [30, 31], lensless FSOIs are simpler and require less packaging efforts. Volume holograms multiplexed in thick polymer film have also been proposed for optical interconnects [32, 33]. The high selectivity of thick Bragg holograms can provide low cross talk noise in optical interconnects.

Volume holograms have more restrict Bragg matching condition, compared to thin holograms, due to the thickness of the holographic medium. Thus, based on the unique property of high selectivity of the reading angle and reading wavelength in thick holographic media, thousands of data pages can be recorded in a small common volume through the multiplexing techniques, such as angular multiplexing [35], wavelength multiplexing [37, 38], phase-coded multiplexing [39], shift multiplexing [40], spatial multiplexing [41], and combinations of multiplexing methods [42, 43]. During the past 50 years, volume holographic technology has been widely used in many other applications, including pattern recognition [44, 45], telecommunication [46-48], and optical neural networks [49].

Shift multiplexing technique has been studied in spherical beam volume holographic storage [40]. The high selectivity of thick Bragg holograms can provide low cross talk noise in free space optical interconnects. The major advantage of using multiplexed volume hologram of two spherical beams is to enable the direct interconnect between dense lattices of spherical light sources and photodetector arrays, thus avoid the collimation of spherical light sources in free-space interconnects. Thus, for free-space optical interconnects, spherical wave volume holograms offer a compact, dense, and fast

solution. Bablumian etc proposed a reconfigurable optical interconnect system by using volume holograms multiplexed in thick bacteriorhodopsin film [50]; however, the diffraction efficiency of the M-type hologram was fairly low (4%- 8%) to achieve strong interconnects.

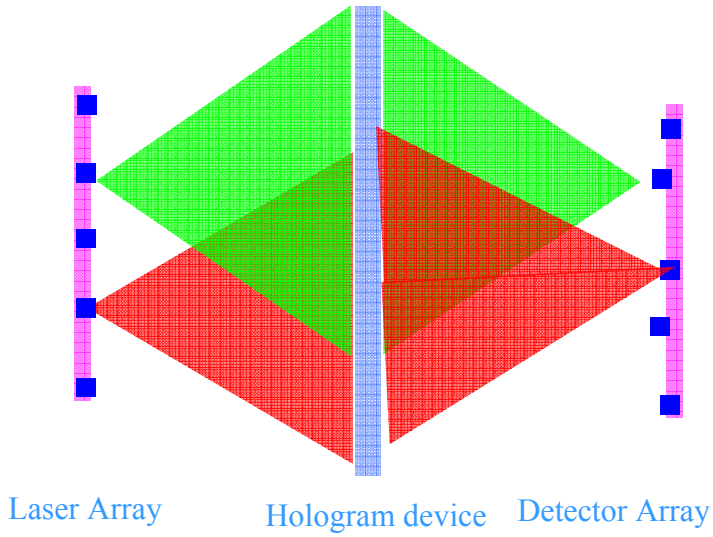

Figure 6.1. The illustration of a free-space optical interconnect by using multiplexed holograms. The light from each source at the laser array is diffracted as a convergent point source and focused at the corresponding target location at the detector array. By changing the hologram device, the interconnect between the source and the target can be reconfigured.

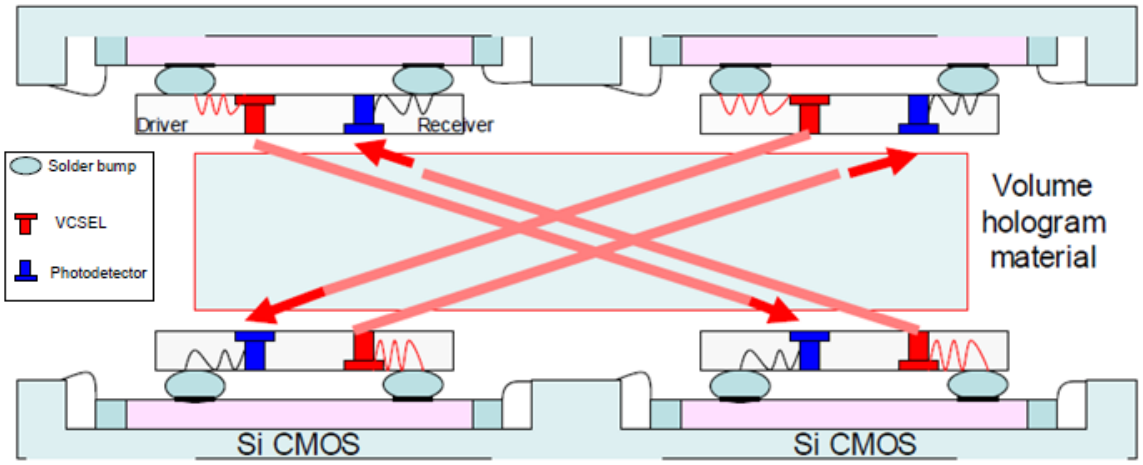

Figure 6.2. The architecture of a free space optical interconnect system by using multiplexed holograms.

Based on the shift multiplexing in spherical beam volume holographic, we propose in this chapter to record spherical beam volume holograms (SBVHs) on a polymer film based on shift multiplexing technique, and then use these volume holograms to build up an interconnect system between the point light source arrays and the detector arrays, as illustrated in Fig 6.1 and Fig 6.2. The following part of this chapter is organized as the followings: First, we recorded a SBVH with high diffraction efficiency by using one convergent spherical beam and one divergent spherical beam. Next, we studied the shift selectivity of the SBVH by observing the intensity change of the diffracted convergent beam when the divergent readout beam was shifted with a computer controlled high precision translation stage. The experimental shift selectivity curve is then compared with the theoretical results. Eight SBVHs are recorded with the same recording setup by evenly shifting the recording medium (i.e., polymer film) to eight different locations. These multiplexed SBVHs are not spatially separated, while they actually share the most common volume in the recording medium, because the space separation of these SBVHs is much less than the size of a single SBVH in the recording

medium. The space separation of these shift locations of the polymer film during recording is also set to be much larger than the shift selectivity of these SBVHs to ensure the negligible cross talk between the adjacent interconnect channels on the detector plane. The optimized recording schedule is also employed during recording to equalize the diffraction efficiency of each SBVH. The wavelength dependence of diffraction efficiency of SBVH is then studied theoretically. Other important system parameters, such as link efficiency and cross talk, are characterized experimentally.

6.2. Study of Shift Selectivity of A SBVH

The SBVH is recorded by the interference of one convergent spherical beam and one divergent spherical beam, as shown in Fig. 6.3. The spherical beams are formed by focusing the collimated beam from a solid-state laser at wavelength $\lambda = 532$ nm with lenses. The distance between the hologram and the divergent point source is d_1 and the distance between the hologram and the convergent point source is d_2. The angle between the axes of the spherical beams is α. The divergent angle of the divergent spherical beam is θ. Both recording beams are TE polarized (E vector perpendicular to the plane of the figure). The recording material is a sample of Aprilis photopolymer [43] with a thickness of 1 mm. It is a photopolymer recording medium which uses the cationic ring-opening mechanism. The thin film polymer holographic media usually offers larger dynamic range than the holographic crystal media, so that multiple strong holograms can be recorded within the same volume of the thin film holographic polymer and provide high link efficiency for free space optical interconnects.

The photopolymer is placed perpendicularly to the axis of the divergent spherical beam. The Aprilis photopolymer has a large dynamic range, and the diffraction efficiency

for a single volume hologram can easily reach above 90%. The system parameters used for recording are: $\theta = 20^{o}$, d_1=4 cm, d_2=4 cm, and α =24.5^{o}. The divergent angle θ of the spherical beam is set to be the same as the divergent angle of vertical cavity surface emitting lasers (VCSELs) or the numerical aperture of stacks of optical fibers or optical channel waveguides, since they are the typical spherical light sources in dense lattices in optical interconnects.

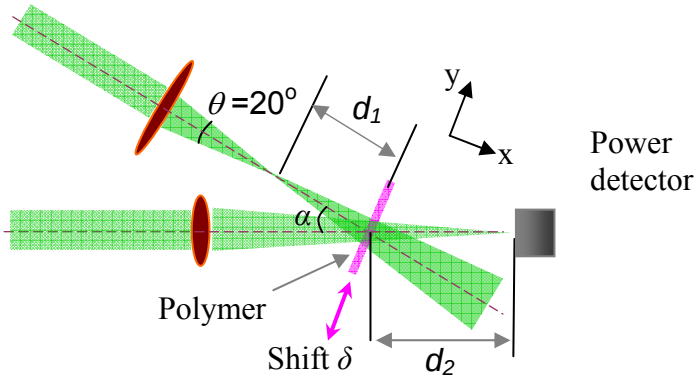

Figure 6.3. Basic schematic of the recoding geometry of the SBVH. θ = 20^{o}, d1 =4 cm, d2 =4 cm, and α =24.5^{o}, λ = 532 nm. The angles are measured in air. The thickness of the polymer film is 1 mm. The size of the hologram is 14 mm by 14 mm.

To study the selectivity of the SBVH, the hologram is then read by using only the divergent beam as shown in Fig. 6.3. The intensity of the diffracted convergent beam is measured by a photodetector placed on the convergent focus point while the polymer is shifted in the direction perpendicular to the axis of the reading divergent beam. The approximate diffraction theory of spherical beam holograms [42] predicts that the diffraction efficiency as a function of shift δ has nulls at integer multiples of the first Bragg null (δ_{Bragg}), the minimum of shift δ required for exactly canceling the

reconstruction of diffracted beam. The experimental and theoretical shift selectivity curves are shown in Fig. 6.4. The first null, i.e., $\delta_{Bragg,}$, occurs at approximately 50 μm, agreeing well with the theoretical prediction. The noticeable asymmetry in the experimental selectivity curve when the reconstructing source is shifted in the opposite direction is mainly due to the asymmetry of the recording geometry, and this selectivity asymmetry is negligible when shift δ is large enough, compared with δ_{Bragg}.

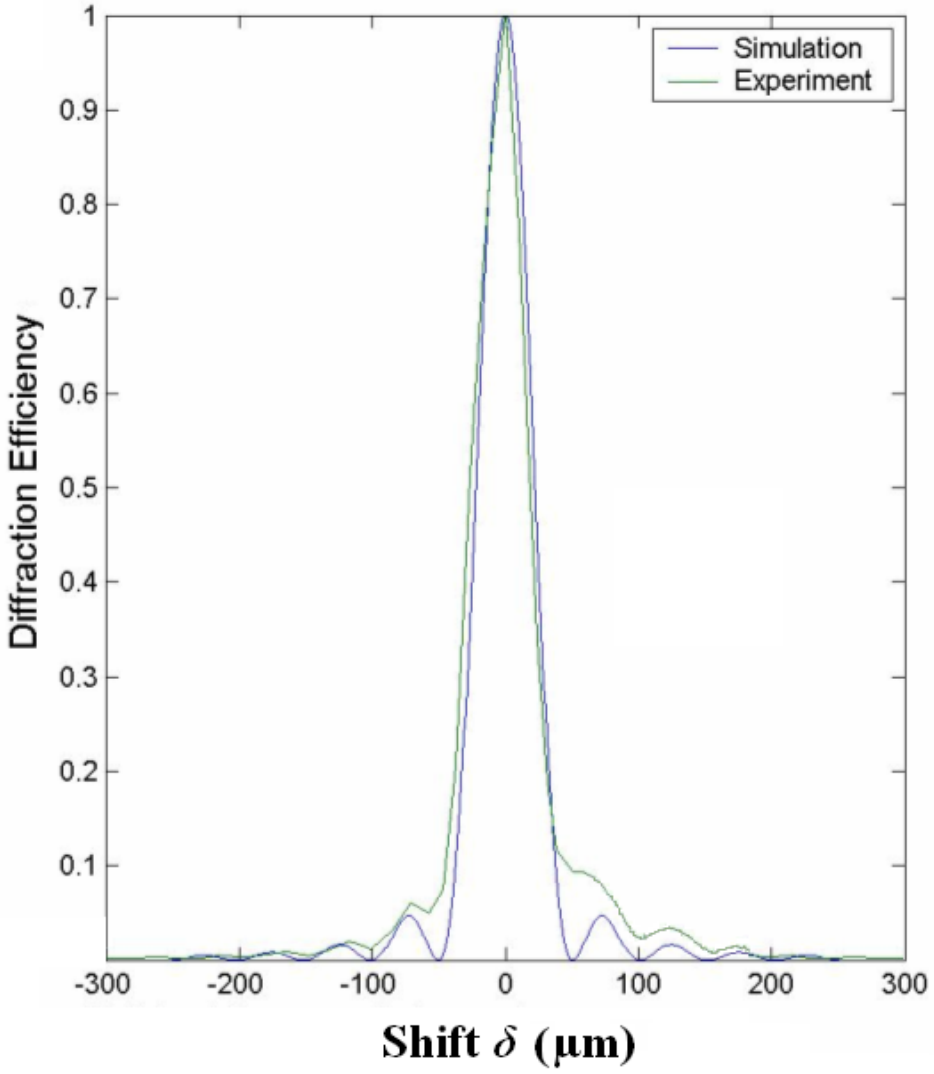

Figure 6.4. Experimental and theoretical selectivity curves (normalized diffraction efficiency versus shift δ).

6.3. Study of the Interconnect System with 8 shift Multiplexed SBVHs

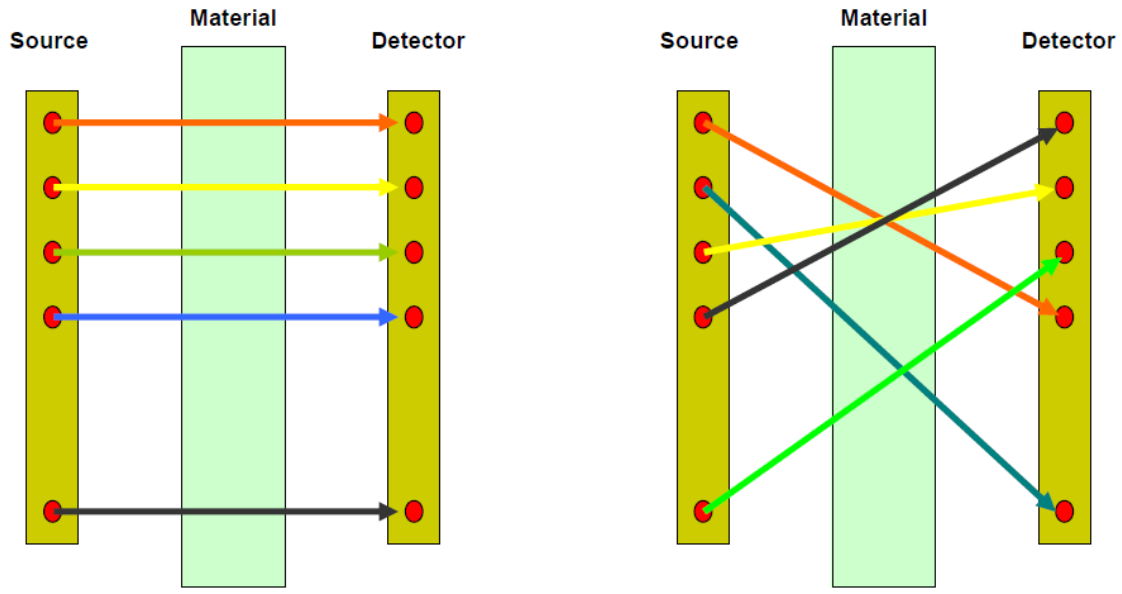

Figure 6.5. Schematic of the different interconnect channel arrangement in the interconnect systems implemented by SBVHs.

Different arrangements for interconnection is possible, so that each laser source can be routed to an arbitrary detector, as illustrated in Fig 6.5, by changing the recording setup for different SBVHs. For simplicity purpose, in this study, the different multiplexed SBVHs are recorded using the same recording setup as shown in Fig. 6.3. The spherical beams are kept the same, and the location of the recording polymer medium is shifted while recording different multiplexed holograms. The distance between sources, i.e., the interconnect density of the light source is limited by shift selectivity. To match the typical channel density of VCSEL array and photodetector array, the shifting distance of the polymer for the next SBVH is set as 250 μm, which corresponds to the fifth Bragg null (5 δ_{Bragg}) of the SBVH. Because the space separation of these shift locations of the polymer film during recording is much larger than the shift selectivity of these SBVHs, the cross

talk between the adjacent interconnect channels on the detector plane is samll. These multiplexed SBVHs are not spatially separated, while they actually share the most common volume in the recording medium, because the space separation of each multiplexed SBVH is much less than the size of a single SBVH (14 mm in diameter) in the recording medium. The maximum number of holograms multiplexed, i.e., the number of the optical interconnect channels, on the polymer depends on the dynamic range of the recording medium and the requirement of the minimum diffraction efficiency of each hologram. The optimized recording schedule is also employed during recording to equalize the diffraction efficiency of each SBVH. Due to the large dynamic range of the Aprilis photopolymer, 8 SBVHs are successfully recorded with high diffraction efficiency (the same with the link efficiency defined in the interconnect system). Figure 6.6 shows that the average diffraction efficiency of the recorded 8 SBVHs is above 60% with small variation.

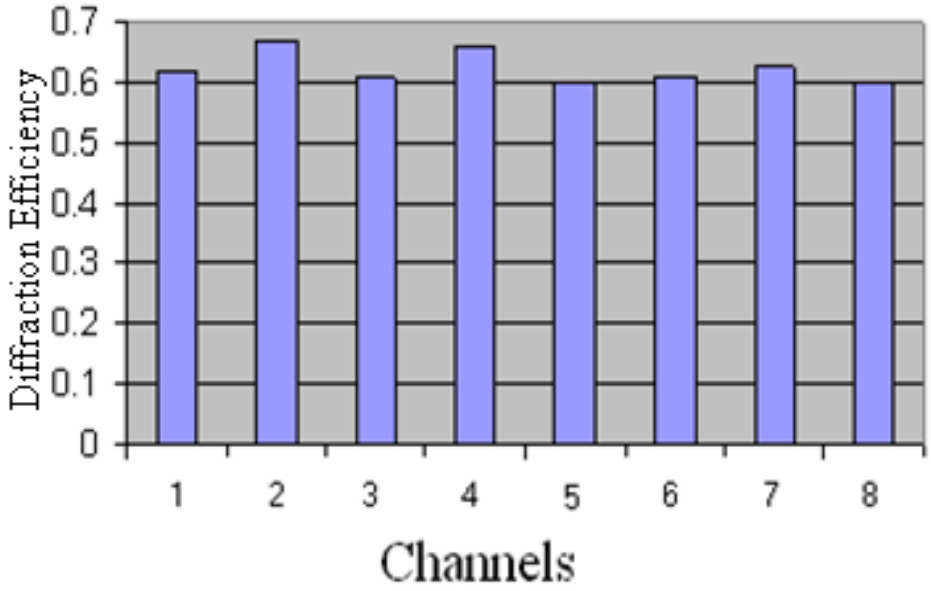

Figure 6.6. Measured diffraction efficiency of 8 channels of shift multiplexed SBVHs.

6.4. Study of Cross Talk of the Interconnect System

Each SBVH establishes a connection channel between a spherical light source and its destination. The spherical light sources can be VCSEL arrays or stacks of optical fibers and optical waveguides, with the destinations being photodetector arrays, or another stack of optical fibers and optical waveguides. Cross talk between adjacent channels is an important system parameter, and is studied experimentally. The recorded SBVHs on the polymer are read by the divergent spherical beams and the diffracted convergent spherical beams are focused at different locations corresponding to the different detectors. The diffraction pattern is detected by a CCD placed on the destination detector plane, as shown in Fig. 6.7. The CCD is tilted along the polymer shift direction. The polymer is shifted to the location where the second SBVH is recorded, such that only the diffraction of the second hologram is Bragg matched. Figure 6.8 shows a CCD picture of the diffraction pattern of the SBVHs on the destination plane, while the 2nd channel connection is established and the signal on the adjacent channels is considered cross talk introduced by the 2nd channel. The measured cross talk is less than -25dB on the adjacent channels. Figure 6.9 shows the combined CCD picture of the diffraction pattern of all 8 SBVHs on the detector plane. The separation between each focused spot is 250 μm, the same with the channel density of the commercial photodetector array. The size of each focused spots is measured as 10 μm (FWHM), which is small compared to the typical aperture of the photodiode (from 50 to 80 μm).

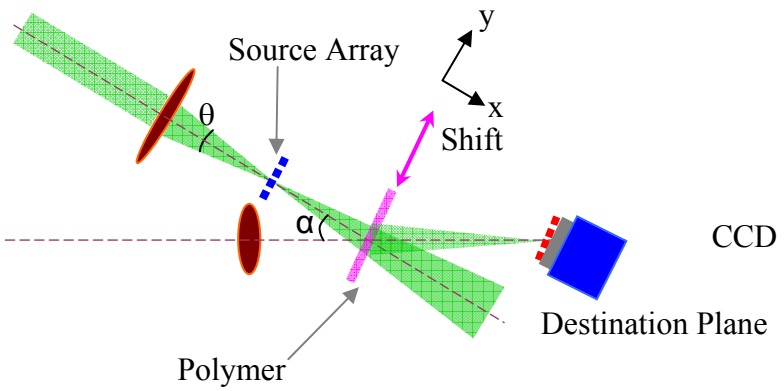

Figure 6.7. Basic schematic of the experimental setup for measuring the cross talk of the SBVHs. $\theta = 20^{o}$, d1 =4 cm, d2 =4 cm, and $\alpha = 24.5^{o}$, $\lambda = 532$ nm. The angles are measured in air. The thickness of the polymer film is 1 mm. The size of the hologram is 14 mm by 14 mm.

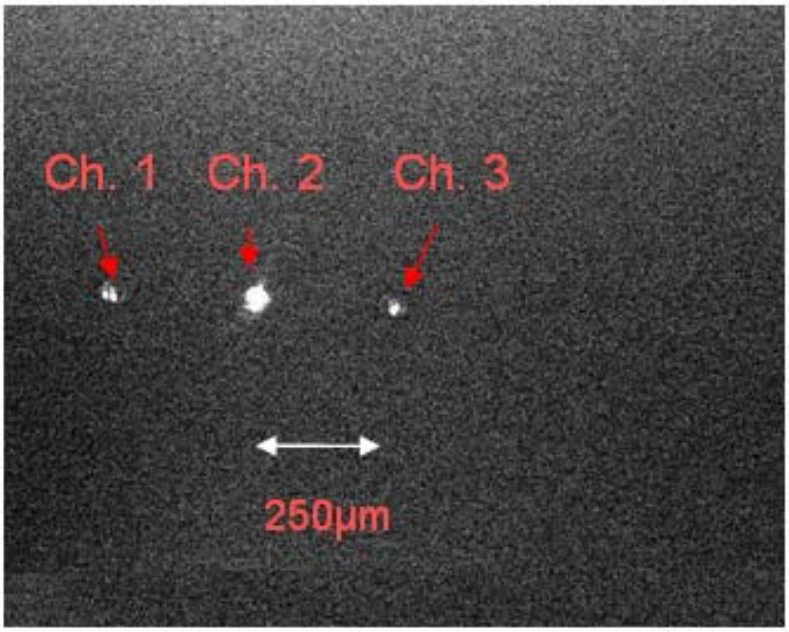

Figure 6.8. A CCD picture shows the diffraction pattern of the SBVHs on the destination plane, while the 2nd channel connection is established and the signal on the adjacent channels is considered cross talk introduced by the 2nd channel. The space separation between the channels is 250 μm.

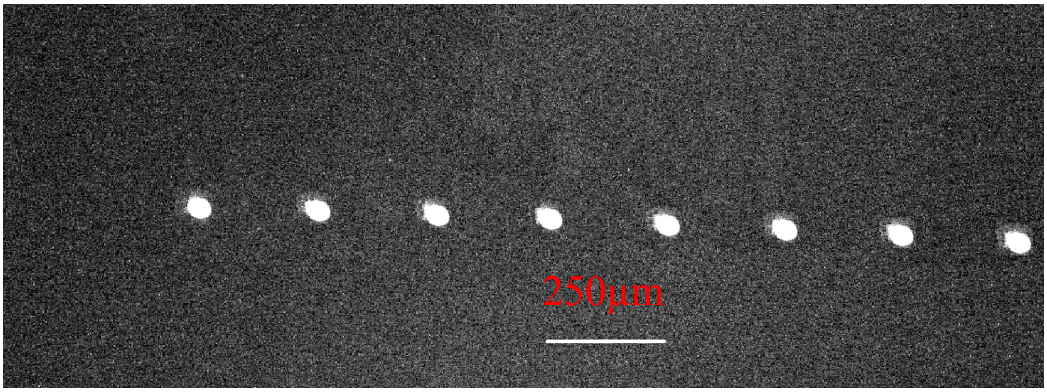

Figure 6.9. The images of the 8 focused beams captured by a CCD placed on the detector plane.

6.5. Study of Thermal Effect and Alignment Tolerance of the Interconnect System

The major challenge to realize reliable free space interconnects is that the system is vulnerable to the external environment, such as temperature fluctuation, vibration, and dust. The VCSEL array is usually used as the light source for optical interconnects as well as for high speed parallel optical data links because of their low threshold currents and simple array integration. The lasing wavelength of VCSEL's is determined primarily by the length, the equivalent refractive index and the lateral size of the cavity. And the operating wavelength of VCSELs varies with the ambient temperature due to the thermal effect. The typical operation temperature of a commercial VCSEL is from 0 ^{o}C to 70^{o}C and the typical temperature coefficient of wavelength tuning is about 0.06 nm/ ^{o}C, so a relatively large wavelength tuning exceeding 4 nm can be observed due to the thermal effect.

SBVH recorded in thick polymer media exhibits wavelength selectivity. The diffraction efficiency of SBVHs decreases, as the reading wavelength of VCSELs was detuned from its optimal value due to the thermal effect. The wavelength Bragg selectivity of SBVHs, $\Delta\lambda_B$, is defined as the wavelength difference as the diffraction

efficiency reach the first null. The wavelength Bragg selectivity of SBVH can be estimated by the plane wave hologram approximation, and it has linear dependence of the reverse of the thickness of the recording material [83]. Figure 6.10 shows that $\Delta\lambda_B$ decreases as the material thickness increases, which means a stricter wavelength selectivity. $\Delta\lambda_B$ is about 0.9 nm at the material thickness of 1 mm, at the given recording geometry in this study. Thus there will be interconnect established, if the wavelength variation of VCSELs due to the thermal effect can not exceed $2*\Delta\lambda_B$, i.e., 1.8 nm. The threshold of the wavelength variation for 3dB interconnect efficiency drop is about 1 nm for 1 mm thick recording media. To guarantee 1 nm wavelength variation for the most commercial VCSELs, the environmental temperature change should be less than 17 ^{o}C. If the ambient temperature fluctuation of the interconnect system exceeds 17 ^{o}C, the use of a thinner recording material will loose the wavelength selectivity of SBVHs. However, as the trade-off, the decrease of the recording material thickness will also loose the shift selectivity of SBVHs, resulting in a higher crosstalk or a lower interconnect density of the free-space interconnect system. Another solution to address the thermal fluctuation for stable interconnects between the VCSELs and the photodetectors is to apply an extra thermal stabilization mechanism, if possible.

The relative positions among the hologram component and two substrates should be precisely controlled to maintain a stable interconnect. The misalignment or vibration tolerance between the SBVH element, the VCSELs array and the detector array can be estimated by the shift selectivity of SBVH. As shown if Fig. 6.4, the misalignment tolerance for 3 dB coupling efficiency drop is about 40 μm along the recording shift direction (i.e., y direction), and is about the same along the direction perpendicular to the

recording plane (i.e., z direction). Because the shift selectivity along the beam propagation direction, i.e., x direction, is much looser than the other directions, the misalignment tolerance in x direction does not need to be considered.

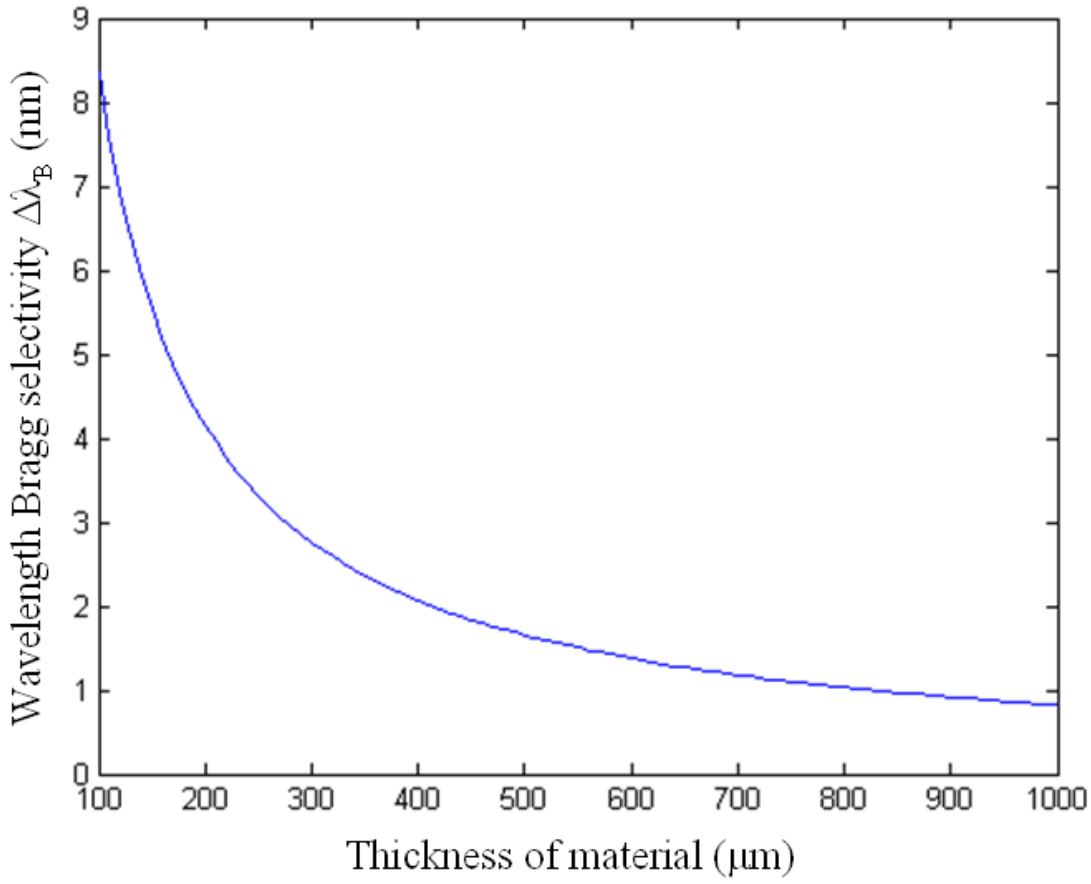

Figure 6.10. The simulation of the wavelength Bragg selectivity versus the thickness of the recording polymer material, given the recording geometry in Fig 6.3.

6.6. Chapter Summary

In summary, we present a novel compact and dense free-space optical interconnect system realized by a single thin-film polymeric volume holographic element. The only element required for the interconnect system is the thin film holographic element between the light source array and detector array. One 2-spherical-beam

hologram is used to link each light source with the corresponding photodetector. We demonstrate an 8-channel free-space optical interconnect using a single volume holographic polymer thin film with a channel pitch of 250 μm. Volume holograms are subsequentially recorded with a recording schedule in the same volume of a photopolymer thin film using shifting multiplexing technique at the wavelength of 532 nm. The interconnect length between the light source and detector arrays is 80 mm, with the average link efficiency above 60% with small variation at the wavelength of 532 nm. The effect of wavelength fluctuation on link efficiency of the volume holograms is studied theoretically. Other important system performances, such as cross-talk, mechanical misalignment tolerances, are characterized theoretically and experimentally. By switching the volume holographic element between the source and the output arrays, it is easy to achieve interconnect reconfiguration.

CHAPTER 7

FUTURE DIRECTIONS AND APPLICATIONS

The research work presented in this thesis focuses on some fundamental studies of optical interconnects for PCB substrates, e.g., developing low-loss optical polymer waveguides with integrated highly efficient out-of-plane couplers for optical interconnect on PCB substrate, as well as the demonstrating of a simple free-space optical interconnect system by using a volume holographic thin film. The research presented in this thesis involves a new type of low-loss polymer waveguides (i.e., capped waveguide) by using contact photolithography with considerable performance improvement over the conventional waveguides. An integrated 45° metal coated micro-mirror with polymer optical waveguides is demonstrated to provide efficient surface normal light coupling between waveguides and optoelectronic devices for optical interconnects, by using a simple method. These fundamental studies prove the feasibility of applying the low loss optical waveguide circuit to the optical interconnects on PCB substrate. However, the integration of the active optoelectronic components, such as VCSELs and photodetectors, along with the optical waveguide circuit on PCB substrate, should be demonstrated. And the high speed performance of the integrated system, such as bit error rate (BER), should be characterized experimentally.

7.1 High Speed Optical Test on the Embedded Optical Interconnect System

Figure 7.1 shows the typical schematic of an embedded guided-wave optical interconnect system on PCB substrate. The elements, involved in providing high-speed

optical communications within a PCB board, are shown in Fig 7.1. These include a VCSEL, a photodetector, embedded micro-lens, surface-normal waveguide couplers (45º micro-mirrors), and a polymer-based channel waveguide functioning as the physical layer of optical interconnects. The VCSEL and the photodetector are fully embedded inside the PCB layer, and the driving electrical modules for the VCSEL and the photodetector are bonded on the surface of the PCB substrate by the flip-chip process. The VCSEL and photodetector modules are connected to the VCSEL and photodetector through electrical vias. Currently, out-of-plane optical deflection is inevitable in most board-to-board or chip-to-chip optical interconnect system. Since the optical path of laser-to-waveguide (or waveguide-to-photodetector) is large in the packaging technologies, it is necessary to insert focusing or collimating elements (e.g., micro-lens array) into optical systems to improve the coupling efficiency. The optical coupling between VCSELs, optical waveguides and photodetectors is based on a single-lens array and on 45° mirrors in the waveguides. In such an optical configuration, VCSELs, photodetectors, and 45° mirrors in the waveguides form out-of-plane alignment along two optical axes perpendicular to each other. In such fully embedded system, the insertion of optoelectronic components into microelectronic systems is much more realistic, because the major stumbling block for implementing optical interconnection onto high performance PCB substrate is the packaging incompatibility. There is no interface problem between the electronic and optoelectronic components on the PCB substrate.

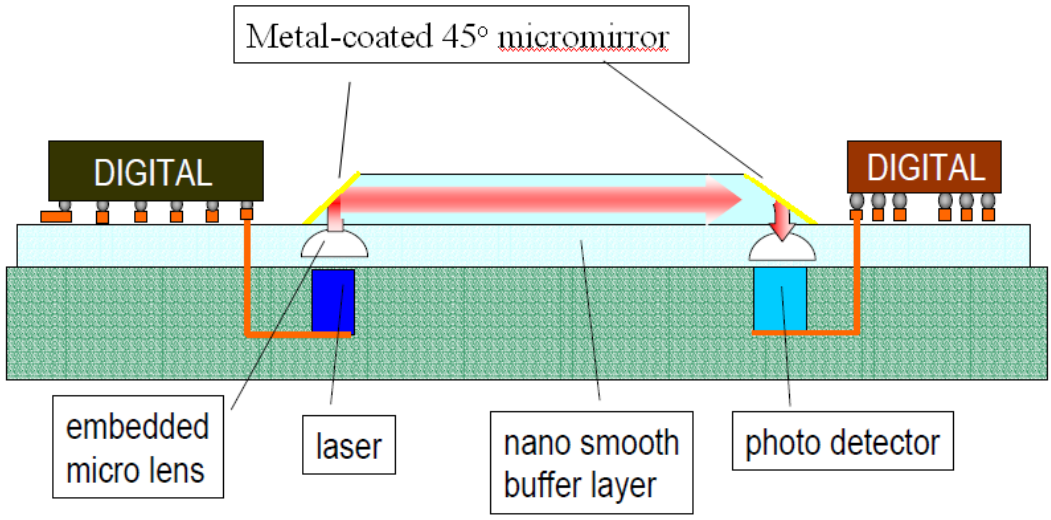

Figure 7.1. The schematic of integration of the active optoelectronics and optical waveguide circuit along with 45° metal coated micro-mirrors for high speed optical interconnects embedded on PCB substrate.

To realize embedded board level optical interconnects, many practical issues need to be addressed such as thermal management, process compatibility, reliability and cost effective fabrication and integration process. Finally, the system performance evaluation needs to be carried on for high speed optical interconnects. For highly reliable operation, system should secure an adequate signal-to-noise ratio, as the current state-of-the-art copper circuit on FR-4 can only operate at a few gigahertz. We should demonstrate more than 10 gigahertz interconnecting rate for each optical waveguide interconnect channel.

As the preliminary study of high speed test for the embedded board level optical interconnects, we have tested the high speed performance of the capped waveguide array with 45º micro mirrors integrated at the end. The modulated optical signal from a single frequency fiber laser modulated by a 40 GHZ electro-optic modulator is coupled into the optical waveguide by 45º TIR micro-mirrors through a 50/125 μm multimode fiber. The operating wavelength of the laser is 1550 nm. After propagation through the waveguide,

the light is coupled out by the surface normal 45º TIR micro-mirrors and collected by a 62.5/125 μm multimode fiber. And the other side of the multimode fiber is connected to the high speed photodector operating at 1550 nm. A high speed oscilloscope is connected to the photodiode for the eye diagram of the signal response. The modulation speed of the electro-optic modulator is controlled by a signal generator at 40 Gbps. The total length of the 50×50 μm^2 multimode optical waveguide channels is 8 cm. Figure 7.2 shows the eye diagrams for the input signal and the output signal of the waveguides with 45º TIR micro-mirrors integrated. Due to the low propagation loss of the capped optical waveguides and the high coupling efficiency of the 45º micro-mirrors, we do not see any noticeable degeneration of high speed signals between the input and output.

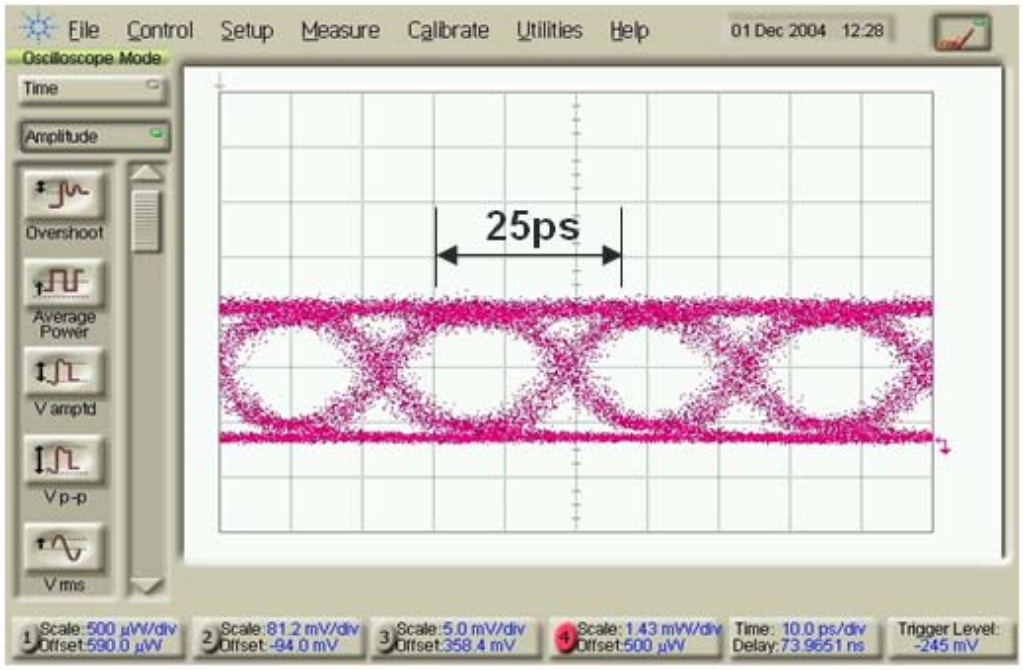

(a)

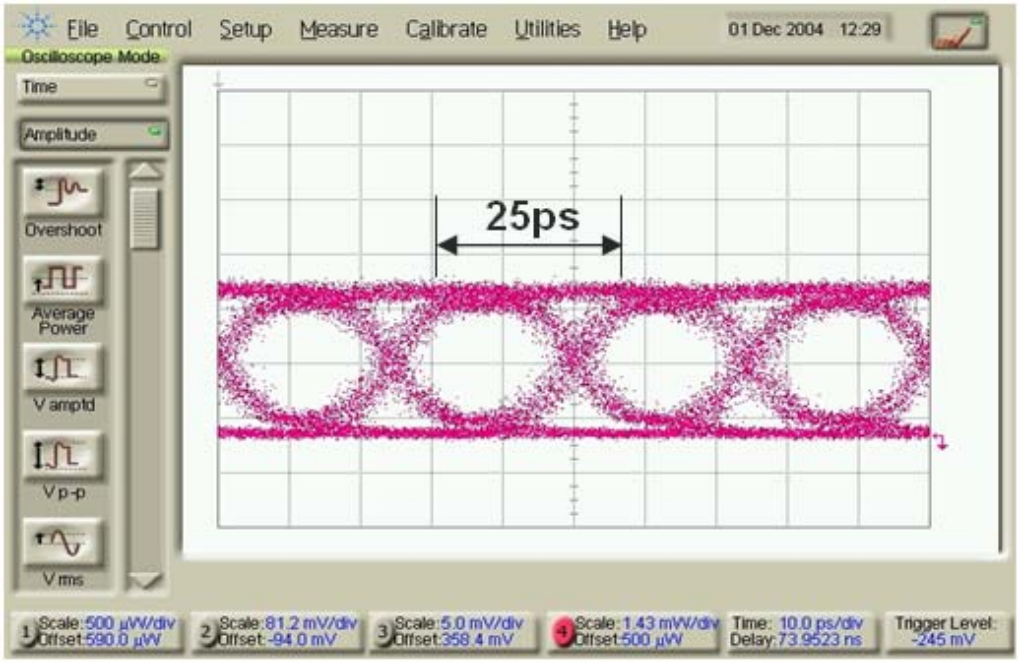

(b)

Figure 7.1. The eye diagrams at 40Gbps of (a) the input signal and (b) the output signal.

CHAPTER 8

CONCLUSIONS

The main focus of this thesis has been the fundamental studies of optical interconnects for PCB substrates. To achieve the high speed optical interconnects on PCB substrate, it is important to demonstrate a low loss optical waveguide circuit along with the efficient surface normal couplers. To be compatible with the PCB industry, the integrated optical waveguide circuit on PCB substrate in this thesis is fabricated by the photolithography using the PCB facilities. The theoretical and experimental investigations on the limitations of using mercury i-line UV proximity photolithography have been carried out, and the metallization techniques for fine copper line formation are explored. The theoretical analysis based on Fresnel diffraction indicates that the key factors that hinder the finer feature size formation through proximity photolithography is the air gap between the photoresist and the mask. An expression for the minimum transferable feature size is obtained from the experiments. The experimental data confirm the validity of the theoretic analysis.

Then, a new type of low-loss polymer waveguides (i.e., capped waveguide) is demonstrated by using contact photolithography with considerable performance improvement over the conventional waveguides. By simultaneously patterning the core and the top cladding layers in capped waveguides, the effect of fabrication defects can be considerably reduced, and the propagation lose is reduced by at least 20% compared to conventional waveguides. To characterize the propagation properties of planar optical

waveguides, a reliable, nondestructive, and real-time technique is developed based on accurately imaging the scattered light from the waveguide using a sensitive CCD camera that has a built-in integration functionality. This technique can be used for real-time investigation of the propagation properties (loss, mode profile, bending properties, etc.) and the fabrication quality of planar waveguides, which provides better sensitivity than other techniques. Using the characterization tool developed, we measured capped waveguides with loss coefficients of 0.065 dB/cm at λ = 850 nm, and 0.046 dB/cm at λ = 980 nm with the accuracy of 0.008 dB/cm.

It is critical to provide highly efficient surface normal light coupling between waveguides and optoelectronic devices for optical interconnects. A simple method is presented in the thesis to integrate 45° TIR micro-mirrors with polymer optical waveguides by an improved tilted beam photolithography (with the aid of de-ionized water) on PCBs. The 45º TIR coupling mirrors are shaped at the ends of the waveguides in one exposure step to provide surface normal light coupling between waveguides and optoelectronic devices by using the low cost PCB facility in a class-1000 substrate laboratory. The slope of the 45º TIR mirrors can be accurately controlled within ±1º with high reproducibility. The average insertion loss of the 45º TIR uncoated mirrors is around 1.6 dB with less than 10% variation.

The coupling efficiency of the 45º TIR mirrors is further improved by metal coating using a single process. The new metal deposition process combines the capped waveguide technique and the tilted beam exposure technique along with a reusable hard metal mask for metal deposition in an E-beam evaporator. This simple process eliminates the usage of traditional lift-off process, and thus greatly simplifies the process and

reduces fabrication cost without sacrificing the coating quality. Furthermore, the common defects induced in the traditional lift-off process (such as retention, ears and redeposition) will be avoided in the new metal deposition process. Micro-mirrors with 150 nm thick silver coating show more than 90% reflection (an insertion loss of 0.46 dB) at both 850 nm and 980 nm. This technique is compatible with PCB manufacturing technology and offers a low-cost solution to large panel board-level manufacturing for optical interconnects.

Parallel free-space beams for board-to-board interconnects, when combined with electronics, offer a potential solution for high speed PCB substrate. For the study of free-space optical interconnects, we demonstrate a novel free-space optical interconnect system realized by a single thin-film polymeric volume holographic element. The only element required for the interconnect system is the thin film holographic element between the light source array and detector array. One 2-spherical-beam hologram is used to link each light source with the corresponding photodetector. We demonstrate an 8-channel free-space optical interconnect using a single volume holographic polymer thin film with a channel pitch of 250 μm. Volume holograms are subsequentially recorded with a recording schedule in the same volume of a photopolymer thin film using shift multiplexing technique at the wavelength of 532 nm. The interconnect length between the light source and detector arrays is 80 mm, with the average link efficiency above 60% with small variation at the wavelength of 532 nm. The effect of wavelength fluctuation on link efficiency of the volume holograms is studied theoretically. Other important system performances, such as cross-talk and mechanical misalignment tolerances, are characterized theoretically and experimentally. By switching the volume holographic

element between the source and the output arrays, it is easy to achieve interconnect reconfiguration.

A brief summary of the main contributions of this research follows:

- I studied the effect of air gap in proximity UV photolithography, and demonstrated sub 10 μm copper circuitry on PCBs for flip-chip application.
- I developed the novel low loss capped polymer waveguides with 20% loss improvement over conventional waveguides.
- I developed a precision non-destructive waveguide measurement technique.
- I integrated 45^{o} polymer TIR micro-mirrors with waveguides by using an easy and cost effective method. The technique is compatible with large scale PCB process.
- I developed a simple process for the metal coating on the surface of 45^{o} polymer micro-mirrors with a reusable hard mask, thus eliminating the regular lift-off process.
- I demonstrated 8 channel high efficient free-space optical interconnect using a holographic element**.**

REFERENCES

1. A. V. Krishnamoorthy and D. A. B. Miller, "Scaling optoelectronic VLSI circuits into the 21st century: A technology roadmap," *IEEE J. Sel. Top. Quantum Electron.* 2(1), 55–76 (1996).

2. J. W. Goodman, F. J. Leonberger, S. Y. Kung, and R. A. Athale, "Optical interconnects for VLSI systems*," Proc. IEEE* 72(7), 850–866 (1984).

3. M. Li, and S. J. Sheard, "Waveguide couplers using parallelogramic-shaped blazed gratings," *Opt. Commun*. 109(3–4), 239–245 (1994).

4. M.Gruber, S. Sinzinger, and J. Jahns, "Optoelectronicmultichip module based on planarintegrated free-space optics," *Proc. SPIE*, *Optics Comput.* 4089 (2000).

5. G. Kim and R. T. Chen, "Three-dimensionally interconnected multi-bus-line bidirectional optical backplane," *Opt. Eng.* 38, 9 (1999).

6. D. H. Hartman, "Radiant Curved Polymer Optical Waveguides on Printed circuit Boards for Photonic Interconnection Use", *Appl. Opt.* 28, 1031-1033 (1988).

7. J.W. Kang, J. Kim, and J.J. Kim, "Optimized Oxygen Plasma Etching of polycarbonate for Low-Loss Optical Waveguide Fabrication", *Jpn. J. Appl. Phys.* 40, 3215-3219 (2001).

8. W.H. Wong, J. Zhou, and E.Y.B. Pun, "Low-loss polymeric optical waveguides using electron-beam direct writing", *Appl. Phys. Lett.* 78(15), 2110-2112 (2001).

9. O.S. Rosch, W. Berhard, R. Miller-Fielder, P. Dannberg, A. Brauer, R. Buestrich, and M. Popall, "High Performance Low Cost Fabrication Method for Integrated Polymer Optical Devices", *SPIE Conference on Linear Optical Properties of Waveguide and Fibers*, 3799, 214-224 (1999).

10. T. Hanemann, H. Ulrich, R. Ruprecht, J. H. Husselt, "Micromolding of Polymer Waveguides*", SPIE Conference on Linear Optical Properties of Waveguide and Fibers*, 3799, 225-229 (1999).

11. R. G. Hunsberger, *Integrated Optics Theory and Technology*, New York, Springer-Verlag (1985).

12. C. Teng, "Precision measurements of the optical attenuation profile along the propagation path in thin-film waveguides," *Appl. Opt.* 32(7), 1051–1054 (1993).

13. J. Wei, X. Xu, Y. Ding, Z. Kang, Y. Jiang, and J. Gao, "Improved method for loss measurements in planar waveguides," *Opt. Lasers Eng.* 45(3), 419–422 (2007).

14. S. Chen, Q. Yan, Q. Xu, Z. Fan, and J. Liu, "Measuring mode propagation losses of integrated optical waveguides: a simple method," *Opt. Commun.* 256(3), 68–72 (2005).

15. Y. Okamura, S. Yoshinaka, and S. Yamamoto, "Measuring mode propagation losses of integrated optical waveguides: a simple method," *Appl. Opt.* 22(23), 3892–3894 (1983).

16. Y. Okamura, S. Sato, and S. Yamamoto, "Simple method of measuring propagation properties of integrated optical waveguides: an improvement," *Appl. Opt.* 24(1), 57–60 (1985).

17. T. A. Strasser and M. C. Gupta, "Optical loss measurement of low loss thin-film waveguides by photographic analysis," *Appl. Opt.* 31(12), 2041–2046 (1992).

18. J. T. Kim, B. C. Kim, M. Jeong, and M. Lee, "Fabrication of a micro-optical coupling structure by laser ablation," *J. Mater. Process. Technol.* 146(2), 163–166 (2004).

19. L. Schares, J. A. Kash, F. E. Doany, C. L. Schow, C. Schuster, D. M. Kuchta, P. K. Pepeljugoski, J. M. Trewhella, C. W. Baks, R. A. John, L. Shan, Y. H. Kwark, R. A. Budd, P. Chiniwalla, F. R. Libsch, J. Rosner, C. K. Tsang, C. S. Patel, J. D. Schaub, R. Dangel, F. Horst, B. J. Offrein, D. Kucharski, D. Guckenberger, S. Hegde, H. Nyikal, C. Lin, A. Tandon, G. R. Trott, M. Nystrom, D. P. Bour, M. R. T. Tan, and D. W. Dolfi, "Terabus: terabit/second-class card-level optical interconnect technologies," *IEEE J. Sel. Top. Quantum Electron.* 12(5), 1032–1044 (2006).

20. N. Herdrickx, J. V. Erps, G. V. Steenberge, H. Thienpont, and P. V. Daele, "Laser ablated micromirrors for printed circuit board integrated optical interconnections," *IEEE Photon. Technol. Lett.* 19(11), 822–824 (2007).

21. S. Garner, S.-S. Lee, V. Chuyanov, A. Chen, A. Yacoubian, W. Steier, and L. Dalton, "Three-dimensional integrated optics using polymers," *IEEE J. Quantum Electron.* 35(8), 1146–1155 (1999).

22. S. Lehmacher, and A. Neyer, "Integration of polymer optical waveguides into printed circuit boards," *Electron. Lett.* 36(12), 1052–1053 (2000).

23. L. Wang, X. Wang, W. Jiang, J. Choi, H. Bi, and R. T. Chen, "45° polymer-based total internal reflection coupling mirrors for fully embedded intraboard guided wave optical interconnects," *Appl. Phys. Lett.* 87(14), 141110 (2005).

24. M. Kagami, A. Kawasaki, and H. Ito, "A polymer optical waveguide with out-of-plane branching mirrors for surface-normal optical interconnections," *J. Lightwave Technol.* 19(12), 1949–1955 (2001).

25. A. L. Glebov, J. Roman, M. G. Lee, and K. Yokouchi, "Optical interconnect modules with fully integrated reflector mirrors," *IEEE Photon. Technol. Lett.* 17(7), 1540–1542 (2005).

26. S. Han, I. Cho, S. Hwang, W. Lee, and S. Ahn, "A high-density two-dimensional parallel optical interconnection module," *IEEE Photon. Technol. Lett.* 17(11), 2448–2450 (2005).

27. N. Hendrickx, J. Van Erps, E. Bosman, C. Debaes, H. Thienpont, and P. Van Daele, "Embedded micromirror inserts for optical printed circuit boards," *IEEE Photon. Technol. Lett.* 20(20), 1727–1729 (2008).

28. T. Yoshimura, M. Miyazaki, Y. Miyamoto, N. Shimoda, A. Hori, and K. Asama, "Three-dimensional optical circuits consisting of waveguide films and optical z-connections," *J. Lightwave Technol.* 24(11), 4345–4352 (2006).

29. K. Y. Hung, H. T. Hu, and F. G. Tseng, "A novel fabrication technology for smooth 3D inclined polymer microstructures with adjustable angles," *Proc. of the International Confer. on Solid State Sensors*, *Actuators and Microsystems*, USA, 821–824 (2003).

30. E.M. Strzelecka, D.A. Louderback, B.J. Thibeault, G.B. Thompson, K. Bertilsson, and L.A. Coldren, "Parallel free-space optical interconnect based on arrays vertical-cavity lasers and detectors with monolithic microlenses," *Appl. Opt.* 37(14), 2811-2821 (1998).

31. G. Li, D. Huang, E. Yuceturk, P. j. Marchand, S. Esener, V. H. Ozguz, and Y. Liu, "Three-dimensional optoelectronic stacked processor by use of free-space optical interconnection and three-dimensional VLSI chip stacks," *Appl. Opt*. 41(2), 348-360 (2002).

32. J. Yeh and R.K. Kostuk, "Free-space holographic optical interconnects for board-to-board and chip-to-chip interconnections," *Opt. Lett.* 21(16), 1274-1276 (1996).

33. G. Lippmann, *J. de Phys.* **3**, 97 (1894).

34. E. N. Leith, A. Kozma, J. Upatnieks, J. Marks, and N. Massey, "Holographic data storage in three-dimensional media," *Appl. Opt.* **5**, 1303-1311 (1966).

35. L. d'Auria, J. P. Huignard, and E. Spitz, "Holographic read-write memory and capacity enchancement by 3-D storage," *IEEE Trans. Magn., MAG*-**9**, 83-94 (1973).

36. K. Curtis, A. Pu, and D. Psaltis, "Method for holographic storage using peristrophic multiplexing," *Opt. Lett.* **19**, 993-994 (1994).

37. G. A. Rakuljic, V. Levya, and A. Yariv, "Optical data storage by using orthogonal wavelength –multiplexed volume holograms," *Opt. Lett.* **17**, 1471-1473 (1992).

38. S. Yin, H. Zhou, F. Zhao, M. Wen, Y. Zang, J. Zhang, and F. T. S. Yu, "Wavelength-multiplexed holographic storage in a sensitive photorefractive crystal using a visible-light tunable diode-laser," *Opt. Commun.* **101**, 317-321 (1993).

39. C. Denz, G. Pauliat, and Roosen, "Volume hologram multiplexing using a deterministic phase encoding method," *Opt. Commun.* **85**, 171-176 (1991).

40. G. Barbastathis, M. Levene, and D. Psaltis, "Shift multiplexing with spherical reference waves," *Appl. Opt.* **35**, 2403-2417 (1996).

41. H. Y. S. Li, and D. Psaltis, "Three dimensional holographic disks," *Appl. Opt.* **33**, 3764-3774 (1994).

42. S. Campbell, X. M. Yi, and P. Yeh, "Hybird sparse-wavelength angle multiplexed optical data storage system," *Opt. Lett.* **19**, 2161-2163 (1994).

43. A. Pu, and D. Psaltis, "High density recording in photopolymer-based holographic 3-D disks," *Appl. Opt.* **35**, 2389-2398 (1996).

44. C. S. Weaver, and J. W. Goodman, "A technique for optically convolving two functions," *Appl. Opt.* **5**, 248-1249 (1966).

45. G. R. Mangasaryan, B. E. Khaikin, and V. S. Khitrova, "Matched filtering on basis of thick holograms for fingerprint identification," *Opt. Comm.* 22, 169-172 (1977).

46. M. C. Parker, A. D. Cohen, and R. J. Mears, **"**Dynamic holographic spectral equalization for WDM,**"** *IEEE Photon. Technol. Lett.* **9**, 529-531 (1997).

47. M. C. Parker, A. D. Cohen, and R. J. Mears, "Dynamic digital holographic wavelength filtering," *J. Lightwave Technol.* **16**, 1259-1270 (1998).

48. A. Sato, M. Scepanovic, and R. K. Kostuk, "Holographic edge-illuminated polymer Bragg gratings for dense wavelength division optical filters at 1550 nm," *Appl. Opt.* **42**, 778-784 (2003).

49. E. G. Paek, and D. Psaltis, "Holographic implementation of a neural network model," *J. Opt. Soc. Am. A* **3**, 32 (1986).

50. A. S. Bablumian and T. F. Krile, "Multiplexed holograms in thick bacteriorhodopsin films for optical memory/interconnections," *Opt. Eng.* 39(11), 2964-2974 (2000).

51. *International Technology Roadmap for Semiconductors, Assembly and Package*, ITRS 2007 Edition.

52. S.C. Johnson, "Flip-chip packaging becomes competitive," *Semiconductor International*, vol. 32, n 5, pp. 10-13 (2009).

53. W. Worobey, and J. Rutkiewicz, "Tantalum thin-film RC circuit technology for a universal active filter," *IEEE Transactions on Parts, Hybrids, and Packaging,* vol. 12, No. 4, pp. 276-282 (1976).

54. M. Mahalingam, "Surface-mount plastic packages-an assessment of their thermal performance," *IEEE Transactions on Components, Hybrids, and Manufacturing Technology*, vol. 12, No. 4, pp. 745-752 (1989).

55. A. Okuno, N. Fujita, and Y. Ishikawa, "High reliability, high density, low cost packaging systems for matrix systems for matrix BGA and CSP by vacuum printing encapsulation systems (VPES)," *IEEE Transactions on Advanced Packaging*, vol. 22, No. 3, pp. 391-397 (1999).

56. V. Kripesh, S.W. Yoon, V.P. Ganesh, N. Khan, M.D. Rotaru, W. Fang, and M.K. Iyer, "Three-dimensional system-in-package using stacked silicon platform technology," *IEEE Transactions on Advanced Packaging*, vol. 28, No. 3, pp. 377-386 (2005).

57. R.R. Tummala, "Foreword special issue on system-on-package (SOP)," *IEEE Transactions on Advanced Packaging*, vol. 27, No. 2, pp. 239-240 (2004).

58. J.C. White, H.G. Craighead, R.E. Howard, L.D. Jackel, R.E. Behringer, R.W. Epworth, D. Henderson, and J.E. Sweeney, "Submicron, vacuum ultraviolet contact lithography with an F2 excimer laser," *Applied Physics Letters*, vol. 44, no. 1, pp. 22-24 (1984).

59. B. Bednar, J. Kralicek, and J. Zachoval, *Resists in Microlithography and Printing*, 2nd ed., Amsterdam, Elsevier Press (1993).

60. M. Born and E. Wolf, *Principles of Optics*, 4th ed., New York, Pergamon Press (1970).

61. Y. Wada and K. Uehara, "Optical limitation in fine pattern photolithography," *Jap. J. Appl. Phys.,* vol 13, pp. 2014 (1974).

62. D. Widmann and K. U. Stein, "Semiconductor technologies with reduced dimensions," *European Solid State Circuits Conference*, vol. 2 (1976).

63. P. Jalonen, "A new concept for making fine line substrate for active component in polymer," *Microelectronics Journal*, v 34, n 2, p 99-107 (2003).

64. R.R. Tummala and M. Swaminathan, *Introduction to SYSTEM-ON-PACKAGE (SOP)*, McGraw Hill (2008).

65. D. Manessis, Y. Shiu-Fang, A. Ostmann, R. Aschenbrenner, and H. Reichl, "Technical understanding of resin-coated-copper (RCC) lamination processes for

realization of reliable chip embedding technologies," *2007 Electronic Components and Technology Conference*, p 278-85 (2007).

66. S. J. Eun, G.C. Hyun, K.W. Chang, and K.S. Young Soo, "Copper metallization on the surface-modified polyimide films by electroless plating method," *Molecular Crystals and Liquid Crystals*, v 492, p 275-82 (2008).

67. F. Liu, G.E. White, V. Sundaram, A.O. Aggarwal, S.M. Hosseini, D. Sutter, and R.R. Tummala, "A novel technology for stacking microvias on printed wiring board," *Proceeedings 53rd IEEE Electronics Components and Technology Conference,* pp. 1134-39 (2003).

68. F. Wang, F. Liu, L. Kong, V. Sundaram, R. Tummala, and A. Adibi, "Proximity printing in sub-10 μm Feature Size Substrate Packaging Technology", Accepted by *IEEE Trans. Of Adv. Packaging* (2010).

69. F. Liu, F. Wang, G. K. Chang, R. Tummala, and A. Adibi, "Capped optical polymeric waveguide", *Optic. Comm.* 28(2), 127-131 (2007).

70. M. Moyniham, B.Sicard, T.Ho, etc., "Progress toward board-level Optical Interconnect technology", *Proceedings of SPIE*, vol. 5731 pp50-62 (2005).

71. F. Wang, F. Liu, and A. Adibi, "Precision measurements for propagation properties of high definition polymer waveguides by imaging of scattered light", *Opt. Eng*. 47(2), 024602 (2008).

72. F. Wang, F. Liu, G. K. Chang, M. Q. Yao, A. Adibi, and R. Tummala, "A real time precision characterization technique for low loss optical polymeric waveguide and lightwave circuits*", Journal of Microelectronics and Electronic Packaging*, 5(1), 26-30 (2008).

73. D. Kim, S. Ahn, I. Cho, D. Im, S. Md. S. Muslim, and H. Park, "Fabrication of thermally stable and cost-effective polymeric waveguide for optical printed-circuit board", *Optics Express,* 16(21), pp. 16798-16805 (2008).

74. N. Bamiedakis, A. Wonfor, R.V. Penty, L. White, J.V. DeGroot, K. Hueston, T.V. Clapp, M. Click, and J. Beals, "A terabit capacity passive polymer optical backplane based on a novel meshed waveguide architecture", *Applied Physics A: Materials Science & Processing*, v 95, n 4, p 983-8 (2009).

75. R. Dangel, C. Berger, r. Beyeler, L. Dellmann, M. Gmur, R. Hamelin, F. Horst, T. Lamprecht, T. Morf, S. Oggioni, M. Spreafico, and B.J. Offrein, "Polymer-waveguide-based board-level optical interconnect technology for datacom applications", *IEEE Trans. Of Adv. Packaging*, v31, n 4, P 759-67 (2008).

76. F. Wang, F. Liu, and A. Adibi, "45 degree polymer micro-mirror integration for board-level three-dimensional optical interconnects", *Opt. Express* 17(13), 10514-10521 (2009).

77. F. Wang, F. Liu, and A. Adibi, "A cost efficient way for metal-coated 45 degree polymer micro-mirror integration for optical interconnects", ready to submit to *Opt. Express* (2010).

78. F.M. Sogandares and E.S. Fry, "Absorption spectrum (340–640 nm) of pure water. I. Photothermal measurements", *Applied Optics*, Vol. 36, Issue 33, pp. 8699-8709 (1997)

79. P. Carlberg, M. Grayczyk, E.L. Sarwe, I. Maximov, M. beck, and L. Montelius, "Lift-off process for nanoimprint lithography", *Microelectronic Engineering*, V 67-68, P 203-7 (2003).

80. M. Hatzakis, B.J. Canavello, and J.M. Shaw, "Single-step optical lift-off process", IBM Journal of Research and Development, 24(4), P 452-460 (1980).

81. Y. Chen, K. Peng, and Z. Cui, "A lift-off process for high resolution patterns using PMMA/LOR resist stack", *Microelectronic Engineering*, V 73-74, P 278-81 (2004).

82. F. Wang, C. Hsieh, O. Momtahan, A. Karbaschi, F. Liu, and A. Adibi, "Free-space optical interconnects with a volume holographic element", ready to submit, (2010)

83. S. Yin, H. Zhou, F. Zhao, M. Wen, Z. Yang, J. Zhang, and F. Yu, "Wavelength multiplexed holographic storage in a sensitive photorefractive crystal using a visible-light tunable diode laser", *Optic. Comm.* 101, 317-321 (1993).

VITA

FENGTAO WANG

Mr. Wang was born in ZhengZhou, China. He received his B.S. (1998) and M.S. (2001) from the Department of Precision Instruments at Tsinghua University (Beijing, China), respectively. He moved to the United States in 2001 and received his M.S.E.E. from the University of Colorado, Boulder in 2003. Then he enrolled in Georgia Tech to pursue a doctorate in Electrical Engineering in Optics and Photonics Group.